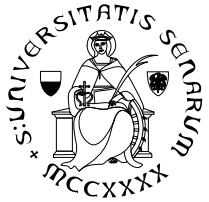

UNIVERSITÀ DI SIENA 1240

Department of Medical Biotechnologies

Doctorate in Genetics, Oncology and Clinical Medicine (GenOMeC)

XXXVI cycle

Coordinator: Prof.ssa Ilaria Meloni

Zika virus induces FOXG1 nuclear displacement and down-regulation

Scientific disciplinary sector: MED/07 - Microbiology and clinical microbiology

PhD Candidate

Giulia Lottini

Università di Pisa

Tutor

Prof.ssa Giulia Freer

Università di Pisa

Supervisor

Prof. Fabio Coppedè

Università di Pisa

Academic year

2022/23

INDEX

1 ABSTRACT

The Zika virus (ZIKV), belonging to the *Flavivirus* genus, is a single-stranded positive-sense RNA virus transmitted through the bites of infected mosquitoes (*Aedes* genus) or sexually. First isolated in 1947 from a primate in Zika Forest in Uganda, it gained little attention until 2016, when an increase in microcephalic newborns born to ZIKV-infected mothers was observed in Brazil and the Pacific islands. In most cases, ZIKV infection in adults is either asymptomatic or presents mild symptoms similar to those caused by other arboviruses. However, when it infects a pregnant woman, ZIKV, due to its ability to cross the placental and blood-brain barriers, can lead to severe congenital malformations in the fetus, including microcephaly. Despite considerable efforts to understand the impact of ZIKV on fetal brain development, the mechanisms linking ZIKV infection and congenital cortical abnormalities are not yet fully understood. Recent research has indicated that fetal ZIKV infection exhibits several molecular and anatomical characteristics similar to congenital disorders associated with Forkhead box G1 (FOXG1) syndromes. FOXG1 is an evolutionarily conserved transcription factor belonging to the Forkhead box protein family. Dysregulation or mutations in FOXG1 have been identified as the cause of various significant human neurological developmental disorders. It plays a crucial role in the development of the telencephalon and early corticogenesis, maintaining the balance between cell replication, differentiation, and apoptosis.

The aim of this dissertation was to scrutinize the impact of ZIKV infection on the subcellular localization of FOXG1. Utilizing plasmids encoding Foxg1 fused with GFP, we transfected A549 cells and observed, *via* confocal microscopy, a reduction in nuclear fluorescence of Foxg1-GFP following ZIKV infection. This result was further corroborated by observing FOXG1 nuclear dislocation after ZIKV infection in neural progenitor cells (NPCs) derived from human induced pluripotent stem cells (hiPSCs), which naturally express FOXG1. Importantly, this phenomenon did not occur following infection with other Flaviviruses, such

as Usutu virus, another Flavivirus, or Chikungunya virus, which belongs to the *Togaviridae* family. Hence, nuclear export of Foxg1 was specifically associated with ZIKV infection.

Subsequently, through western blot (WB) analysis in both transiently and endogenously FOXG1-expressing cells, we detected a downregulation in the expression of this transcription factor after ZIKV infection. To ascertain whether ZIKV infection selectively affected FOXG1 or also impacted other transcription factors involved in neural differentiation, we infected hiPS-NPCs with ZIKV. Remarkably, we did not observe any alterations in SRY (sex determining region Y)-box 1 (SOX1) and SOX2 expression or subcellular localization, suggesting that ZIKV effect was specific to FOXG1. This led us to hypothesize that the compromised transcription factor activity of FOXG1 due to ZIKV infection resulted in the dysregulation of its downstream genes. To test this hypothesis, we infected hiPS- NPCs with ZIKV and analyzed the expression of genes associated with cell replication and apoptosis. We observed upregulation of *CDKN1A* and *CDKN1B*, alongside downregulation of *CCND1* in infected hiPS-NPCs, in contrast to uninfected cells.

To delve deeper into the cellular mechanisms responsible for the reduction in nuclear and total FOXG1 levels, we explored the role of Akt-mediated phosphorylation at the level of threonine 271 (T271) in Foxg1, and how its presence or absence influenced nuclear export following ZIKV infection. By transfecting plasmids encoding Foxg1-GFP T271A (a phospho-defective mutant) and Foxg1-GFP T271D (a phospho-mimetic mutant), we observed no reduction in nuclear fluorescence of both Foxg1 mutants, emphasizing the pivotal role of T271. This phosphorylation event is orchestrated by the Akt pathway, which is activated through Akt phosphorylation (pAkt). Consequently, we probed for variations in pAkt/Akt levels following ZIKV infection to ascertain whether the infection triggered an increase in active pAkt. Although we did not observe changes in protein levels of PTEN, a negative regulator of the Akt pathway, after ZIKV infection, our results suggested alterations in pAkt/Akt levels following 24 h of

ZIKV infection. However, it is important to note that other molecules and regulatory mechanisms may also be involved in Foxg1 phosphorylation.

In our quest to investigate which additional regions of FOXG1, apart from T271, contributed to the nuclear displacement triggered by ZIKV, we transiently transfected cells with various murine Foxg1 fragments fused to GFP. Confocal imaging of these fragments revealed that while the localization of N-terminal and central Foxg1 fragments remained unaffected following ZIKV infection, both human and murine C-Foxg1-GFP fragments exhibited significant alterations. This suggests that the mechanisms responsible for subcellular delocalization and functional loss of FOXG1 predominantly hinge on the C-terminal portion of FOXG1.

To further elucidate the potential mechanisms underlying FOXG1 downregulation, we examined the role of the ZIKV protease NS2B-NS3. FOXG1 harbors a ZIKV serine protease cutting motif, prompting us to transiently transfect A549 cells with the Foxg1-GFP construct and the NS2B-NS3 plasmid. However, our confocal imaging did not reveal colocalization between NS2B-NS3, which primarily resided in the cytoplasm, and Foxg1, which was predominantly nuclear. Consequently, we did not detect any protease activity against FOXG1, even after forcing protease and FOXG1 physical interaction by disrupting A549 cells transiently expressing both exogenous proteins.

Next, we turned our attention to growth factors (GFs), as several studies have associated fibroblast growth factor 2 (FGF2) with ZIKV infection, stem cell self-renewal, and neural development. Given the importance of GFs in the activation of the Akt signaling pathway and considering that ZIKV infection led to increased Akt activation, we hypothesized that GFs expression and release might be affected by ZIKV infection, subsequently influencing FOXG1 nuclear export and downregulation. Initially, we measured FGF2 secreted by ZIKV-infected cells, along with cells infected with Usutu virus (USUV) and Chikungunya virus (CHIKV) and compared them to cells transfected with Poly(I:C). This analysis revealed secretion of 1.5 ng/ml

of FGF2 following 72 h of ZIKV infection, and we also observed an increase in *FGF2* mRNA expression in ZIKV-infected hiPS-NPCs cells compared to mock-infected cells. Intriguingly, we found that treating A549 cells with recombinant FGF2 resulted in an increase in ZIKV infection. Furthermore, when we treated with FGF2 A549 cells transiently expressing FOXG1 infected with ZIKV, a subsequent WB analysis did not reveal any significant changes in FOXG1 expression. Additionally, we experimented with NES cells, a model of human neural stem cells that are typically maintained in a medium supplemented with FGF2 and EGF2. Interestingly, following ZIKV infection, we did not observe the typical FOXG1 displacement in these cells. Moreover, when we maintained A549 and hiPS-NPCs in a medium supplemented with GFs and subjected them to ZIKV infection, the treatment with GFs effectively prevented FOXG1 displacement.

In summary, our research findings suggest that ZIKV specifically targets the nuclear factor FOXG1, resulting in its export and downregulation. This phenomenon is mediated through T271 phosphorylation, activation of the Akt signaling pathway, and the modulation of GFs expression. These insights contribute to our understanding of the mechanisms underlying the development of microcephaly in fetuses following congenital ZIKV infection.

2 LIST OF ABBREVIATIONS

aa	Amino acids
Akt	Protein Kinase B
bp	Base pairs
BSA	Bovine Serine Albumin
C	Capsid
Ca^{2+}	Calcium ion
CDKN1A	Cyclin-Dependent Kinase Inhibitor 1A
CHIKV	Chikungunya Virus
CKI	Casein Kinase I
CTCF	Corrected Total Cellular Fluorescence
DAG	Diacylglycerol
DMEM	Dulbecco's Modified Eagle Medium
E	Envelope
ER	Endoplasmic Reticulum
ERK	Extracellular signal-Regulated Kinase
FBS	Fetal Bovine Serum
FGF	Fibroblast Growth Factor
FGFR	Fibroblast Growth Factor Receptor
FHD	Forkhead Domain
FOXG1	Human Forkhead Box G1 (Foxg1 in mice, FoxG1 in other chordates)
GBD	Groucho Binding Domain
GFs	Growth Factors
GOI	Gene of Interest
EM	Extracellular Matrix

hiPSCs	Human-Induced Pluripotent Stem Cells
HFAs	Human fetal astrocytes
HIV-1	Human Immunodeficiency Virus 1
HS	Heparan Sulfates
IF	Immunofluorescence
IFN	Interferon
IP_3	Inositol 1,4,5-trisphosphate
JBD	JARID1B Binding Domain
LTR	Long Terminal Repeat
MAPK	Mitogen-Activated Protein Kinase
MOI	Multiplicity of Infection
MIT	Mitochondrial Domain
NES	Neuroepithelial Stem Cell
NPCs	Neural Progenitor Cells
NS	Non Structural
NSCs	Neural Stem Cells
O/N	Overnight
PBS	Phosphate Buffered Saline
PDK1	Pyruvate Dehydrogenase 1
pi	post infection
PI3K	Phosphoinositide 3-Kinase
PIP_2	Phosphatidylinositol 4,5-Bisphosphate
PIP_3	Phosphatidylinositol Trisphosphate
PKC	Protein Kinase C
PLCγ	Phospholipase Cγ

PLVs	Pseudotyped Lentiviral Vectors
PTEN	Phosphatase and Tensin Homolog
TBK1	TANK-Binding Kinase 1
prM/M	Membrane Glycoprotein
RT	Room Temperature
ROI	Region of Interest
SOX	SRY (sex determining region Y)-box
ssRNA+	Single-stranded positive-sense RNA
ssRNA-	Single-stranded negative-sense RNA
STAT	Signal Transducer and Activator of Transcription
TBS	Tris Buffered Saline
TGN	Trans-Golgi Network
USUV	Usutu Virus
VSV	Vesicular Stomatitis Virus
VSVG	VSV Virus Glycoprotein G
WB	Western Blot
WHO	World Health Organization
ZIKV	Zika Virus

3 INTRODUCTION

Zika virus (ZIKV) is a unique member within the *Flavivirus* genus of the *Flaviviridae* family that is associated with intricate complications in fetal neural development, most notably microcephaly. Despite ongoing research efforts, the precise mechanism through which ZIKV infection contributes to congenital cortical development disorders remains a subject of ongoing investigation. The link between ZIKV infection and microcephaly was first described through epidemiological data, which pointed to an increase in the incidence of microcephaly cases concomitant with the ZIKV epidemic outbreak in Brasil in 2015 (Brasil et al., 2016a; Brasil et al., 2016b). Confirmation of this association came to light when the ZIKV's genome was discovered and sequenced in the amniotic fluid of a microcephalic fetus in Brazil during the year 2016 (Calvet et al., 2016).

The maternal-fetal interface is typically guarded by innate immunity, a robust defense mechanism that effectively shields it from invading pathogens. However, ZIKV has displayed a remarkable ability to circumvent these natural defense mechanisms, thereby gaining access to the developing fetus, crossing the maternal-fetal barrier (El Costa et al., 2016). Furthermore, a study conducted by Tang et al. in 2016 provided compelling evidence that ZIKV exhibits a distinct tropism for specific cellular targets, notably neural progenitor cells (NPCs), neural stem cells (NSCs), and the blood-brain barrier (Tang et al., 2016). Upon infection, ZIKV leads these cells to cell cycle arrest, increased apoptosis, and inhibition of differentiation. The susceptibility of NPCs to viral infection and the ability of ZIKV to infiltrate the developing fetal brain by breaching the maternal-fetal barrier collectively suggest a pivotal role for ZIKV in causing aberrations in cerebral development (C. Li et al., 2016).

Several studies have explored the impact of ZIKV infection on the regulatory network governing brain development. These effects manifest as a dysregulation of critical factors involved in immune response, expression of differentiation-associated genes, such *Ntn1* and

Ephb2, impairment of apoptotic pathways through Caspase-3 increased expression and cleavage of factors involved in cell cytokinesis and mitotic abscission as Septin-2 (Dang et al., 2016; Li et al., 2016; Tang et al., 2016; Li et al., 2019). The implication of such fundamental developmental processes underscores the complex and multifaceted nature of the influence of ZIKV infection on neural development (Figure 1).

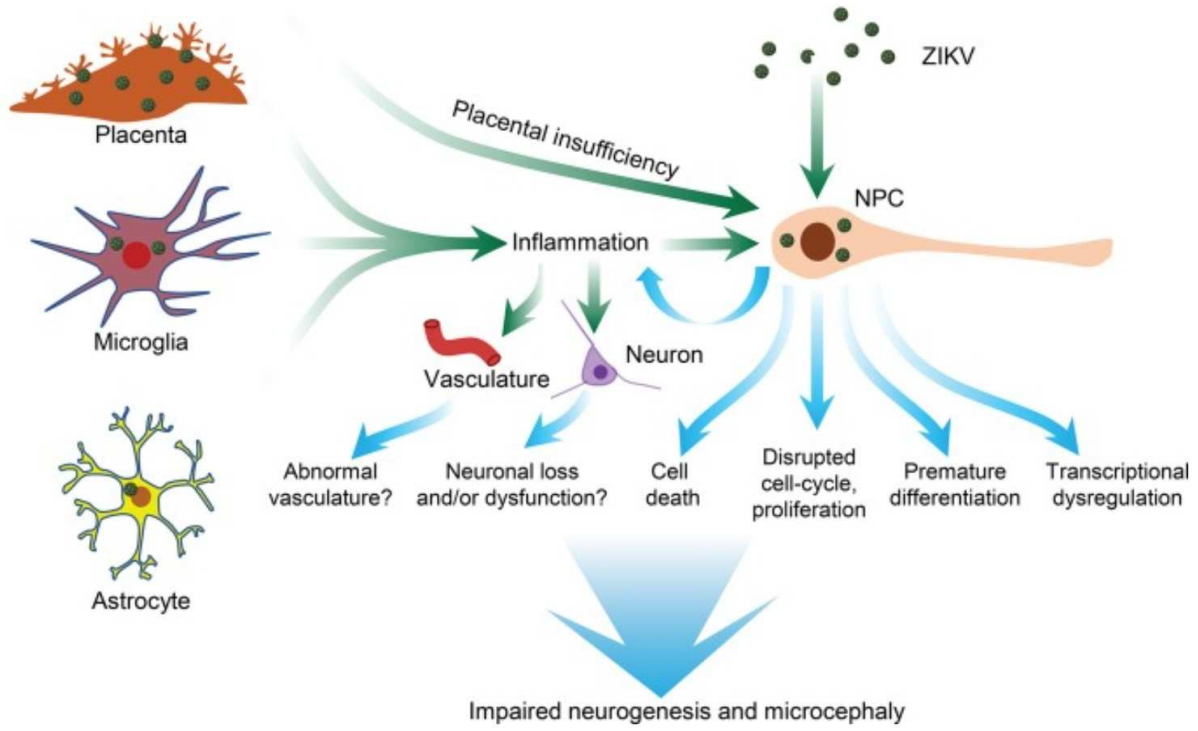

Figure 1. **Mechanisms underlying brain development disruption following ZIKV infection.** The upper portion illustrates the fact that ZIKV directly infects NPCs in the developing brain and activates the innate immune response, potentially leading to dysregulation of genes involved in cell cycle, neurogenesis, and apoptosis, resulting in increased cell death, cell cycle interruption, reduced proliferation, and premature differentiation. ZIKV infection within the placenta and in glial cells, including astrocytes and microglia, is shown to be potentially able to lead to placental insufficiency and immune response activation (inflammation), which may have effects on NPCs, neurons, and vascularization, ultimately altering neurogenesis and causing microcephaly (Wen et al., 2017).

3.1 Flaviviruses

Flavivirus, a genus of the *Flaviviridae* family, consists of single-stranded positive-sense RNA viruses (ssRNA+). Within this viral genus, a diverse array of prevalent human pathogens can be found, which are primarily transmitted through mosquito or tick bites. These viruses have evolved to exploit both vertebrate and invertebrate hosts for their replication, as reviewed by Rey and colleagues (Rey et al., 2017). Notably, some of these viruses possess the potential to spread dramatically worldwide, causing epidemics, as underscored by the expanding endemicity regions of Dengue virus and ZIKV. Such adaptability and potential for global impact have brought Flaviviruses to the forefront of scientific research and public health concerns.

At a structural level, Flaviviruses present as virions with an icosahedral capsid, covered by a lipid bilayer containing the viral receptor. The fully matured viral particle has a diameter of approximately 50 nm, making them remarkably compact. Flaviviral genome consists of 10,800 base pairs (bp), encoding for a cap at the 5' untranslated regions and lacking a poly-A tail typically found in mRNA molecules. Upon entering the host cell cytoplasm, the viral genome appears as a naked RNA entity that swiftly undergoes translation into a single polyprotein, within the endoplasmic reticulum (ER). This polyprotein is cleaved into three structural peptides and seven non-structural (NS) proteins, each with a specialized role in replication. This cleavage process is tightly orchestrated by cell proteases before the viral protease take over (Figure 2A).

The three structural peptides encoded within this polyprotein serve as the structural elements of the viral particle including the capsid (known as C), the envelope (E), and the membrane glycoproteins (prM/M). The C protein is located in the cytoplasm of infected cells, where it forms a nucleocapsid complex with viral RNA. Following viral endosomal membrane fusion, the viral genome remains associated with C dimers to evade RNA sensors and host nucleases. Additionally, the C protein acts as an RNA chaperone, aiding in the formation of nucleocapsid

buds in the endoplasmic reticulum, contributing to the creation of viral particles. The PrM protein is situated beneath the E-protein layer and plays a crucial role in virion maturation (Figures 2B and 2C). Both the M and E proteins are organized in icosahedral symmetry, composed of 60 repeated units. The E protein is essential for binding and membrane fusion processes in conjunction with surface proteins. It consists of three domains, with domain I involved in envelope structure organization, while domains II and III participate in receptor binding and monomer interaction, respectively. The E protein serves as the primary target for antibodies (Mukhopadhyay et al., 2005).

Conversely, the seven NS orchestrate key processes such as transcription and replication, ensuring viral survival and propagation within the host cell. Moreover, these proteins possess the ability to subvert the host's antiviral defense mechanisms. In particular, NS1 glycosylation is pivotal for efficient viral release, virulence, and replication. It exists in three forms: monomeric, dimeric and hexameric (the secreted protein). NS2A is a multifunctional, hydrophobic, membrane-associated protein involved in RNA replication and modulation of the host's antiviral interferon (IFN) response. NS2B collaborates with the C-terminal protease domain of NS3 to form a serine protease complex responsible for cleaving the viral polyprotein. NS4A and NS4B proteins determine viral pathogenesis and contain multiple hydrophobic membrane regions; NS4B plays a role in forming membrane constituents of the viral replication complex and localizing NS3 within membranes. Finally, NS5 consists of two domains: the C-terminal RNA-dependent RNA polymerase and the N-terminal methyltransferase (Lin et al., 2018).

Regarding their replicative cycle, Flaviviruses enter target cells through endocytosis, by membrane receptors like the Gas6-AXL complex. Once inside the host cell, within the acidified endosomes, the nucleocapsid releases the viral genetic material. Once translation begins, the polyprotein is delivered to the ER. The NS proteins come together to form the replication

complex, facilitating the invagination of the ER membrane to generate replication organelles. These replication complexes are responsible for duplicating the viral RNA *via* a ssRNA- intermediate, resulting in the production of a ssRNA+. This RNA is subsequently enclosed within new nucleocapsids and enveloped, ultimately giving rise to immature virions (Van Den Elsen et al., 2021). Then, to become infectious, these immature particles are addressed to the Trans-Golgi network (TGN), where they reach full maturation through cleavage by furin (Yu et al., 2008). At the end, mature virions exit *via* the secretory pathway, a sophisticated network of cellular compartments and vesicles. As the virions are released into the extracellular milieu, they can potentially begin new infections, either in neighboring cells within the same host or when transmitted to other susceptible hosts, to propagate and perpetuate the infection, starting a new replication cycle (Figure 2D) (Chiramel & Best, 2018).

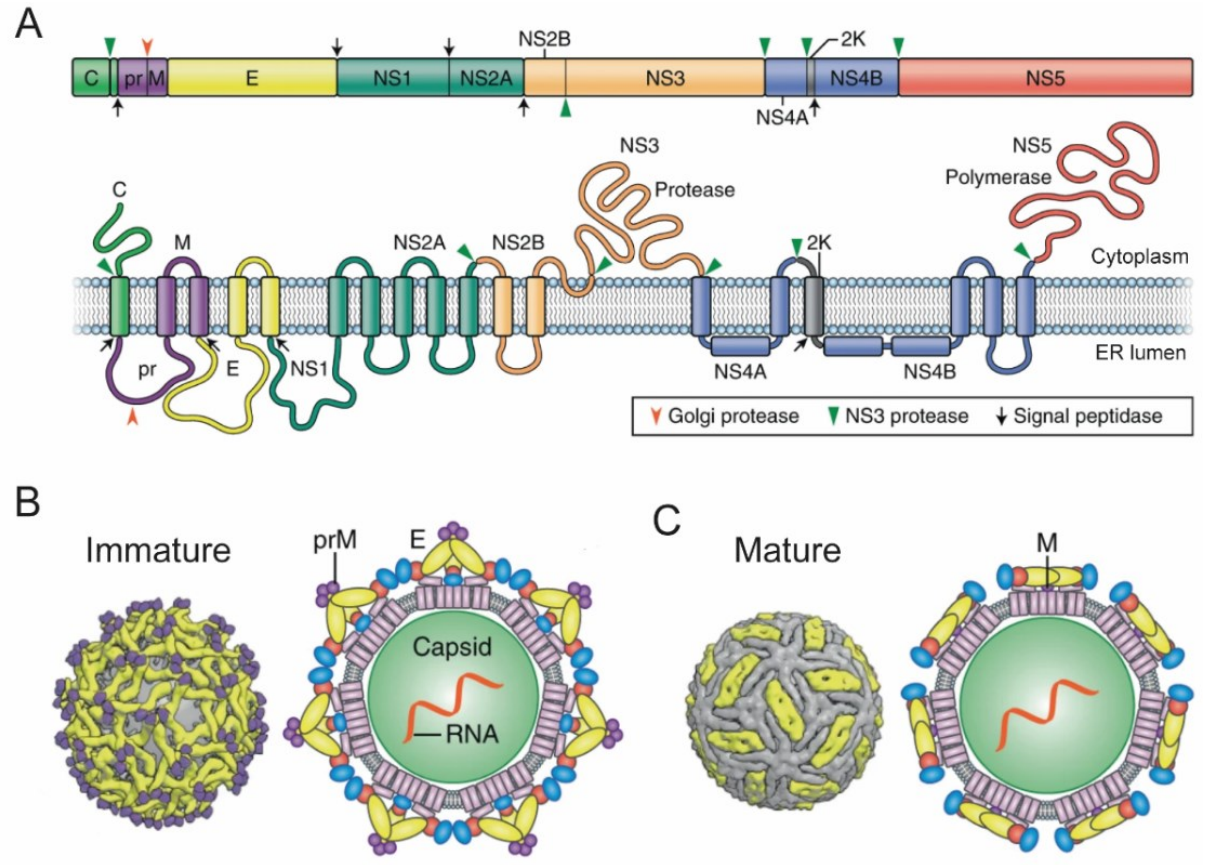

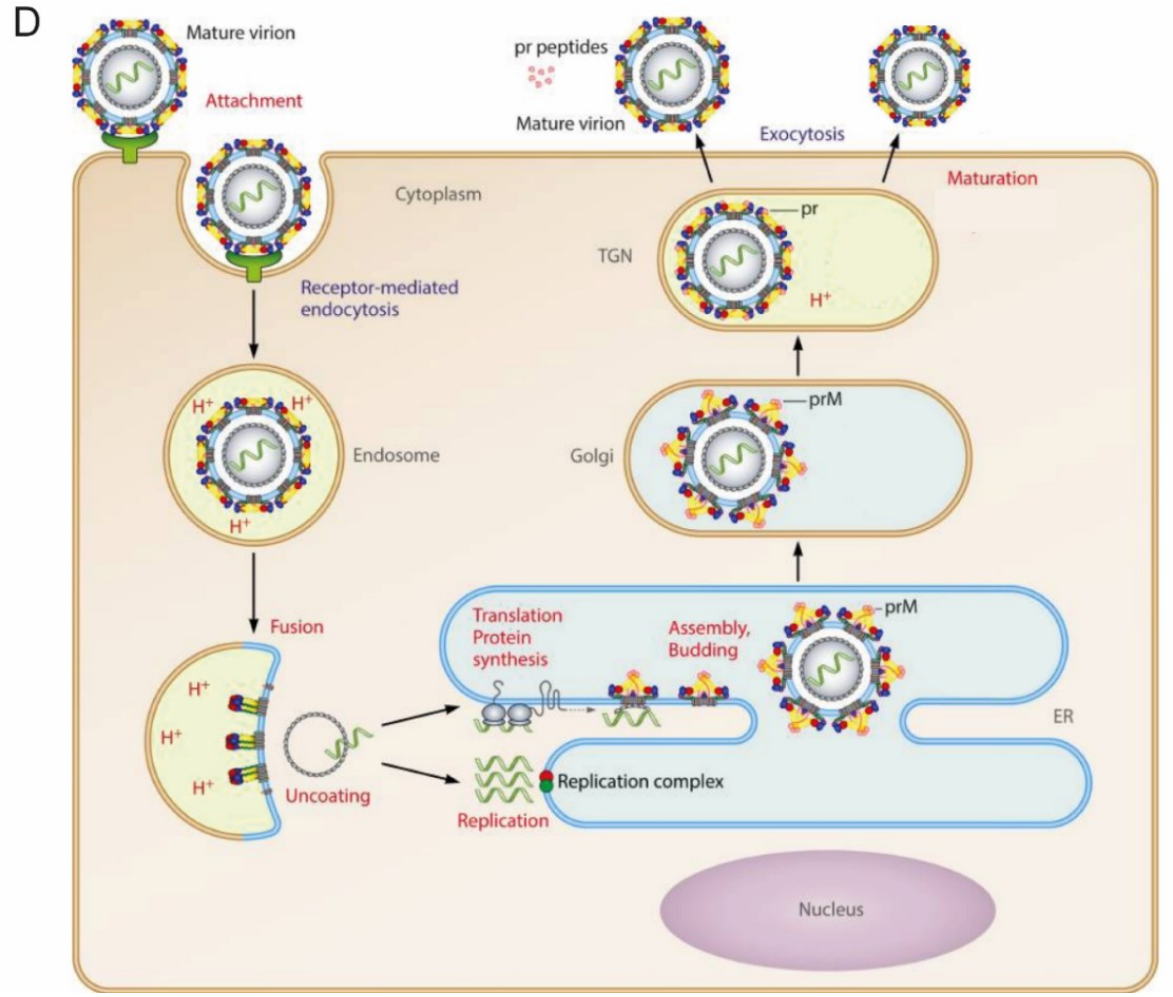

Figure 2. **Flavivirus structure and replication.**

(A) Flaviviruses possess a single open reading frame that undergoes translation within the ER, coding for a polyprotein. This polyprotein is subsequently subjected to cleavage, a process facilitated by both viral and host cell proteases. This proteolytic activity results into three structural proteins (C, prM, and E) and seven NS proteins.

(B) In most Flaviviruses, folding of E proteins in the ER is facilitated by their interaction with prM after their synthesis. During the formation of virions, prM is integrated into the viral envelope as heterotrimeric prM–E spikes, assuming icosahedral symmetry. Incorporation of prM is indispensable to prevent conformational changes in the E protein, which could lead to unintended fusion of virions with host cell membranes during their release.

(C) In mature virions, E proteins are organized as antiparallel dimers. Each mature virion incorporates ninety E dimers, arranged in a pattern with a symmetrical configuration of an icosahedron (Pierson & Diamond, 2020).

(D) The virus enters the host cells through receptor-mediated endocytosis, followed by membrane fusion triggered by the acidic pH within the endosome. This fusion process enables

release of the viral RNA into the host cell. Viral protein synthesis and the assembly of new virus particles occurs primarily at the ER membrane. Immature virions undergo transport via the exocytic pathway. Within the TGN, a drop in pH triggers structural alterations, that enable the cleavage of prM by the host cell protease furin, leading to the formation of mature and infectious virions, that are released in extracellular compartment (Heinz & Stiasny, 2017).

3.1.1 ZIKV: the only Flavivirus associated to birth defects

ZIKV was initially discovered in the Zika forest of Uganda in 1957. Over time, it spread to affect human populations in Africa, India, and Asia, eventually reaching Brazil (Sager et al., 2018). Initially, ZIKV received little attention in the medical community, and its clinical significance was considered low. Indeed, the majority of ZIKV infections in adults tend to be asymptomatic or present with mild, flu-like symptoms, including joint pain, skin rash, and conjunctivitis (Hayes, 2009). However, a significant turning point occurred in 2013 in French Polynesia. During this time, a notable increase in cases of Guillain-Barrè syndrome was reported, along with a concerning rise in congenital neurological defects, such as microcephaly (Mlakar et al., 2016; Smith & Mackenzie, 2016). These alarming changes in ZIKV pathogenicity culminated in the ZIKV infection/microcephaly outbreak in Brazil in 2015 and prompted the World Health Organization (WHO) to declare the ZIKV epidemic a global public health emergency, highlighting the importance of continued research, monitoring, and public health measures (Zanluca et al., 2015).

ZIKV is primarily transmitted to humans through *Aedes* mosquito bites. Additionally, human-to-human transmission can occur through blood and blood products, sexual contact, or vertically from mother to child (Figure 3A) (Hasan et al., 2018). Notably, ZIKV, compared to other Flaviviruses, displays a unique tropism for cells lining the maternal-fetal interface. To replicate within host cells, ZIKV must overcome the intrinsic cellular responses that trigger the release of type I IFN, inducing the degradation of the IFN-regulated transcriptional activator STAT2 (Signal transducer and activator of transcription 2) (Wen et al., 2017).

Like other viral infections, ZIKV infection induces the production of type I and III IFNs in placental trophoblasts, as well as pro-inflammatory cytokines, resulting in antiviral gene expression (Bayer et al., 2016; Quicke et al., 2016). In line with this, blocking IFN receptor signaling with an anti-receptor antibody has been shown to enhance transplacental ZIKV infection. Moreover, ZIKV infection in the placenta can lead to trophoblast apoptosis and vascular damage, ultimately compromising the placental barrier's protective function against viral infection and potentially allowing ZIKV transmission to the fetus (Miner et al., 2016). Inflammatory responses, vascular damage, a reduced number of fetal capillaries, and irregular trophoblast morphology are clinically significant outcomes of infection, as placental insufficiency is associated with intrauterine growth restriction (Ornelas et al., 2017). The fetal brain's exposure to cytokines not only triggers cell death but also disrupts the differentiation and proliferation of NPCs, contributing to the intricate mechanisms leading to ZIKV-induced microcephaly (Figure 3B) (Wen et al., 2017).

NS proteins of the virus are responsible for cytopathogenic effects during viral infection (Liang et al., 2016). Moreover, research has suggested that glycosylation of the E protein contributes to ZIKV pathogenesis, potentially facilitating attachment and infection of lectin-expressing leukocytes (Carbaugh et al., 2019).

In March 2016, the WHO declared a scientific consensus that ZIKV was a causative factor in the neurological disorders known as Guillain-Barré syndrome, microcephaly, and other congenital brain abnormalities (Krauer et al., 2017). As a result, numerous studies have focused on investigating the link between ZIKV infection and congenital brain anomalies, including microcephaly, in infants born to mothers infected during the first trimester of pregnancy. It is during this period that the neurological development of the central nervous system occurs (Faizan et al., 2017).

To comprehend the mechanisms and pathogenesis of ZIKV infections, studies have been conducted, employing advanced tools, such as human-induced pluripotent stem cells (hiPSCs), as well as neurospheres and organoids derived from human cells. These experiments have been further substantiated by in vivo studies on animals and immortalized cell lines. The results from various research groups have consistently indicated a strong tropism of ZIKV for NPCs in the cerebral cortex (Cugola et al., 2016; Garcez et al., 2017; Gladwyn-Ng et al., 2018; Himmelsbach & Hildt, 2018; Li et al., 2016; Tang et al., 2016). Collectively, this data suggests that ZIKV disrupts the progression of the cell cycle and triggers a cascade of apoptotic and autophagic cell deaths, ultimately leading to microcephaly. A recent study even reported that the effects induced by ZIKV in NPCs look like those caused by numerous genetic mutations underlying severe microcephaly in mice (El Ghouzzi et al., 2016; Zhang et al., 2016). These insights underscore the critical role of ZIKV in interfering with the delicate processes of neural development, shedding light into the mechanisms that contribute to the development of microcephaly and related neurological disorders.

A study by Onorati and colleagues highlighted efficient infection of neuroepithelial stem cell (NES) derived from human cerebral cortex and spinal cord by ZIKV, as opposed to neurons. Infection resulted in a reduction in cell density, an increase in apoptotic cells with condensed chromatin, nuclear fragmentation, and a decrease in proliferation levels. Notably, primary ZIKV-infected cells in the human fetal brain were identified as radial glial cells, capable of transmitting the infection to neurons. An intriguing observation was the relocalization of phosphorylated TANK-binding kinase 1 (pTBK1) from centrosomal positions in the cytoplasm to mitochondria in the presence of ZIKV. Since TBK1 plays crucial roles in innate antiviral immune signaling, mitotic division, and cell proliferation, these findings suggest that this mechanism links ZIKV infection to specific associated phenotypes (Onorati et al., 2016).

Within ZIKV-infected brains, a significant loss of cells is evident, likely accounting for cortical lesions and post-natal neurological dysfunction, including secondary microcephaly and cognitive deficits, which collectively constitute the congenital ZIKV syndrome (Subissi et al., 2018; Van der Linden et al., 2018). These data and reports have dispelled the notion of a random association between ZIKV infection and the observed neurological impairments in fetuses infected *in utero* (Alfano et al., 2019). Primary microcephaly, present at birth, or secondary microcephaly, which occurs after birth, arises from an imbalance between the production of progenitor cells and cell death. This imbalance results in a reduced number of neurons and glia within the brain, leading to a smaller brain size. This clinical condition is associated with severe congenital defects, with the measurement of head circumference, typically assessed at the occipito-frontal diameter, falling at least 3 standard deviations below the population average (Figure 3C) (Passemard et al., 2013).

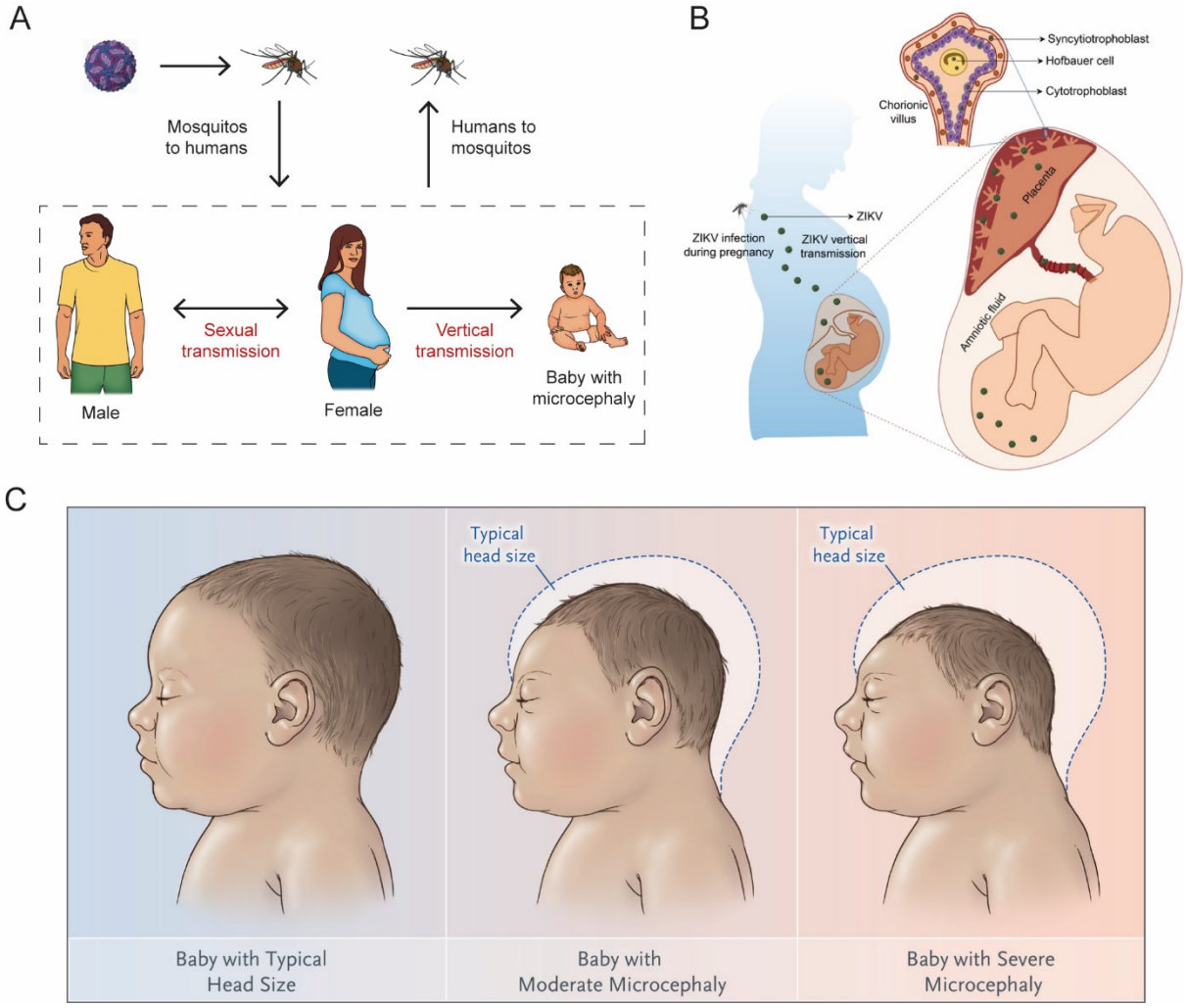

Figure 3. **ZIKV transmission and associated microcephaly.**

(A) ZIKV can be transmitted through various means, aside from mosquito bites. It can spread through sexual contact, especially from men to women. ZIKV can persist in semen for an extended period, possibly up to six months, longer than in other bodily fluids. Another significant mode of transmission is from an expectant mother to her child during pregnancy or around the time of birth, potentially resulting in symptoms like microcephaly and specific brain damage patterns. Additionally, the virus can be transmitted through blood transfusions and breastfeeding (adapted from Rossi et al., 2018).

(B) ZIKV is transmitted to a pregnant woman through the bite of an infected mosquito, subsequently leading to vertical transmission from the infected mother to the fetus by infecting placental trophoblasts and macrophages, disrupting and crossing the placental barrier (Wen et al., 2017).

(C) Representation of the head size of a typical healthy newborn, compared to infants with moderate or severe microcephaly associated with vertical ZIKV infection. Microcephaly at

birth is associated to a range of brain malformations, resulting from a more or less severe failure of neurogenesis (Petersen et al., 2016).

3.1.2 Usutu virus: a Flavivirus not associated with microcephaly

Usutu virus (USUV), which also belongs to the *Flavivirus* genus, is not associated with congenital brain disorders, but since it is very similar to ZIKV, it can be used to demonstrate how microcephaly is selectively induced only by ZIKV and not by other viruses.

USUV was first identified in South Africa in 1959, and it is named after the Usutu River. When introduced to Europe, USUV caused significant outbreaks among birds, as observed in Austria in 2001 and reported in countries like Hungary, Italy, and Germany. Since then, its geographical distribution has rapidly expanded, with a marked increase in circulation, especially in recent years. Birds, particularly songbirds, are the primary reservoir of USUV. Mosquitoes become infected when they feed on infected birds, and then they can transmit the virus to other birds and occasionally to humans through their bites. This makes it similar in transmission to other mosquito-borne viruses like West Nile virus (Clé et al., 2019).

The symptoms of USUV infection in humans are typically mild or asymptomatic, and most people who are infected do not experience any noticeable illness. In rare cases, it can lead to more severe symptoms such as fever, rash, headache, and muscle and joint pain. Severe cases are more common in individuals with weakened immune systems. However, due to the limited number of cases, the full clinical spectrum associated with USUV is not yet fully understood, and specific antiviral treatments for this infection have not been developed to date (Gill et al., 2020).

3.2 Chikungunya virus: an arbovirus not causing microcephaly

Chikungunya virus (CHIKV) belongs to the *Togaviridae* family, *Alphavirus* genus. Like ZIKV, it is a mosquito-borne pathogen that can infect humans but is not associated with microcephaly

at birth. CHIKV is characterized by symptoms such as severe joint and muscle pain, skin rashes, and fever. For this reason, as USUV, can be used as a good negative control in studies that show how only ZIKV impairs expression of neural differentiation-associated genes.

This virus is primarily transmitted by *Aedes aegypti* and *Aedes albopictus* mosquitoes in tropical and subtropical regions. CHIKV was originally identified in Tanzania in 1952. Since then, like others, it has spread to various parts of the world and, over the past 15 years, it has caused severe epidemics in Africa, Asia, the Indian Ocean, and more recently, in the Caribbean and the Americas (Silva & Dermody, 2017).

CHIKV is an enveloped virus with an icosahedral nucleocapsid shell. It is a small virus, approximately 70 nm in diameter, with a ssRNA+ genome of approximately 11,800 nucleotides, a 5'-cap and a poly-A tail at the 3' end. CHIKV encodes several proteins, including NS proteins involved in replication (nsP1, nsP2, nsP3, and nsP4) and structural proteins (capsid, E1, and E2) that make up the viral particle's outer structure. CHIKV enters host cells by attaching to specific receptors, like Mxra8 (Matrix-remodeling-associated protein 8), on the cell's surface and through receptor-mediated endocytosis. Once inside the cell, the viral envelope fuses with the endosomal membrane, releasing the viral RNA genome and nucleocapsid into the cell's cytoplasm. The viral RNA serves as a template for the synthesis of a large polyprotein that is subsequently cleaved by viral and host proteases into individual functional proteins, including NS and structural proteins. New viral particles are assembled in the cytoplasm, where the structural proteins, capsid, E1, and E2, interact with the replicated RNA and migrate to the ER, where they are incorporated into the viral envelope. Assembled viral particles bud from the cell's membrane, acquiring their lipid envelope. Once mature, they are released often leading to cellular damage in the process. These newly formed viruses can then infect neighboring cells and continue the replication cycle (Schnierle, 2019).

3.3 Microcephaly associated to the FOXG1 transcription factor

The severe impact of ZIKV on brain development and long-term consequences of perinatal infection closely resemble congenital alterations at the anatomic, symptomatological, or molecular levels caused by mutations or downregulation of Forkhead Box G1 (FOXG1 in humans, Foxg1 in mice, FoxG1 in other chordates) (Kaestner et al., 2000). FOXG1 is a transcription factor involved in brain development and its haploinsufficiency in humans is associated with significant differences in brain size and altered intellectual development in early childhood, while homozygous mutations are typically fatal (Hou et al., 2020). Abnormalities caused by mutations in FOXG1 belong to a distinct clinical entity known as "FOXG1-related encephalopathy" associated with Rett syndrome (Wong et al., 2019). Results have provided evidence that mutations in the N-terminal region, which are among the most common mutations, and large deletions of FOXG1 lead to a more severe FOXG1 syndrome, although genotype-phenotype correlations are not necessarily direct in recurrent mutations (Vegas et al., 2018). Therefore, reduced dosage of FOXG1 results in microcephaly, severe intellectual disability, epilepsy, schizophrenia, infantile spasms, autism spectrum disorder, and is associated with congenital Rett syndrome (Figure 4).

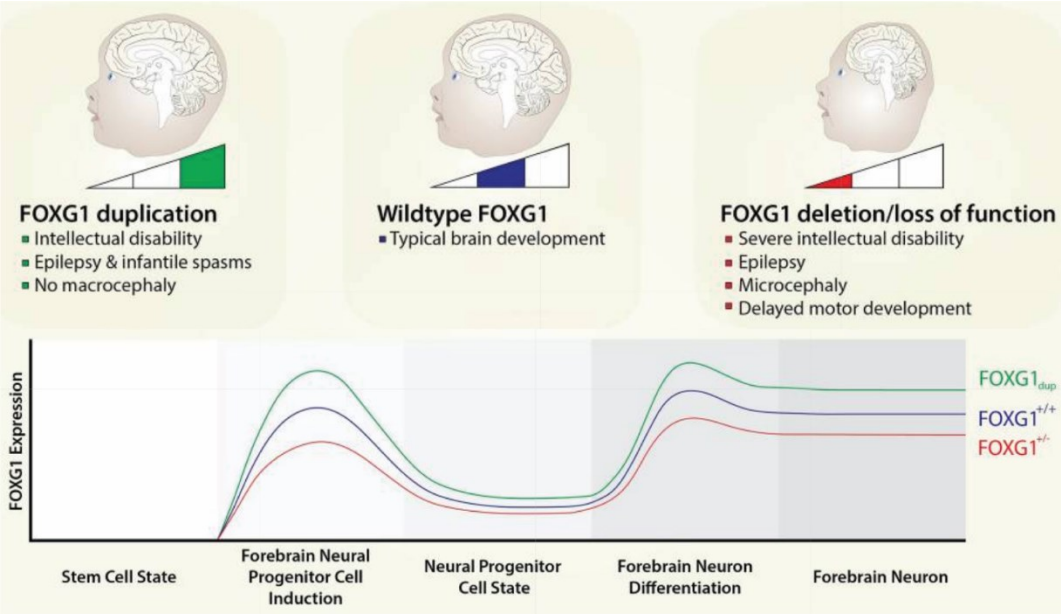

Figure 4. **FOXG1 dosage in neurodevelopment.**

FOXG1 expression patterns transitioning from a stem cell state to forebrain neurons, with induction and maintenance states defined. FOXG1 is among the earliest genes to be expressed in the mammalian telencephalon and its expression is activated in advance of the terminal differentiation of forebrain neurons, possibly even before the differentiation of forebrain neural progenitors. Variations in FOXG1 dosage, resulting from deletions, duplications, or mutations that cause functional gain or loss, give rise to a multifaceted range of cellular effects, holding significant implications for human diseases, particularly neurodevelopmental disorders (Hettige & Ernst, 2019).

3.4 Forkhead box transcription factors family

FOXG1 belongs to the Forkhead box (Fox) transcription factors superfamily, which are proteins characterized by a DNA-binding domain approximately 110 residues long with a structured conformation featuring two loops, often referred to as "wings," connecting three alpha-helical domains, known as the Forkhead domain (FHD), which resembles a fork-like shape. The various Fox transcription factors bind to a similar DNA sequence, albeit with varying affinities, due to their highly conserved DNA-binding motif (Hettige & Ernst, 2019). One remarkable aspect of Fox transcription factors is their evolutionary conservation. They are found in a wide range of organisms, from simple invertebrates like worms to complex vertebrates like humans.

This conservation suggests that Fox proteins play fundamental roles in regulating gene expression and controlling various biological processes throughout evolution.

The *forkhead* gene was initially identified in *Drosophila melanogaster*. Subsequently, it was demonstrated that this gene is crucial for the normal development of the intestine, and its absence results in a characteristic "head hole" appearance (Weigel et al., 1989). Following this discovery, a series of genes called *Fox* were identified in multiple organisms (Golson & Kaestner, 2016). The different *Fox* families are characterized by sequence differences, excluding the FHD, allowing for differential regulation and functional diversification among them. Fox proteins participate in numerous physiological processes, including embryonic development and organogenesis, cell cycle regulation, metabolism control, maintenance of stem cells, and signal transduction. The role of Fox proteins in development is well-known, but many *Fox* genes continue to be expressed in post-embryonic stages, suggesting functions that are yet to be clarified (Hettige & Ernst, 2019). For instance, studies have shown how Fox transcription factors provide regulation in adult neurogenesis, the process of generating new neurons in the adult brain. Indeed, certain Fox transcription factors are key regulators of neural stem cell maintenance and differentiation in the adult brain. This highlights their role in ongoing brain plasticity and the potential for therapeutic interventions in neurodegenerative diseases or brain injuries (Genin et al., 2014).

The *Fox* superfamily is quite extensive, with a varying number of family members depending on the organism. In humans, there are 44 known *Fox* genes, each potentially regulating different sets of target genes and processes. In mammals, this family of transcription factors is subdivided into subclasses ranging from "A" to "S". This classification helps to organize and understand the diversity of these transcription factors based on sequence similarities (Hettige & Ernst, 2019).

3.4.1 FOXG1

Like all members of this family, FOXG1 is characterized by the presence of the highly conserved FHD, which is essential for recognizing specific DNA sequences. Evolutionarily conserved, it consists of 481 aa in mice and 489 aa in humans. It is encoded by a gene located on chromosome 14q12, expressing for a protein of 79.3 kDa. FOXG1 consists of the FHD, which comprises three alpha helices and a beta sheet, in addition to a 10-residue Histone Demethylase JARID1B (JBD)-binding domain and a 20-residue Groucho-binding domain (GBD) (Figure 5A). The aa sequence from the FHD to the C-terminus is highly conserved, while the N-terminal domain is more variable among different species (Bredenkamp et al., 2007).

FOXG1 plays a significant role in brain development, where alterations in its expression significantly affect the formation and function of the mammalian cerebral cortex. FOXG1 is expressed in various cell types within the nervous system, such as the cerebral cortex and telencephalon, and has a pleiotropic role in anterior brain development (Pauley et al., 2006).

FOXG1 is considered a pioneering transcription factor, as it is one of the earliest expressed in nervous system cells and can modify chromatin structure to enable other factors to bind (Hettige & Ernst, 2019). Furthermore, it maintains the expansion of the neural proliferation pool and regulates the pace of cortical neurogenic progression. It is involved in facilitating the formation of the cortical layer and corpus callosum, promoting dendrite elongation, and maintaining neural plasticity (Wong et al., 2019). Additionally, overexpression or loss-of-function of FOXG1 can lead to tumorigenesis (Figure 5B).

FOXG1 antagonizes major cell cycle pathway components, including the FOXO/SMAD pathway, which promotes cortical neuron differentiation. In particular, FOXG1 inhibits FOXO/SMAD complexes through competition for binding sites or direct association. This antagonism reduces the expression of cyclin-dependent kinase inhibitor 1A (*CDKN1A*/p21),

preventing cell cycle exit and promoting stem cell pool expansion, facilitating prolonged proliferation of FOXG1-expressing cells (Figures 5C and 5D) (Seoane et al., 2004).

The proper spatiotemporal expression of FOXG1 is essential for the normal development of the telencephalon, where FOXG1 is regulated by numerous morphogens such as BMPs, WNTs, FGF8, and SHH and within the telencephalon, it primarily acts as a transcriptional repressor. Indeed, FOXG1 action prevents premature differentiation of the neural progenitor cell pool by actively remaining within the nucleus, where it can exert its repressive action, both DNA-binding dependent and independent (Hettige et al., 2023).

The ability to keep neural progenitor cells in a proliferative and undifferentiated state appears to depend on its nuclear localization, which is regulated by Casein Kinase I (CKI) and Protein Kinase B (Akt). Phosphorylation by CKI on serine 19 of FOXG1 induces its nuclear import and retention. Phosphorylation on threonine 226 (T226) of FOXG1 induced by FGF and mediated by Akt, on the other hand, results in export and cytoplasmic localization, leading to loss of transcription factor function and induction of neuronal differentiation. The Regad research group has indeed demonstrated, through experiments on *Xenopus*, that the nuclear export of FOXG1 depends exclusively on the pathway mediated by Akt-induced phosphorylation at T226. Therefore, the signaling of CKI and FGF converges in an antagonistic regulation of FOXG1, which in turn controls prosencephalic neurogenesis (Regad et al., 2007). Another study has shown that Akt also mediates phosphorylation on T271 of FOXG1, promoting the survival of post-mitotic differentiated neurons (Dastidar et al., 2011).

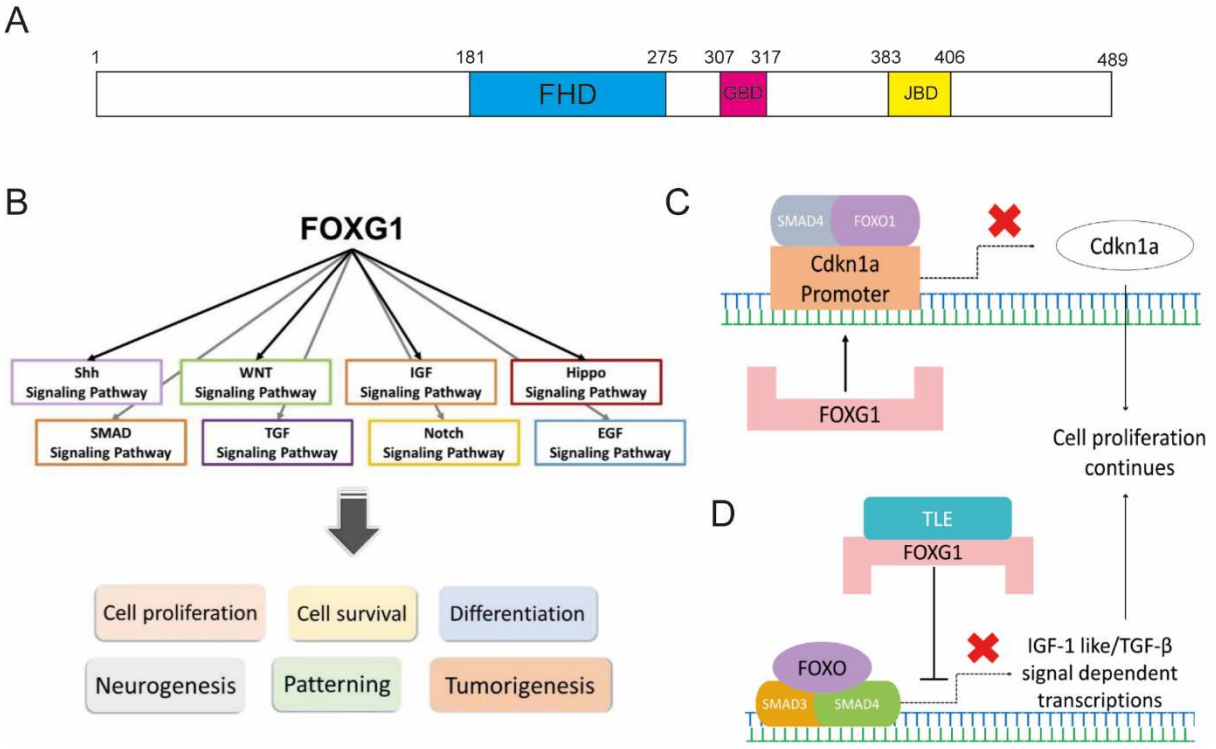

Figure 5. **FOXG1 sequence and regulation pathway.**

(A) Graphic representation of the human transcription factor FOXG1 highlighting FHD, Forkhead domain (blue), GTB, GROUCHO/TLE-Binding domain (pink) and JBD, JARID1B Binding Domain (yellow). The numbers above the figure refer to aa residues.

(B) FOXG1 interacts with various components of different pathways crucial in neurodevelopment, such as the Wnt, Notch, SMAD, IGF, and Shh signaling pathways. These interactions play pivotal roles in promoting the proliferation, survival, and differentiation of neurons and other cell types. Due to their significant influence on neurogenesis and telencephalon patterning, these interactions may also be implicated in tumorigenesis.

(C) FOXG1 (pink) suppresses *CDKN1A* expression by binding and associating with SMAD4 (grey) and FOXO1 (purple) complexes at the *CDKN1A* promoter, thereby preventing cell cycle exit and stopping differentiation.

(D) TLE-FOXG1 complex suppresses the IGF-1like/TGF-β signaling pathway, mediated by FOXO (purple)-SMAD3 (orange)-SMAD4 (green). This repression inhibits apoptosis while promoting growth and proliferation (Wong et al., 2019).

3.5 Pseudotyped lentiviral vectors to improve FOXG1 transiently expression

FOXG1 is endogenously expressed in NPCs, that can be obtained from hiPSCs after cerebro-cortical induction, recapitulating early stages of human neurodevelopment. We can observe FOXG1 expression also in NES cells that are neurogenic and display positivity for neuroprogenitor markers like SRY (sex determining region Y)-box 1 (SOX1) and (Onorati et al., 2016). However, at times, it may be necessary to induce the expression of FOXG1 in cell lines like human lung adenocarcinoma A549, which do not naturally express it. To achieve this, it is possible to transiently transfect the cells with plasmids encoding the gene of interest, in this case, *FOXG1*, or to transduce the cells with pseudotyped lentiviral vectors (PLVs) carrying the *FOXG1* gene. PLVs are widely employed as gene delivery vehicles due to several advantages they offer, including the integration of the carried gene into the host genome, the ability to transduce both dividing and non-dividing cells, and a wide range of tissue tropisms depending on the envelope protein used for pseudotyping.

In general, PLVs are viral vectors that combine the capsid proteins of a lentivirus, such as human immunodeficiency virus 1 (HIV-1), with the receptor envelope glycoprotein of another virus that exhibits a broad cellular tropism, such as the vesicular stomatitis virus glycoprotein G (VSVG). The recombinant genome of a PLV maintain the structural features of HIV-1 genome, such as the long terminal repeat (LTR) sequences and packaging signals (Ψ), but it is replication-related genes defective. In their place, the gene of interest, regulated by a strong heterologous promoter, is delivered, and inserted into host cells (King et al., 2016).

PLVs are produced through transfection of HEK-293T cell line, which possesses the SV40 T antigen that enhances vectors production (Merten et al., 2016). During the production of these particles, recombination events can occur and to prevent the restoring of the viral particle's ability to replicate, different plasmid are administered as follows:

1. A packaging plasmid, which contains the structural genes of HIV-1, necessary for the formation of the lentiviral capsid, reverse transcription of the lentiviral genome, and its integration into the cellular genome;
2. A plasmid containing the transgene that should be delivered, *FOXG1*, flanked by truncated HIV-1 LTR sequences containing Ψ;
3. A plasmid coding for the VSVG envelope protein;
4. A plasmid coding for HIV-1 Rev protein that enhances the export of viral mRNA from the nucleus to the cytoplasm (Gutierrez-Guerrero et al., 2020).

Once assembly in packaging cells has occurred, it is possible to collect the PLVs and use them to transduce the cell line of interest to express transiently FOXG1 (Figure 6).

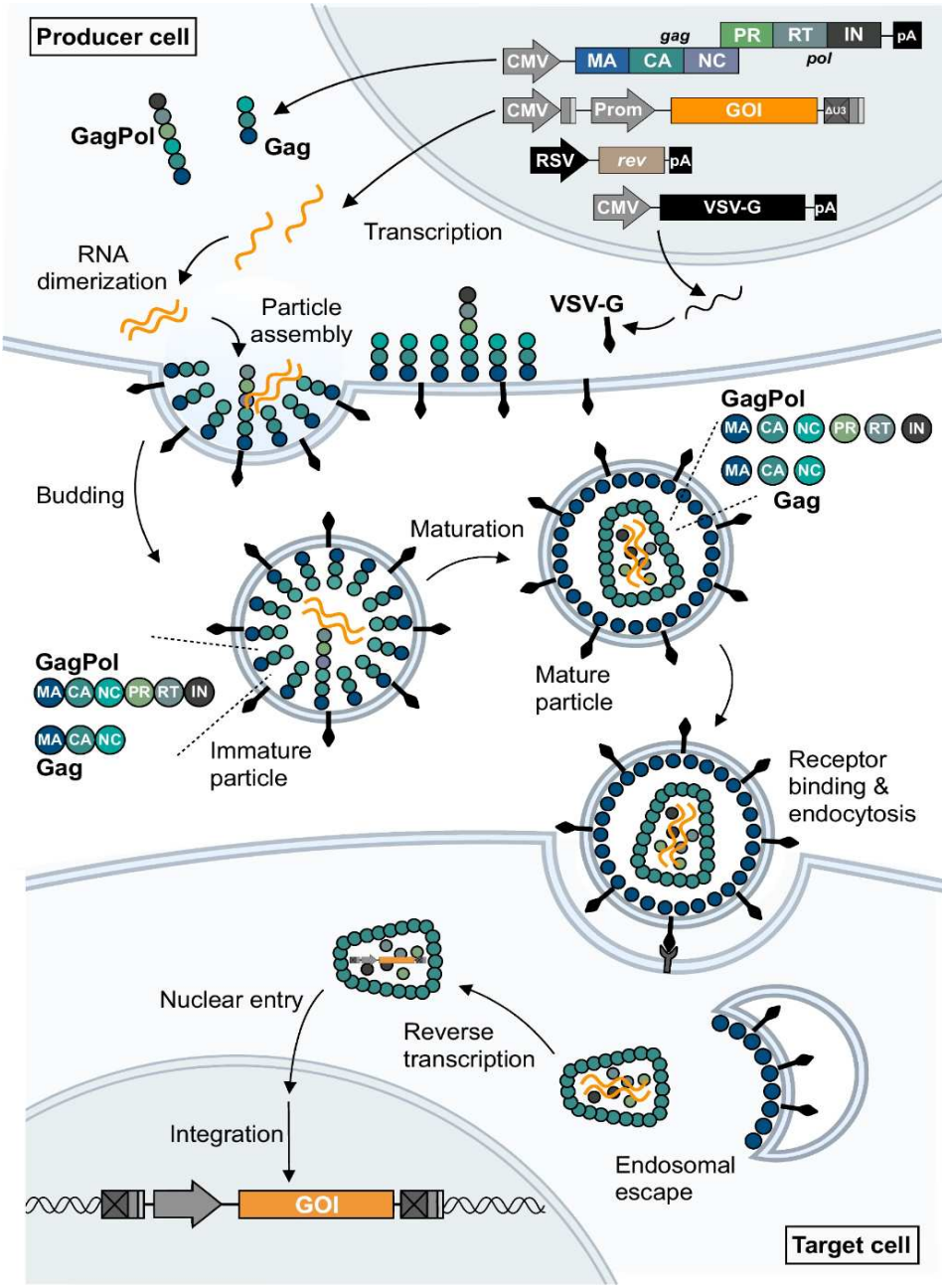

Figure 6. **PLVs production and transduction.**

This process begins by transfecting producer cells with four plasmids, initiating the transcription of key components, including Gag and GagPol polyprotein precursors, the VSVG envelope glycoprotein, Rev, and the transfer vector carrying the gene of interest (GOI) to be inserted into the target cells. During this process, nascent lentiviral particles are packaged with dimerized ssRNA encoding the GOI, flanked by viral cis-elements necessary for RNA packaging and reverse transcription. Initially, budding of lentiviral particles leads to the formation of immature particles. These immature particles undergo maturation, which involves cleavage of the Gag and GagPol polyproteins, as well as the formation of the viral core. Once matured, the lentiviral particles enter target cells through receptor-mediated endocytosis,

releasing the viral core into the cytoplasm. Subsequently, reverse transcription of the single-stranded RNA from the transfer vector occurs, resulting in the formation of double-stranded DNA. This DNA is then transported into the nucleus, where it integrates into the genome of the target cell (Wolff & Mikkelsen, 2022).

3.6 Fibroblast growth factors

Recent studies showed that ZIKV induces fibroblast growth factor 2 (FGF2) expression and FGF2 facilitates virus replication and spread and that in ZIKV-infected pregnant women, blood concentration of FGF2 correlates with the severity of the affected fetuses (Kam et al., 2017; Limonta et al., 2019). Moreover, growth factors (GFs) are active in neural development and essential for maintaining NSC self-renewal and for this reason could impact on the interaction between ZIKV and FOXG1 (Onorati et al., 2016).

FGFs are encoded by a family of 22 genes with a highly conserved core sequence. Canonical FGFs are divided into subfamilies 1, 4, 7, 8, 9, secreted for local autocrine/paracrine actions; subfamily 11, instead are intracellularly retained factors and subfamily 15/19, refers to as "endocrine" or "metabolic" FGFs (Lottini et al., 2023). FGFs are associated with the extracellular matrix (EM) and are shielded from protease digestion by heparan sulfates (HS), which remain bound to them even when they interact with their FGF receptors (FGFRs). This HS interaction is crucial for FGFR binding and activation (Prudovsky, 2021).

Among them, FGF2, also known as basic FGF, has four isoforms, with only the lightest being secreted, while the heavier isoforms function within the cells where they are produced. FGF2 is secreted through a distinctive ER-independent process that relies on phosphatidylinositol 4,5-bisphosphate (PIP_2) on the inner plasma membrane leaflet and HS on the outer leaflet where it binds. FGF2 exhibits greater stability than FGF1 (Schäfer et al., 2004).

FGF activity is regulated through various mechanisms, including sequestration of secreted FGF on the EM, modulation of FGFR production, splice variants, and FGFs themselves. When FGFs

bind to FGFRs on the cell surface, trimeric complexes form involving HS, FGF, and FGFR. These complexes are then internalized. Within the cytoplasm, FGFRs tyrosine kinase domains autophosphorylate, recruiting cellular cofactors. Subsequent phosphorylation can activate four pathways:

- Phospholipase Cγ (PLCγ) pathway: PLCγ binds to the phosphorylated Y766. When activated, PLCγ degrades PIP_2 in lipid vesicles, generating two second messengers: inositol 1,4,5-trisphosphate (IP_3), which triggers calcium ion (Ca^{2+}) release from ER, and diacylglycerol (DAG), which activates protein kinase C (PKC) on the membrane.
- STAT pathway: STAT-1, -3, and -5 transcription factors translocate to the nucleus. STAT proteins play crucial roles in cytokine responses, inflammation, and cancer progression. STAT1 is anti-apoptotic and has tumor-suppressing and potentially antiviral activities.
- MAPK/ERK (Mitogen-Activated Protein Kinase/Extracellular Signal-Regulated Kinase) pathway: Activation of the Ras-Raf-MEK-ERK pathway occurs, with FRS2α serving as a key docking protein that is constitutively associated with the intracellular domain of FGFR. Once activated, FRS2α can associate with other proteins, initiating a kinase cascade involving serine/threonine kinases such as AR-AF/BRAF/CRAF, MEK1/2, and ERK1/2.
- PI3K (phosphoinositide 3-kinase)-Akt signaling pathway: Activation of this pathway occurs when FRS2α associates with the GAB1 protein. This pathway plays a role in cell survival, growth, and proliferation (Figure 7)

FGFs play crucial roles in tissue development, especially during fetal organogenesis, and are essential for tissue repair in response to injury in adults. Additionally, FGFs are significant players in tumorigenesis, making them a focus of anti-cancer research. They also play roles in

responding to infections, both in repairing cytopathic effects and triggering immune responses (Ornitz & Itoh, 2015).

Most viruses have evolved strategies to stimulate cell metabolism as they require an active cellular environment for replication. As a result, FGFs may have a vital role in viral replication. Interestingly, insect viruses heavily rely on FGF, even carrying their own *FGF* (*vFGF*) gene, which is expressed during viral replication and allows arboviruses dissemination within their arthropod vectors (Means & Passarelli, 2010).

Recently, FGF2 was found to be dramatically upregulated in ZIKV-infected Sertoli cells (Kumar et al., 2018). Moreover, Limonta et al. have revealed that ZIKV infection in human fetal astrocytes (HFAs), the most abundant cell type in the brain, leads to a substantial increase in the expression and secretion of FGF2. FGF2 expression has been shown to enhance ZIKV replication and dissemination in HFAs and fetal brain explants. The pro-viral effect of FGF2 is partly mediated by suppressing the IFN response. Therefore, it is hypothesized that ZIKV replication in HFAs is supported by the presence of FGF2, contributing to the emergence of neurodevelopmental disorders associated with *in utero* ZIKV infection. Blocking FGF2 and its downstream signaling significantly inhibited ZIKV replication in HFAs and fetal brain explants, confirming a correlation between ZIKV infection and FGF2 (Limonta et al., 2019).

Moreover, the ZIKV African strain exhibited a lower capacity to stimulate the release of FGF2 compared to the more pathogenic Asian and Brazilian strains (Hung & Huang, 2021). This observation has led to the hypothesis that substantial changes in ZIKV may have contributed to its transition from a mild disease to a severe cause of microcephaly, with an increased ability to induce FGF release possibly playing a pivotal role. Supporting this notion, a study by Kam et al. found that individuals acutely infected with ZIKV displayed elevated serum levels of FGF2 further bolstering the proposed role of FGF in ZIKV pathogenicity (Kam et al., 2017).

These findings shed light on the intricate interactions between ZIKV and key cellular components in the developing fetal brain, emphasizing the role of FGF2 in promoting viral replication and potentially contributing to the neurological complications observed in cases of *in utero* ZIKV infection.

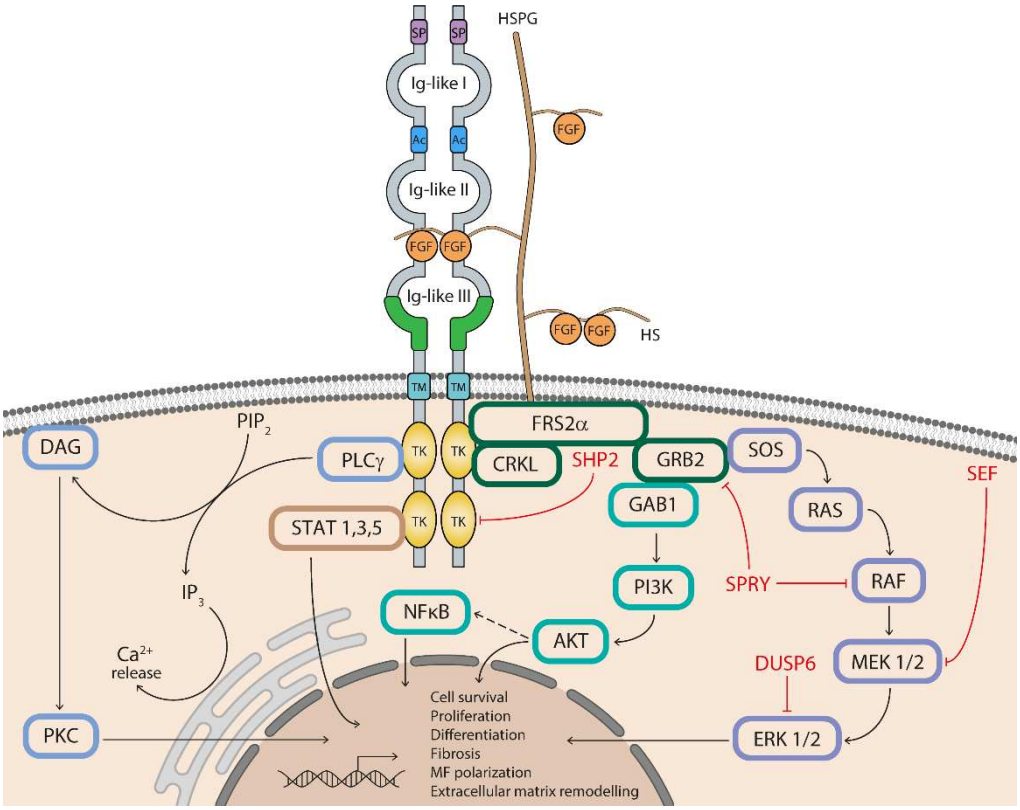

Figure 7. **FGF signaling pathways.**

FGFs signaling is initiated through the binding of FGF to FGFR-HS, which triggers receptor dimerization and phosphorylation of the FGFR intracellular TK domain. This activation leads to the engagement of four main downstream pathways: RAS-MAPK (purple), PI3K-Akt (green), PLCγ (light blue), and STAT (brown). Active PLCγ hydrolyzes PIP2, resulting in the production of DAG and IP3, which induces the release of Ca2+ and subsequent activation of PKC. In the presence of CRKL, FGFR phosphorylation facilitates the recruitment of FRS2α, a critical docking protein involved in two independent complexes: FRS2α-GRB2-SOS, activating the RAS-MAPK pathway, and FRS2α-GRB2-GAB1, activating PI3K/Akt. The activation of the NFκB transcription factor is a result of the latter two complexes. Additionally, FGFR also triggers the activation of STAT1, STAT3, and STAT5 pathways.

These diverse signaling pathways play multiple roles in cell survival, proliferation, differentiation, metabolism, fibrosis, macrophage (MF) polarization, and EM remodeling. FGFR signaling is subject to negative regulation by various proteins (highlighted in red), including SHP2, SEF, SPRY, and DUSP6 (Lottini et al., 2023).

3.6.1 Akt signaling pathway

Akt signaling pathway, also known as the PI3K-Akt pathway, is a signal transduction pathway that promotes survival and growth in response to extracellular signals. Key proteins involved in this pathway are PI3K and Akt. It is an intracellular signaling pathway associated with various aspects of cellular functions, playing a role in quiescence, survival, and growth under physiological conditions, as well as in pathological disorders. This pathway can be activated by various signals such as hormones, GFs, and other well-defined biochemical mechanisms that lead to Akt activation (Revathidevi & Munirajan, 2019).

Among the GFs that activate the signaling cascade involving Akt, FGFs are prominent. FGF binds to the receptor, and its signaling pathway branches out to the MAPK pathway or the PI3K pathway to phosphorylate Akt (Regad et al., 2007). Akt is synthesized in the cytosol in an inactive state, and under the influence of insulin, it translocates to the plasma membrane where it is phosphorylated to form pAkt (Gray & Coster, 2016). PI3K plays an essential role in Akt translocation to the membrane due to Akt high affinity for phosphatidylinositol trisphosphate (PIP_3). The interaction between Akt and PIP_3 results in conformational changes in Akt and the exposure of phosphorylation sites on T308 in the kinase domain and S473 in the C-terminal domain (Abeyrathna & Su, 2015). Akt is partially activated following T308 phosphorylation by pyruvate dehydrogenase 1 (PDK1) (phosphoinositide-dependent). Complete activation is achieved through S473 phosphorylation, which can be catalyzed by various proteins, including PDK2, integrin-linked kinase, mammalian target of rapamycin complex (mTORC), and DNA-dependent protein kinase (DNA-PK). After stimulation, PIP_3 levels decrease, and Akt activity is attenuated by dephosphorylation by serine or threonine phosphatases. PTEN (Phosphatase

and tensin homolog) acts as a tumor suppressor within this pathway. It plays a crucial role in negative regulation by removing the 3-phosphate group from PIP_3, effectively converting it back into PIP_2. Loss of PTEN function results in the over-activation of Akt, which, in turn, is associated with uncontrolled cell proliferation, reduced apoptosis, and heightened tumor angiogenesis (Figure 8) (Phin et al., 2013).

Akt can also be activated through a PI3K-independent pathway. This pathway, dependent on GFs, inflammation, DNA damage, heat shock, hypoxia, and oxidative stress, comes into play when PI3K activity is inhibited. Other studies demonstrate that Akt can be activated in response to heat shock or an increase in calcium ions (West et al., 2002).

Intriguingly, it has been demonstrated that ZIKV NS4A and NS4B play a role in inhibiting the Akt-mTOR signaling pathway, which, through phosphorylation events and other molecular processes, leads to the induction of autophagy, known to enhance virus replication, and impedes neurogenesis (Chiramel & Best, 2018; Liang et al., 2016). According to Liang et al., ZIKV NS4A and NS4B initiate a significant suppression of phosphorylation on T308 and S473 of Akt, subsequently reducing phosphorylation on S2448 of mTOR, thus initiating the autophagic process (Liang et al., 2016). This intricate interplay between ZIKV and the cellular autophagy machinery highlights the virus's ability to manipulate host cell processes to promote its own replication and pathogenesis.

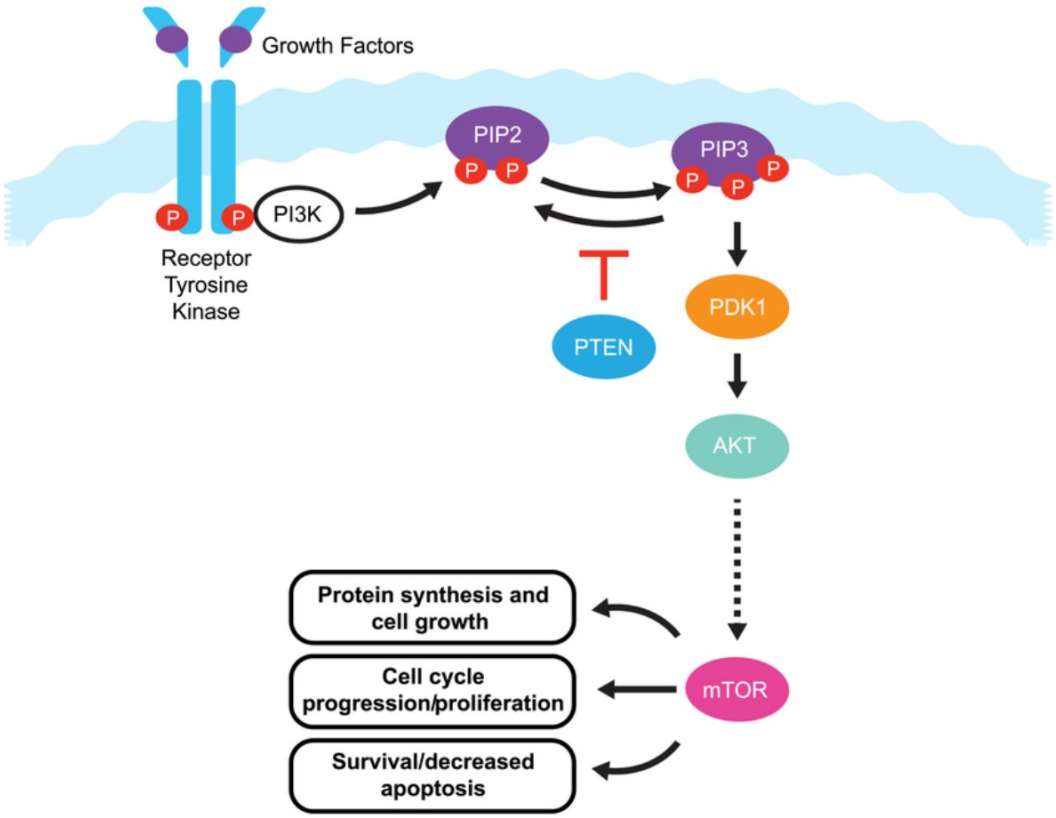

Figure 8. **PI3K/PTEN/Akt signaling pathway.**

When GFs bind to receptor tyrosine kinases, it triggers the activation of the receptor complex. This, in turn, recruits and activates PI3K. Once activated, PI3K converts PIP2 into PIP3. PIP3 then serves as a mediator for the phosphorylation of Akt by PDK1. Phosphorylated Akt, in its active form, exerts its influence on a wide range of substrates within the cell. Notably, one of its pivotal targets is mTOR, a protein intimately involved in processes like cell growth, proliferation, and cell survival. PTEN, converting PIP3 back into PIP2, is a negative regulator of Akt pathway (Phin et al., 2013).

4 AIM OF THE DISSERTATION WORK

The mechanistic link between ZIKV infection during pregnancy and subsequent congenital cortical anomalies, including microcephaly, remain relatively unexplored. This dissertation aims to assess the impact of ZIKV infection on the transcription factor FOXG1. We questioned whether this transcription factor, which is essential for proper telencephalic development, undergoes dysregulation following ZIKV infection. Observations regarding FOXG1 levels and localization in the presence or absence of ZIKV could highlight a correlation between the subcellular localization of FOXG1 and ZIKV infection. Changes in localization, following ZIKV infection, might suggest a potential loss of function of the transcription factor, which acts primarily within the nucleus.

To investigate this, we transfected A549 cells with plasmids encoding Foxg1 fused with GFP and, using confocal microscopy, analyzed the levels of nuclear and cytoplasmic fluorescence in the absence and presence of ZIKV infection. Then we asked if the dysregulation of Foxg1 in response to ZIKV was specific to this virus. To address this, we compared the results obtained after ZIKV infection with those obtained after infection with a virus of the same genus as ZIKV such as USUV and another arbovirus with ssRNA+ genome, not belonging to the genus *Flavivirus*, such as CHIKV. We also assessed the effect of ZIKV infection on cells expressing FOXG1 endogenously, such as hiPS-NPCs, confirming a reduction in FOXG1 expression and its translocation from the nuclear compartment to the cytoplasm, following ZIKV infection. By using hiPS-NPCs, we were also able to evaluate the impact of ZIKV on other transcription factors involved in neuronal differentiation, such as SOX1 and SOX2 and on FOXG1 downstream genes. We indeed hypothesized that, following the relocation of FOXG1 from the nucleus to cytoplasm, its transcription factor activity might be compromised, leading to the dysregulation of these genes, involved in cell replication and apoptosis, that are targeted by FOXG1.

Phosphorylation at T226 induced by Akt is known to lead to the nuclear export of FOXG1 transcription factor (Regad et al., 2007). Therefore, we investigated whether modifications at T271, also phosphorylated by Akt, might affect the nuclear exit of FOXG1. This could suggest that changes in cellular levels of pAkt/Akt, possibly stimulated by ZIKV infection, influence the nuclear translocation of the transcription factor. We conducted WB analyses of pAkt/Akt and PTEN levels in the presence or absence of ZIKV infection. To explore the additional FOXG1 regions, apart from T271, that played a role in nuclear translocation in response to ZIKV, we generated sequential deletions of Foxg1-GFP and FOXG1-GFP fusion constructs at both its N- and C-termini. Later, we found in the literature that FOXG1 possesses a cleavage sequence for the ZIKV NS2B-NS3 protease (Morazzani et al., 2019). We transfected A549 cells with Foxg1-GFP and NS2B-NS3 plasmids to assess whether the protease could impact the localization of FOXG1 and potentially lead to its degradation. Finally, we evaluated the role of GFs because we learned from literature that ZIKV infection is associated with FGF2 and that FGF2 levels are associated with severe microcephaly (Kam et al., 2017; Limonta et al., 2019). To study the role of FGF2 in our model, we infected A549 with ZIKV and measured FGF2 secreted. Conversely, we treated A549 with FGF2 and evaluated its impact on both ZIKV infection and FOXG1 expression and localization. Surprisingly we found that ZIKV infection on FOXG1 is modulated by the presence of GFs.

Altogether, the results obtained from these analyses could contribute to understanding the mechanisms involved in the development of microcephaly following congenital ZIKV infection and highlight a possible correlation between ZIKV infection, changes in FOXG1 transcription factor behavior, and the onset of microcephaly.

5 MATERIAL AND METHODS

5.1 Cell culture

5.1.1 A549 cells maintenance

A549 are alveolar epithelial cells derived from a human adenocarcinoma and were developed as a cell line by Giard in 1972 (Giard et al., 1973). A549 cells are suitable for our research because are permissive to ZIKV. The cells are grown in Dulbecco's Modified Eagle Medium (DMEM) High Glucose (4.5 g/L glucose) with 1 mM L-glutamine. In culture, the cells were maintained with 10% Fetal Bovine Serum (FBS, Sigma, #F7524). No antibiotics were added. Once they reached confluence, the cells were detached and split at dilutions ranging from 1:10 to 1:5. All the cells were routinely tested for mycoplasma (Lai et al., 2022).

5.1.2 hiPS-NPC maintenance and derivation

We derived neural progenitor cells from hiPSCs, as previously reported (Sousa et al., 2017). Briefly, hiPSCs were dissociated into single cells in StemFlex medium (Thermo Fisher Scientific; #A3349201)) in Matrigel coated dishes containing 10 μM Y-27632, until confluent. Then, we performed the dual SMAD inhibition protocol changing the StemFlex medium with a neural induction medium (1:1 Dulbecco's minimum essential medium/F12 (DMEM/F12) (Gibco #11330-032) and Neurobasal medium (Gibco #21103-049) with addition of B27 supplement (1:50, Gibco, #175040-44), N2 supplement (1:100, Gibco, #17502-048), 20 μg/ml insulin (Sigma, #I9278), L-glutamine (1:100, Gibco, #25030-081), MEM Non-Essential Amino Acids (1:100, Gibco, #11140-050) and 2-mercaptoethanol (1:1,000, Gibco, #21985)), supplemented with 100 nM of LDN-193189 (StemCell Technologies, # 72144), 10 μM of SB-431542 (Merck, # 616464-5MG) and 2 μM of XAV939 (StemCell Technologies, # 72674). The medium was changed daily until day 11. At day 12, the cells were dissociated with Accutase

and maintained in a neural differentiation medium (Neurobasal medium (Gibco #21103-049) with addition of B27 supplement (1:50, Gibco, #175040-44), N2 supplement (1:100, Gibco, #17502-048), L-glutamine (1:100, Gibco, #25030-081), with Y-27632 (10 μM), to increase cell viability.

5.1.3 NES cells maintenance

NES cells were cultured as already reported (Dell'Anno et al., 2018; Onorati et al., 2016). Briefly, NES cells were maintained in NES medium (Dulbecco's minimum essential medium/F12 (DMEM/F12) (Gibco #11330-032) with addition of B27 supplement (1:1,000, Gibco, #175040-44), N2 supplement (1:100, Gibco, #17502-048), 20 ng/ml FGF-2 (Gibco, #13256029), 20 ng/ml EGF (Gibco, #PHG0311), 1.6 g/l glucose, 20 μg/ml insulin (Sigma, # I9278) and 5 ng/ml BDNF (Gibco, #PHC7074)) in poly-L-ornithine (0.01%, Sigma, #P4957), laminin (5 μg/ml, Invitrogen #23017-015) and fibronectin (1 μg/ml, Corning, #354008) coated dishes. In order to preserve their optimal growth and neurogenic properties, the medium should be changed every 2-3 days and the cells should be passaged 1:2-3 when they are confluent, once every 5-7 days (~0.5–1 x 105 cells/cm2).

5.1.4 HEK 293T cells maintenance

HEK 293 are human embryonic kidney cells derived from a spontaneously miscarried female fetus. This cell line was immortalized in 1973, by the integration of adenovirus 5 (Ad5) genome fragment into chromosome 19 (Graham et al., 1977). HEK 293T, in particular, are very efficiently transfectable with DNA, due to the expression of SV40 large T antigen. Indeed, transfected DNA plasmids that carry the SV40 origin of replication can efficiently replicate in HEK 293T maintaining a high copy number and increasing the amount of recombinant protein produced (Dubridge et al., 1987). The cells are maintained in DMEM High Glucose (4.5 g/L glucose) with 1 mM L-glutamine and 10% FBS (Sigma, #F7524). No antibiotics were added.

Once they reached confluence, the cells were detached and split at dilutions ranging from 1:10 to 1:5. All the cells were routinely tested for mycoplasma (Lai et al., 2022).

5.2 Viral stocks and expansion

The following viral strains were purchased from Public Health England: ZIKV Ug 1308258v, strain MP1751 (Accession number: KY288905.1), CHIKV 0704221v, and USUV 1105081v. ZIKV Br isolate Brazil/2016/INMI1 (009V-00880) was supplied by the National Institute for Infectious Diseases L. Spallanzani IRCCS. All viruses were expanded on VERO E6 cells and titrated as plaque-forming units.

For expansion, VERO E6 cells were used, as these cells are permissive for ZIKV replication. Cells were plated in T75 flasks, and once they reached 60% confluence, were infected with 150 µl of virus (stock) diluted in 1 ml of DMEM High Glucose supplied with 2% FBS and incubated at 37°C with 5% CO_2 for 1:30 h. After the incubation period, DMEM High Glucose medium containing 2% FBS was added to reach a total volume of 15 ml and flask was incubated for 4 days. After 4 days, the flask was frozen at -80°C and then, was rapidly thawed. The medium was collected in a vial, then centrifuged at 700 *g* for 10 min. Finally, the supernatant was collected, aliquoted, and frozen at -80°C until further use as stock.

5.3 DNA constructs

All the constructs used in the study have been mostly generated by standard PCR strategy or by digestion with restriction enzymes (Figures 18A-18I). Plasmid constructs containing the cDNA coding for the whole mouse Foxg1 fused to GFP (Foxg1-GFP WT (wild type)) and 234-391-GFP fragments were previously described (Pancrazi et al., 2015).

Mouse Foxg1 aa 1-171 cDNA was amplified by PCR using GFP-Foxg1 WT as DNA template and a forward primer incorporating the XhoI restriction site that occurs in the Foxg1 cDNA.

Forward primer: 5'-ACTCGAGCATGCTGGACATGGGAGATAGG-3'. The reverse primer was 5'-GGATCCCCATGTATTAAAGGGTTGGAAG-3', incorporating a BamHI restriction site. The amplification product was purified and cleaved with XhoI/BamHI and ligated to the corresponding restriction sites in the vector pEGFP-N1 (Clontech, USA).

Foxg1-T271D-GFP (phospho-mimetic T271-ACG were changed in Asp-GAC) and Foxg1-T271A-GFP (phospho-defective T271-ACG were changed in Ala-GCG) were purchased at IDT, Belgium.

Mouse Foxg1 aa 315-489 cDNA was amplified by PCR using GFP-Foxg1 as DNA template. The forward primer was 5'-GGTACCAATGAGCACTTTGAGTTACAACGG-3', incorporating a KpnI restriction site and a start codon before the codon coding for aa 315. The reverse primer was 5'-GGATCCCCATGTATTAAAGGGTTGGAAG-3', incorporating a BamHI restriction site. The amplification product was purified and cleaved with KpnI/BamHI and ligated to the corresponding restriction sites in the vector pEGFP-N1 (Clontech, USA).

The GFP-Foxg1 aa 428-481 construct was generated digesting Foxg1-GFP with SmaI and BamHI. The excised fragment was cloned in frame into the corresponding restriction sites of pEGFP-C2 (Clontech, USA).

Plasmids encoding for human FOXG1 fused to GFP to the C-termini (FOXG1-GFP WT) was purchased from Origene (Cat: RG207964).

FOXG1-No tag was generated digesting human FOXG1-GFP with NotI (blunt) and EcoRI, creating a stop codon before GFP. The excised fragment, containing human FOXG1 with 3 modified aa to the C-termini, was blunted with SI Nuclease (ThermoFisher). Also, pcDNA3.1(-) (Clontech, USA) vector was digested with AflII and EcoRI and then blunted. Then, fragment and linearized vector were digested with EcoRI and ligated.

Constructs encoding for the N- and C- parts of FOXG1 (1–280 and 280–481 respectively), were purchased at IDT, Belgium. N-FOXG1-GFP and C-FOXG1-GFP were generated digesting

respectively N-FOXG1 and C-FOXG1 with BamHI and XhoI. Also, FOXG1-GFP WT (cat. RG207964) was digested with BamHI and XhoI and purified as empty linear vector. Both excised FOXG1 fragment were ligated to vector RG207964, to the corresponding restriction site.

Plasmid encoding ZIKV protease (NS2B-NS3) was developed by Lei et al. (Lei et al., 2016). It consists of 47 residues (49-95) of NS2B and 170 residues (1-170) of NS3pro, according to the genome sequence of the Brazilian isolate BeH923339 (GenBank: KU729217.2). The NS2B and NS3 chains are connected by a Gly4-Ser-Gly4 linker. To stabilize the construct against autoproteolytic cleavage, Arg95 of NS2B was replaced by Ala and Arg29 of NS3 was replaced by Gly. In addition, cysteine residues 80 and 143 of NS3 were replaced by serine, to avoid the formation of intermolecular disulfide bonds. The construct, that was amplified by PCR and digested with NdeI and XhoI for ligation with the pET-15b vector (Novagen), was, then, digested again with NdeI and XhoI and ligated to the corresponding restriction sites in the vector pcDNA3.1(-) (Clontech, USA).

FOXG1-pLENTI was amplified by PCR using FOXG1-GFP WT as DNA template. The forward primer, incorporating the SpeI restriction site, was 5'-TGCTTAACTAGTTTAATGTATTAAAGGGTTGGAAGAA-3' and the reverse primer was 5'-TAAGCATCTAGAATGCTGGACATGGGAGATAGGA-3', incorporating a XbaI restriction site, that occurs both in FOXG1 cDNA. T. The amplification product was purified and cleaved with XbaI and SpeI. Also, plasmid pLENTI-Ace2-Puro (Addgene, #155295) was cleaved with XbaI/SpeI and purified as empty linear pLENTI vector. FOXG1 fragment was then ligated to the corresponding restriction sites in the vector.

pLenti-FOXG1-mGFP-Puro (RC207964L4) was purchased at Origene. psPAX2 (#12260), pMD2.G (#12259) and pET11d_Rev (#119322), for PLVs assembly were purchased at Addgene.

5.4 Transfection

Transfection is a process that allows the introduction of exogenous nucleic acids into eukaryotic cells with the aim of genetically modifying cells. To perform immunofluorescence (IF) staining and confocal imaging A549 cells (about 40,000) were plated at 70% confluence onto Lab-Tek chamber slides. The next day, 500 ng of the relevant plasmid DNA was diluted in 50 µl of Opti-MEM™ (Reduced Serum Media, GIBCO) and was mixed with 1 µL of Lipofectamine (2,000) (11668-027, Invitrogen,) also diluted in 50 µl of Opti-MEM™. Following the manufacturer's instructions, the transfection mix was incubated 15 min, to let liposomes containing the plasmid DNA to form in suspension. After the incubation period, 100 µl of DNA + Lipofectamine reaction mixture was added by gently dripping it into each well and then the wells were returned to the incubator at 37°C with 5% CO_2, O/N.

Instead, to perform WB analysis, about 200,000 A549 (70% confluence) were plated onto 6-well plates. The following day 5 µg of the relevant plasmid DNA was diluted in 500 µl of Opti-MEM™ and was mixed with 5 ml of Lipofectamine (2,000) (11668-027, Invitrogen) also diluted in 500 µl of Opti-MEM™. Transfection mix was incubated and added to cells as previously described.

Poly(I:C) (P0913, Sigma) transfection is performed with some changes in protocol. Poly(I:C) is an immunostimulant that mimics double-stranded RNA and because of its toxicity, transfection is performed using a final concentration of 200 ng/ml. Moreover, transfection mixture that was added to cells, was replaced with fresh medium after 6h of incubation.

5.5 Infection

Infection of A549 was performed 24h post-transfection or transduction. Cells were infected with 1 Multiplicity of infection (MOI) of ZIKV, USUV and CHIKV that were diluted in a final volume of 150 µl of DMEM High Glucose without FBS when infection were performed onto

chamber slides and 500 µl of DMEM High Glucose when cells were plated on 6-well plates. After 1:30 h of adsorption at 37 °C, 5% CO_2, the virus diluted in DMEM High Glucose was removed and replaced with DMEM High Glucose supplemented with 2% FBS.

hiPS-NPC and NES cells were infected following differentiation. Viruses were diluted at 1 MOI in DMEM F12 without FBS and incubated, to allow adsorption for 1:30 h in the incubator at 37 °C, 5% CO_2. Once removed the inoculum, hiPS-NPC and NES cells were maintained with one-half conditioning medium and one-half fresh medium for hiPS-NPCs and NES cells.

5.6 PLVs production and transduction

PLVs consist of lentiviral replication defective vectors, bearing glycoproteins derived from other enveloped viruses and delivering a transgene of interest, as FOXG1, to transiently expression in permissive cells. For PLVs production, $4*10^6$ HEK 293T cells were seeded in T-75 flask, so that they will be confluent at 70% the next day. To perform cell transfection were prepared two different mixtures following and scaling-up Carnell et al. protocol:

1. 650 µl of Opti-MEM™ containing 5.2 µg of FOXG1-pLENTI plasmid, 3.2 µg of packaging plasmid (psPAX2), 2.8 µg of envelope plasmid expressing VSV-G (pMD2.G) and 2.4 µg of pET11d_Rev.
2. 650 µl of Opti-MEM™ containing 140 µl of PEI branched 41.2 µM (408727, Sigma).

First mixture was added to the second one, and incubated for 20 min, RT, following briefly vortexing (Carnell et al., 2017). Then, reaction mixture was added by gently dripping it into flask, that returned to the incubator at 37°C with 5% CO_2, O/N. Supernatant of transfected cells, containing packaged PLVs, were collected after 72 h and centrifuged for 15 min at 800 *g*. Supernatant was collected and added with a final concentration of sterile 50 mM Tris-HCl, pH=7,5 in order to store it to -80°C.

PLVs can be used to transiently express FoxG1 in A549, following transduction. 200,000 A549 cells were seeded at 70% confluence in 6-well plate. The following day PLVs were quickly thawed at 37°C and added with a final concentration of 10 µg/ml of polybrene (TR-1003, Sigma). Then, cells exhausted medium was replaced with 1,4 ml of PLVs and plate was centrifuged for 1 h at 1800 *g* and 37°C to allow PLVs transduction. Following "spinoculation" cells supernatant was removed and replaced with fresh DMEM High Glucose, supplied with 2% FBS. Cells were incubated at least 24 h to express FoxG1.

5.7 Immunofluorescence

Cultured cells were fixed in 4% Paraformaldehyde for 12 min at RT (Room Temperature). After two washes of 3 min with PBS-Triton X-100 (PBSX) (0.1% (vol/vol) Triton X-100 in PBS Ca^{2+}/Mg^{2+} 1X) cells were permeabilized for 10 min with permeabilization solution (0.5% (vol/vol) Triton X-100 in PBS Ca^{2+}/Mg^{2+}1X) and blocked for 1 h with blocking solution (3% BSA (Bovine Serum Albumin, Sigma, #A3059), 0.3% (vol/vol) Triton X-100 in PBS Ca^{2+}/Mg^{2+}1X). Cells were incubated with primary antibodies, diluted in antibody solution (3% BSA, 0.2% (vol/vol) Triton X-100 in PBS Ca^{2+}/Mg^{2+}1X) at 4°C O/N:

- Flavivirus NS1 protein (ab214337, (D/2/D6/B7) clone, Abcam, 1:400)
- FoxG1 (ab214337, Abcam, 1:500)
- Zika virus NS3 protein (GTX133309, Genetex 1:1,000)
- Zika virus Capsid protein (GTX133317, Genetex 1:1,000)
- Zika virus NS2B protein (GTX133318, Genetex 1:1,000)
- Chikungunya virus native protein (MA5-18181, A54Q clone, Invitrogen, 1:50)
- Usutu virus native protein (MA5-18281, F50F clone, Invitrogen, 1:50)
- SOX2 (ab5603, Millipore, 1:400),
- Tubulin (mca77g, Bio-Rad, 1:500)

- SOX1 (4194, Cell signaling, 1:200)
- pHH3 (06-570, Millipore, 1:500)
- cleaved CASP3 (ab3623, Millipore, 1:200)

The next day, cells were washed with PBSX three times for 3 min and then incubated for 1 h at RT with Alexa Fluor® secondary antibodies (Goat anti-mouse Alexa Fluor 568 (Thermo Fisher Scientific A11031, 1:1,000), Goat anti-rabbit Alexa Fluor 647 (Thermo Fisher Scientific A21245, 1:1,000), Goat anti-rabbit Alexa Fluor 488 (Thermo Fisher Scientific A11008, 1:1,000)) and DAPI (D1306, Invitrogen, 1 µg/ml) diluted in antibody solution. After two washes of 3 min with PBSX and one wash of 3 min with PBS Ca^{2+}/Mg^{2+}, the fixed cells were mounted on microscope slides to perform confocal analysis. All images were acquired using a laser scanning confocal microscope (Nikon, Eclipse Ti), a laser scanning confocal microscope Zeiss LSM 9.10 (Carl Zeiss) or Operetta CLS high-content imaging device (PerkinElmer, Hamburg, Germany).

5.8 Measurement of the nuclear-cytoplasmatic percentage of fluorescence

Using ImageJ software (https://imagej.nih.gov/ij/), a ROI (Region Of Interest) was drawn to select the nucleus and the total cell area (cytoplasm and nucleus) of each cell and to measure the intensity of fluorescence in each selection in the channel of interest. Moreover, one small circle was selected out of each cell to measure the background fluorescence. The following parameters were measured:

- ROI Area: the number of pixels into the ROI
- Mean Gray Value: $\frac{\sum \text{gray intensity of pixels into the ROI}}{\text{number of pixels into the ROI}}$
- Integrated Density: $ROI\ Area \times Mean\ Gray\ Value$

Then, the Corrected Total Cellular Fluorescence (CTCF) was calculated:

- $CTCF_{\text{total}} = IntDen_{\text{total}} - (ROI\ Area_{\text{total}} \times Mean\ Gray\ Value_{\text{background}})$
- $CTCF_{\text{nuclear}} = IntDen_{\text{nuclear}} - (ROI\ Area_{\text{nuclear}} \times Mean\ Gray\ Value_{\text{background}})$
- $Nuclear\ fluorescence\ \% = \frac{\text{CTCF}nuclear}{\text{CTCF}total} \times 100$

Once obtained these values, the target marker nuclear fluorescence of mock and infected cells was compared.

5.9 Measurement of infection percentage

Percentage of infection showed in section 6.3 and 6.13 was analyzed with Harmony 4.6 software (PerkinElmer Hamburg, Germany). We used the following building blocks: Find Nuclei > Find Cytoplasm > Calculate intensity properties (ZIKV C - Alexa 647) > Select population: Infected cells > Define results:

- $Infection\ \% = \frac{N°\ of\ infected\ cells}{N°\ of\ total\ cells} \times 100$

Percentage of FOXG1 positive cells showed in section 6.3 was analyzed with Harmony 4.6 software (PerkinElmer Hamburg, Germany). We used the following building blocks: Find Nuclei > Find Cytoplasm > Calculate intensity properties (FOXG1 - Alexa 488) > Select population: FOXG1 positive cells > Define results:

- $FOXG1\ \% = \frac{N°\ of\ FOXG1\ positive\ cells}{N°\ of\ total\ cells} \times 100$

About 45 fields were analyzed per well using 40× water objective, as previously described (Lai et al., 2021).

5.10 Reverse-Transcriptase quantitative PCR

To perform RT-qPCR total RNA was extracted with QIAzol Lysis Reagent (QIAGEN, Hilden, Germany) according to the manufacturer's instructions. Total RNA (200 ng) was reverse-transcribed in cDNA and amplified by using QuantiNova SYBR Green RT-PCR kit (QIAGEN®, Hilden, Germany) following the manufacturer's protocol. The forward and reverse primers were:

- 5'-TGGACGCAGACCTTGAGAAC-3' and 5'-GGGCACCTTTACTACGAATGC-3' for *FOXG1*;
- 5'-GCGGAGGAGAACAAACAGATC-3' and 5'-GAGGGCGGATTGGAAATGAAC-3' for *CCND1*;
- 5'-CTCTCAGGGTCGAAAACGGC-3' and 5'-GCGGATTAGGGCTTCCTCTTG-3' for *CDKN1A*;
- 5'-CGCAGGAATAAGGAAGCGACC-3' and 5'-GGCATTTGGGGAACCGTCTG-3' for *CDKN1B*;
- 5'-TGAGTTCCCTCAGCCGTTACCT-3' and 5'-GAGGTTTCCTCTGGTCCTGGTA-3' for *PTEN*;
- 5'-CTGGCTATGAAGGAAGATGGA-3' and 5'- TGCCCAGTTCGTTTCAGTG-3' for *FGF2*;
- 5'-AGCTGAACGGGAAGCTCACT-3' and 5'-AGGTCCACCACTGACACGTTG-3' for *GAPDH*.

RT-qPCR was performed in 20 µl with the following parameters: an activation step of 95°C for 10 min, followed by 40 cycles of 95°C for 10 sec, 60°C for 15 sec, and 72°C for 15 sec, and a melt curve step of 95°C for 15 sec, 60°C for 1 min, and 95°C for 15 sec. The generation of specific PCR products was confirmed by melting curve analysis. The data were analyzed using the $2^{-\Delta\Delta Ct}$ method with all samples normalized to GAPDH and mock condition.

5.11 Protein extraction and subcellular fractionation

Cells were lysed in ice, following ice-cold PBS washing, with RIPA buffer 10x (Sigma, #20-188), protease inhibitor (Pierce Protease Inhibitor Tablet, Thermo Scientific, #A32963), and phosphatase inhibitor 10x (Phosphatase Inhibitor Cocktail 3, Sigma, #P0044).

For subcellular fractionation cells were washed once with ice-cold PBS and then incubated on ice for 5 min in 200 µl buffer A (10 mM Tris-Cl, pH 7.5, 3 mM MgCl2, 10 mM KCl, 0.1 mM EDTA, 0.5% NP40 and protease inhibitor cocktail). Cells were centrifuged at 600 *g* at 4°C for 5 min. Supernatant was collected and used as the cytosolic fraction. The pellet was washed once at 600 *g* at 4°C for 5 min with buffer A without NP40, then resuspended in 200 µl buffer C (20 mM HEPES, pH 8.0, 0.4 M NaCl, 7.5 mM MgCl2, 0.2 mM EDTA, 0.21 mM EGTA, 1 mM DTT, and protease inhibitor cocktail). Sample were incubated for 1 h at 4°C in rocking plate and resulting homogenates were centrifuged for 10 min at 16,000 *g* at 4°C. The pellet was washed once again at 16,000 *g* at 4°C and resuspended in 75 µl of dH2O. This was used as the nuclear fraction (Ma et al., 2019).

5.12 Western Blotting

Following protein cell lysis and protein extraction, samples were sonicated (50% amplitude and 10s pulse settings) with Laemmli 5x (0.175 M Tris HCl pH =6.8, 35% glycerol, 2% SDS, 5% 2-mercaptoethanol, 0.05% bromophenol blue) and boiled at 70°C for 10 min. Next, lysates were run in Mini-PROTEAN® Tetra Cell system (Bio-Rad), in hand-cast 12% Acrylamide/Bis-acrylamide gel and Running buffer, at 200V for 45 min. Following, gels were transferred on nitrocellulose membrane, 0.45 µm pore size, (GE10600002, Sigma) with Mini Trans-Blot® Module (Bio-Rad) in Transfer buffer at 350 mA for 1 h. The membrane was washed with TBST (0.05% Tween v/v in TBS) for 5 min in rocking plate at RT and incubated with Blocking solution (skim milk or BSA, 5% w/v, in TBST or PBST following primary antibody instruction)

for 1 h in rocking plate at RT, washed with TBST or PBST for 2 min in rocking plate at RT, and finally incubated with primary antibodies at 4°C O/N in rocking plate:

- FoxG1 (ab214337, Abcam, 1:1,000) in skim milk 5% w/v in PBST
- Tubulin (3873, Cell signaling, 1:8,000) in skim milk 1% w/v in PBST
- Zika virus NS3 (GTX133309, GeneTex, 1:2,000) in skim milk 5% w/v in PBST
- Zika virus NS2B (GTX133318, GeneTex 1:1,000) in skim milk 5% w/v in PBST
- Actin (A5441, Sigma, 1:2,000) in BSA 5% w/v in PBST
- Histone H3 (GTX122148, GeneTex 1:1,000) in BSA 5% w/v in TBST
- GAPDH (MA5-15738, Invitrogen, 1:2,000) in skim milk 2% w/v in PBST
- pAkt (9271S, Cell signaling, 1:1,000) in BSA 5% w/v in TBST
- Akt pan (2920S, Cell signaling, 1:2,000) in BSA 5% w/v in TBST
- PTEN (9552S, Cell signaling, 1:1,000) in BSA 5% w/v in TBST
- FGF2 (ab208687, (EPR20145-219), Abcam 1:1,000) in BSA 5% w/v in TBST
- Flavivirus NS1 protein (ab214337, (D/2/D6/B7) clone, Abcam, 1:1,000) in skim milk 5% w/v in PBST
- Chikungunya virus E1 (GTX135187, GeneTex, 1:5,000) in skim milk 5% w/v in PBST
- DDX58 (RIG-I, GTX132517, GeneTex, 1:1,000) in skim milk 5% w/v in PBST

The next day, the membrane was washed 3 times with TBST or PBST for 5 min in rocking plate at RT and incubated with secondary antibodies conjugated to peroxidase (Goat anti-Rabbit IgG, A0545, Sigma, 1:40,000 and Goat anti-Mouse IgG, A9044, Sigma, 1:80,000) diluted in antibody solution for 1h at RT in rocking plate. Finally, after 3 x 10 min-washes in TBST or PBST, the membrane was revealed using ECL substrates (#1705061 or #1705062, Bio-Rad) with Chemidoc system. Expected size of WB bands: 70 kDa for FoxG1, 69 kDa for ZIKV NS3, 50 kDa for Tubulin, 15 kDa for ZIKV NS2B, 42 kDa for Actin, 17 kDa for Histone H3, 37 kDa

for GAPDH, 60 kDa for pAkt, 60 kDa for Akt, 54 kDa for PTEN, 18,22,24 kDa for FGF2, 100 kDa for USUV NS1, 55 kDa for CHIKV E1, 100 kDa for RIG-I.

5.13 ZIKV NS2B-NS3 proteolytic assay

To assess proteolytic activity of ZIKV NS2B-NS3 towards FOXG1, A459 were seeded in 6-well plate and transduced with FOXG1-PLVs. The following day FOXG1 transiently expressing A549 were infected with 1 MOI of ZIKV Br and transfected with ZIKV NS2B-NS3 or control plasmid pcDNA3.1(-) (Clontech, USA). Next 24h cells were lysed with RIPA buffer supplemented with protease inhibitor and incubated at 37°C for 4h. Then, cell lysates were immediately put in ice and Laemmli 5x was added to perform WB.

5.14 ELISA

Supernatants from mock or infected or treated A549 were collected at indicated time points (24-96 h), and secreted FGF2 was quantified using an enzyme-linked immunosorbent assay (ELISA). 96-well plate was coated with FGF2 capture antibody (ab208687, (EPR20145-219), Abcam 1:600) diluted in 50 µl of PBS, pH=7.2, sealed with parafilm and incubated at 4°C, O/N. The next day wells were aspirated to remove capture antibody and washed 3 times with 100 µl of PBST (0.05% Tween v/v in PBS). 50 µl of blocking buffer (1% BSA w/v in PBS) were added to each well and incubated for 1 h at RT in rocking plate. FGF2 standards were prepared diluting 2-fold FGF2 (F-0291, Sigma), from 4,000 pg/ml to zero in diluent buffer (0.05% Tween v/v and 0,1% BSA v/w in PBS). After incubation period blocking was removed, samples or FGF2 standards were added to each well and incubated for 2 h at RT in rocking plate. Then, samples were aspirated, and plate was washed 3 times with 100 µl of PBS. FGF2 detection antibody conjugated with biotin (ab84027, Abcam 1:4,000), was diluted in diluent buffer and 50 µl were incubated for 1 h at RT in rocking plate. Antibody was removed and wells were

washed with PBST, 3 times. Then, 50 µl of streptavidin-HRP conjugate (RABHRP3, Sigma, 1:120) were diluted in diluent buffer and added for 45 min at RT in rocking plate. Following incubation time, solution was removed, and plate was washed 3 times with 100 µl of PBST. Finally, 50 µl of TMB liquid substrate was incubated in dark condition and when it started to color (about 10-15 min later), 50 µl of stop solution was added (#900-T00, Peprotech). The absorbance was immediately read at 450 nm using a plate reader (Varioskan™ LUX, Thermo Fisher).

5.15 FGF2 release and stimulation assays

To assess FGF2 expression and release, A549 were plated in 6-well plate at 70% confluence. The following day A549 were infected with 1 MOI of ZIKV Br, 1 MOI of USUV and 1 MOI of CHIKV, transfected with 200 ng/ml of Poly(I:C) (P0913, Sigma), transfected with a total of 5 µg of pcDNA3.1(-) (Clontech, USA) and transduced with 1.4 ml of FOXG1-PLVs. After 24 h, 48 h, 72 h and 96 h cell culture supernatant from each sample were collected to perform ELISA and cells were lysed to perform WB.

For FGF2 treatment and neutralization assays, 10,000 A549 were seeded in 96 well plates. The following day cells were:

- pretreated with different concentration of rFGF2 performing 2-fold dilution in complete medium, from 16 ng/ml to 0.25 ng/ml. Pretreated A549 were infected with 1 MOI of ZIKV Br and then treated again with the same rFGF2 concentrations already used, in DMEM High Glucose with 2% FBS;
- infected with 1 MOI of ZIKV Br and treated with 2-fold dilution (from 16 ng/ml to 0.25 ng/ml) of rFGF2 in DMEM High Glucose with 2% FBS, after the time of incubation of ZIKV Br adsorption;

- treated with 2-fold dilution of neutralizing anti-FGF2 antibody (05117, Millipore) from 16 µg/ml to 1 µg/ml, following 1 MOI ZIKV Br infection.

Cells were fixed, stained for IF imaging and analyzed using Operetta High-Content Imaging System (Perkin Elmer).

To study the role of FGF2 on FOXG1 expression, A549 were seeded in 6-well plates and then transduced with FOXG1-PLVs. The following day A549 transiently expressing FOXG1 were:

- pretreated with 15 ng/ml rFGF2 for 24 h, infected with 1 MOI of ZIKV Br or USUV and treated again with 15 ng/ml FGF2 for further 24 h;
- infected with 1 MOI of ZIKV Br or USUV and treated with 2.5 ng/ml FGF2 for 24 h;
- treated with 15 µg/ml of neutralizing anti-FGF2 antibody after infection with 1 MOI of ZIKV Br or USUV.

Cell lysates were extracted 24 h pi (post-infection) and was performed WB analysis.

5.16 Statistical analysis

Data are mean ± SD values from at least three separate experiments after blinded analyses. Differences between groups were analyzed using appropriate tests as reported for individual figures. Values of all significant correlations are given with degree of significance indicated (* $p < 0.05$, ** $p < 0.01$, *** $p < 0.001$, **** $p < 0.0001$). Total cell number for each experiment is indicated in legends. Data were analyzed with ImageJ software and plotted with GraphPad Prism 7 software.

6 RESULTS

6.1 ZIKV infection produces FOXG1 nuclear displacement.

FOXG1 is specifically associated with the development of the forebrain and, as for many transcription factors, its subcellular localization is predominantly nuclear. Mutations or alterations in the *FOXG1* gene are linked to a rare neurodevelopmental disorder called FOXG1 syndrome that affects the brain, causing severe intellectual disability, developmental delays, and a range of neurological symptoms (Florian et al., 2012). Because FOXG1 disorders and congenital ZIKV infection display common clinical traits, we first investigated the impact of ZIKV infection on FOXG1 expression.

Because of the modest dissimilarity between human and murine FoxG1 sequences we decided to take advantage of readily available murine Foxg1 constructs, shorter by only 8 aa than human (481 aa mouse vs. 489 aa human) (Kaestner et al., 2000; Pancrazi et al., 2015). We transfected murine Foxg1 fused to the GFP at its C-terminus (Foxg1-GFP) in A549, a well-accepted substrate for the infection of a large plethora of viruses, including ZIKV. 24 h later we infected A549 transiently expressing Foxg1 with 1 MOI of ZIKV Ug MP1751, Uganda strain and 24 h pi we fixed and stained cells, immunolabeling for the ZIKV NS1. We quantified the nuclear-to-total ratio of Foxg1-GFP signal and observed that Foxg1-GFP localized to the nucleus in uninfected cells, while, after ZIKV infection, it was displaced from the nuclear compartment to the cytoplasm (Figures 9A and 9B).

Next, to verify the effect of ZIKV also in endogenously expressing FOXG1 cells, we employed NPCs obtained from hiPSCs, which recapitulate early stages of human neurodevelopment after cerebro-cortical induction. We infected hiPS-NPCs with 1 MOI of ZIKV Ug and 48 h pi we performed IF analysis, labelling FOXG1 and ZIKV NS1 proteins. In uninfected hiPS-NPCs, we observed that FOXG1 was mostly localized within the nuclear compartment, as previously

reported in normal neuroprogenitors in the developing human telencephalon (Onorati et al., 2014). Conversely, ZIKV-infected hiPS-NPCs displayed FOXG1 dislocation towards the cytosol (Figures 9C and 9D).

Moreover, because ZIKV-related microcephaly was generally found in patients infected by the Brazilian strain of ZIKV (ZIKV Br) during the 2015 outbreak, we investigated whether ZIKV Br had similar effects on FOXG1 as the Uganda strain. hiPS-NPCs were infected with the Brazil/2016/INMI1 ZIKV strain that induced, 48 h and 72 h pi, significant FOXG1 displacement to the cytoplasm (Figures 9E and 9F). Moreover, in most experiments that will follow, we infected with both ZIKV strains and we observed comparable results. For this reason, from now on, experiments are performed infecting with ZIKV Br, if not otherwise stated.

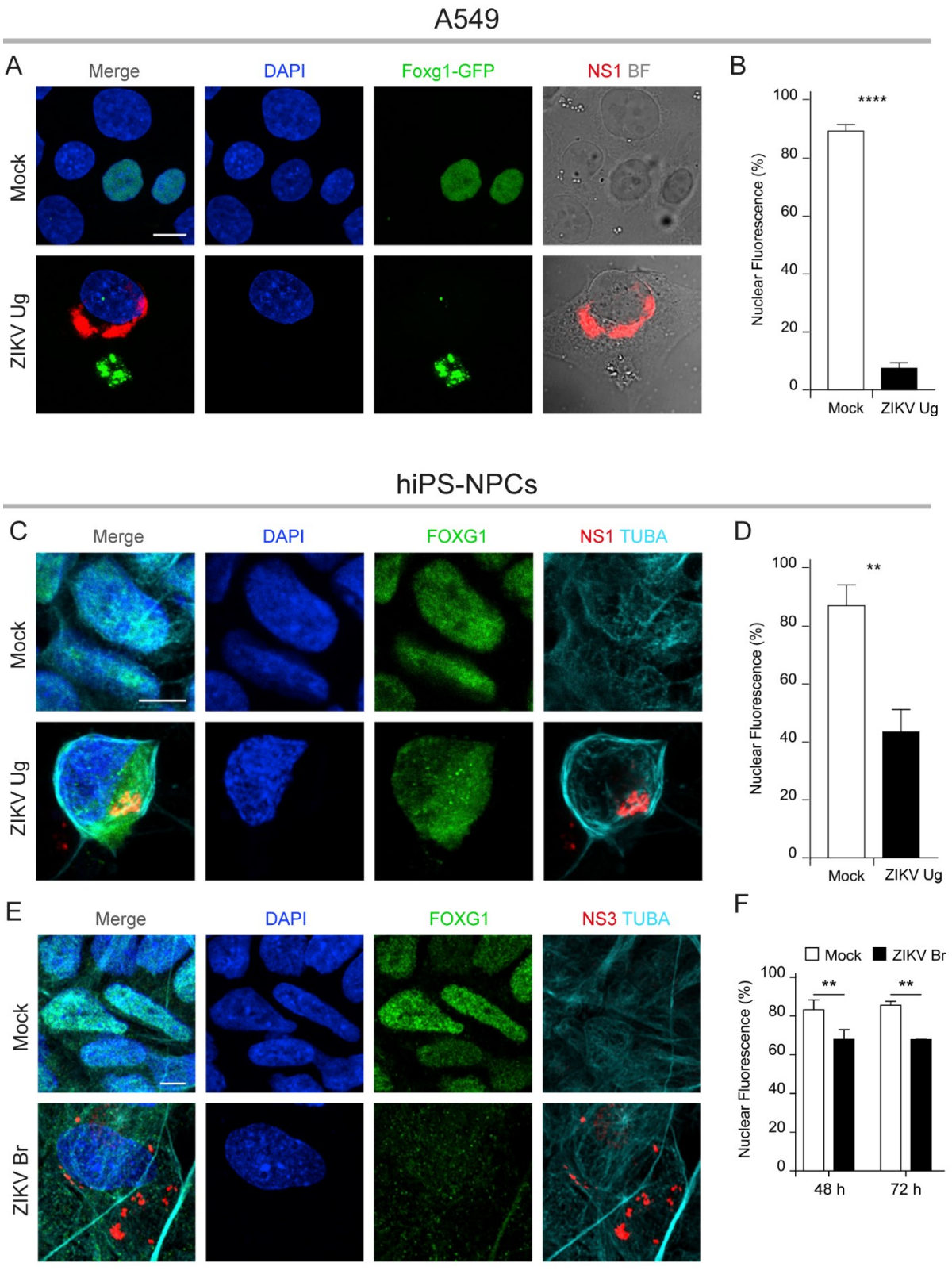

Figure 9. **Mislocalization of FOXG1 after ZIKV infection in A549 and hiPS-NPCs cells.** (A) Representative confocal images of Foxg1-GFP transfected A549 cells, mock- and infected with 1 MOI of ZIKV Ug. ZIKV NS1, DAPI and bright field (BF) are shown. Analyses were performed at 24 h pi. Scale bar, 10 µm.

(B) Bar plot indicating the ratio of Foxg1 nuclear fluorescence on total fluorescence in mock- and ZIKV Ug-infected conditions. Data are shown as mean ± SD (total cells, n = 37), $p < 0.0001$; unpaired Student's t test with Welch's correction.
(C) Representative confocal images of FOXG1, ZIKV NS1, TUBA (α-tubulin), and DAPI in hiPS-NPCs, mock- and infected with 1 MOI of ZIKV Ug. Analyses were performed at 48 h pi. Scale bar, 10 μm.
(D) Bar plot indicating the ratio of FOXG1 nuclear fluorescence on total fluorescence in mock- and ZIKV Ug-infected conditions. Data are shown as mean ± SD (total cells, n = 40), $p < 0.01$; unpaired Student's t test.
(E) Representative confocal images of FOXG1, Brazilian ZIKV (ZIKV Br) NS3, TUBA (α-tubulin), and DAPI, in hiPS-NPCs mock- and infected with 1 MOI of ZIKV Br. Analyses were performed at 48 h pi. Scale bar, 5 μm.
(F) Bar plot indicating the ratio of FOXG1 nuclear fluorescence on total fluorescence in mock- and ZIKV Br-infected conditions at 48 h and 72 h pi (total cells, n = 240), $p < 0.01$. Data are shown as mean ± SD; two-way ANOVA, post hoc Tukey's test.

6.2 ZIKV infection produces FOXG1 downregulation.

Next, we also evaluated whether ZIKV infection affected on FOXG1 protein expression, as well as its displacement to the cytoplasm. We performed WB analysis on both A549 transiently transfected with untagged human FOXG1 (Figures 10A and 10B) and hiPS-NPCs (Figures 10C and 10D), infected or not with ZIKV Br and we observed that following ZIKV Br infection we had a reduction of FOXG1 protein levels in both infected samples. Altogether, these findings show that ZIKV-induced FOXG1 reduction occurs both in hiPS-NPCs endogenously expressing FOXG1, as well as in A549 expressing exogenous FOXG1.

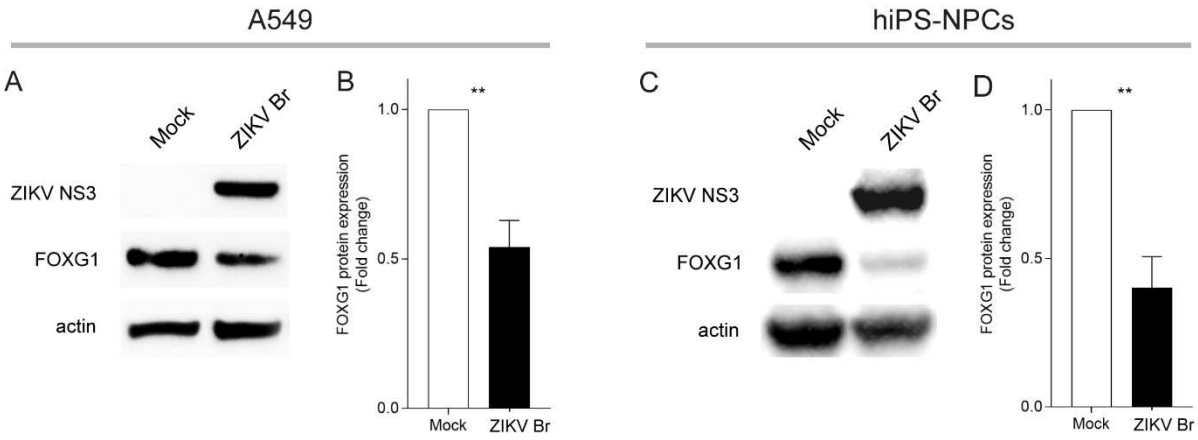

Figure 10. **Downregulation of FOXG1 after ZIKV infection in A549 and hiPS-NPCs cells.**

(A) WB analysis of A549 transiently transfected with FOXG1, mock- or infected with 1 MOI of ZIKV Br. Cell lysates are extracted 24 h pi to compare FOXG1 protein level in mock- and ZIKV Br-infected A549 transiently expressing FOXG1. Actin, as loading control, is shown in both sample and ZIKV NS3 in infected cells.

(B) Densitometric analysis of (A). Bar plot indicating fold change in FOXG1 protein expression, in mock- and ZIKV Br-infected A549 transiently expressing FOXG1, normalized to actin. Data are shown as mean ± SD. (n = 4), $p < 0.01$; unpaired Student's t test.

(C) WB analysis of hiPS-NPCs, mock- and infected with 1 MOI of ZIKV Br. 48 h pi cells are lysed to compare FOXG1 protein level in mock- and ZIKV Br-infected hiPS-NPCs, endogenously expressing FOXG1. Actin, as loading control, is shown in both samples and ZIKV NS3 in infected cells.

(D) Densitometric analysis of (C). Bar plot indicating fold change in FOXG1 protein expression, in mock- and ZIKV Br-infected hiPS-NPCs, normalized to actin. Data are shown as mean ± SD. (n = 3), $p < 0.01$; unpaired Student's t test.

6.3 Transduction improves FOXG1 transient expression in A549 and following infection.

In several experiments, we observed that, following A549 transfection with FOXG1 plasmids, we had a reduction in ZIKV infection efficiency, possibly due to type I IFN signaling activation. Indeed, there is evidence that transfection induces type I IFN activation and response, which set up an antiviral state in cells, thereby protecting them from infection (Koyama et al., 2008;

X.-L. Li et al., 1998). Moreover, we also had low transfection efficiency because, even if direct transfection results in very high FOXG1 expression in cells, this can be very non-uniform (some cells can contain many copies while others carry very few or none). In order to manage all these problems, we decided to employ PLVs with VSVG, carrying *FOXG1*. PLVs are largely used as gene-delivery vehicles because of many advantages, such as integration of carried gene into host genome, transduction of both dividing and non-dividing cells and broad tissue tropisms depending on envelope protein used for pseudotyping (Sakuma et al., 2012).

For this reason, we transfected HEK 293T cells to produce PLVs carrying FOXG1-GFP as explained in section 5.6 and, 72 h later, we collected and clarified supernatants containing PLVs. Then, we spinoculated A549 with FOXG1-GFP-PLVs, adding a final concentration of 10 µg/ml polybrene to improve transduction efficiency, and, in parallel, we transfected A549 with FoxG1-GFP as usual to compare the two transient gene-delivery systems. The next day we infected with 1 MOI of ZIKV Ug and 24 h pi we stained ZIKV C. Following A549 transduction, we obtained higher FOXG1-GFP transient expression, compared to transfection with Foxg1-GFP (Figures 11A and 11C). Moreover, we found that ZIKV infection rate is higher when A549 are transduced, compared to infection performed after transfection (Figures 11A and 11B).

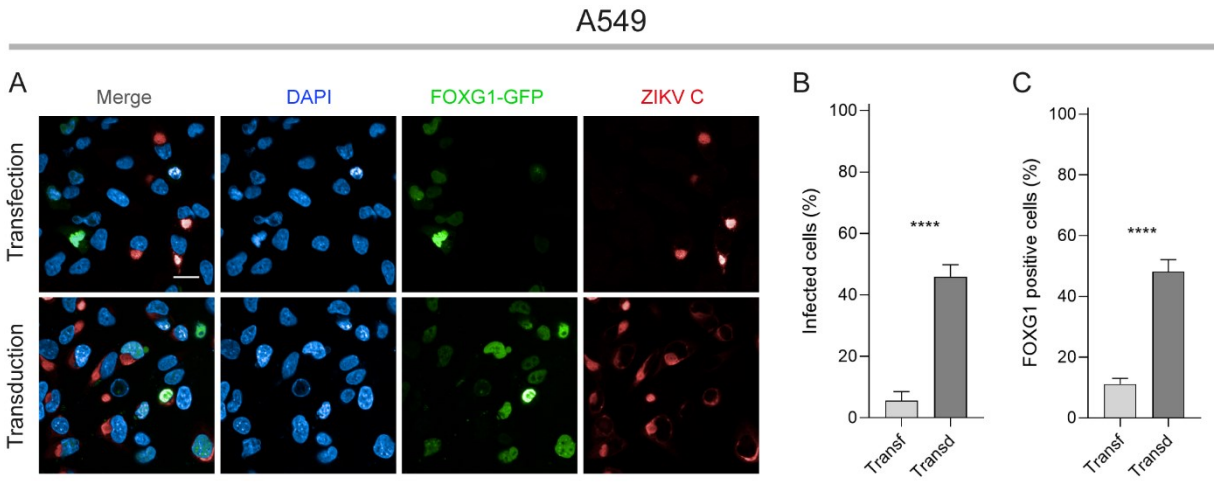

Figure 11. **FOXG1 transduction in A549 improves transgene expression.**

A) Confocal images of Foxg1-GFP-transfected and FOXG1-GFP-transduced A549 cells, both infected with 1 MOI of ZIKV Ug and fixed 24 h pi. ZIKV C, DAPI are also shown. Scale bar, 20 μm.
(B) Bar plot indicating ZIKV Ug infection efficiency expressed as percentage, in *FOXG1*-transiently transfected (Transf) or transduced (Transd) A549. Data are shown as mean ± SD (n = 9), $p < 0.0001$; unpaired Student's t test.
(C) Bar plot indicating the percentage of FOXG1 transiently expressing cells, in transfected (Transf) or transduced (Transd) A549. Data are shown as mean ± SD (n=9), $p < 0.0001$; unpaired Student's t test.

6.4 ZIKV infection affects FOXG1 expression into the nucleus.

Next, we subcloned untagged human *FOXG1* in PLV packaging plasmid pLENTI-Ace2-Puro to produce PLVs carrying untagged *FOXG1*. This way, we could transduce A549 to obtain *FOXG1* expression, avoiding transfection of *FOXG1* and the consequent innate immunity activation, possibly impinging on following infection efficiency.

To perform WB analysis, we transduced A549 with FOXG1-PLVs and the following day we infected with 1 MOI of ZIKV Br. Then, 24 h pi, to analyze FOXG1 expression following ZIKV infection in different cellular compartments, we performed subcellular fractionation following the protocol reported in section 5.11. We analyzed total, cytoplasmic, and nuclear fractions of FOXG1-transduced, ZIKV Br-infected cells by WB. To verify that we obtained separated cellular fractions, we stained for Histone H3 that is supposed to be expressed only in nuclei, and GAPDH, that instead is a cytosolic protein. The results confirmed that, in FOXG1-transduced A549, the protein is found in the total and nuclear, but not the cytoplasmic fraction. After infection, we could not observe FOXG1 protein in cytoplasmic fractions, but we did notice a reduction in both total and nuclear fractions (Figures 12A and 12B).

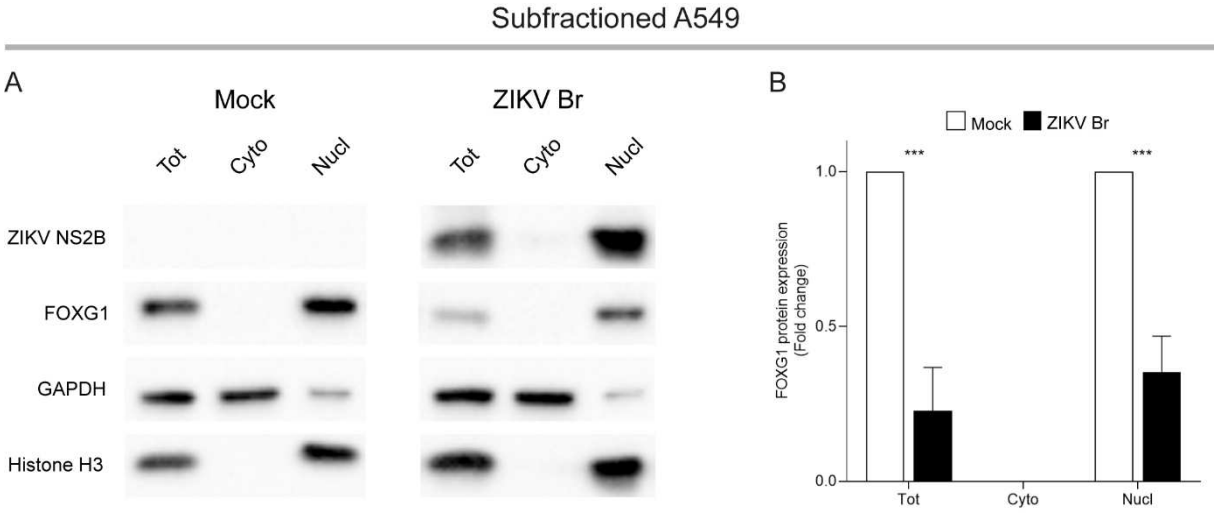

Figure 12. **Nuclear content of FOXG1 is downregulated following ZIKV infection.**
(A) WB analysis of total lysates (Tot), cytoplasmic (Cyto) and nuclear (Nucl) fractions of A549 transduced with untagged human FOXG1-PLV, comparing of FOXG1 protein expression in mock- and ZIKV Br-infected samples. ZIKV NS2B is shown to confirm infection, GAPDH as loading control of cytoplasmic fraction and histone H3 of nuclear fraction.
(B) Densitometric analysis of (A). Bar plot indicates fold change in FOXG1 protein expression normalized to histone H3. Data are shown as mean ± SD. (n = 2), $p < 0.001$; two-way ANOVA, post hoc Tukey's test.

6.5 ZIKV infection induces dysregulation in FOXG1 downstream genes and impacts on cell cycle progression and survival.

Because FOXG1 was downregulated following ZIKV infection, we analyzed how ZIKV affected *FOXG1* transcription. For this reason, we infected hiPS-NPCs with 1 MOI of ZIKV Br and we collected RNA samples at different time points. We performed RT-qPCR using primers and protocols discussed in section 5.10 and we found that there is a transcriptional reduction of FOXG1 72 h pi, but not earlier (Figure 13A).

Then, to evaluate the effects of FOXG1 displacement/reduction following ZIKV infection, we explored the kinetics of expression of several known FOXG1 target genes, focusing on cell replication and apoptosis (Cargnin et al., 2018; Kumamoto & Hanashima, 2017; Seoane et al., 2004; Zhao et al., 2021). We verified the expression of genes involved in the p53-dependent

cell-cycle arrest, including *CDKN1A* (p21) and *CDKN1B* (p27), and *CCND1* (Cyclin D1), in mock- and ZIKV Br-infected hiPS-NPCs. *CDKN1A* and *CDKN1B* were upregulated, while *CCND1* was downregulated in infected hiPS-NPCs 72 h pi (Figures 13B, 13C and 13D), implying a possibly negative effect of ZIKV on cell cycle progression, i.e. decrease in mitotic index, and activation of apoptosis, as a consequence of p53-dependent cell-cycle arrest (Xiong et al., 2020). Then we studied the kinetics of ZIKV Br-infected hiPS-NPCs by IF with phosphorylated histone H3 (pHH3), as marker of proliferation and cleaved caspase 3 (cCASP3), as marker of apoptosis. Consistently with the previous data, ZIKV infection caused significant decrease in pHH3 (Figure 13E) and substantial increase in cCASP3 (Figure 13F) 72 h pi, but not at earlier time points. Collectively, these results suggest a link between ZIKV infection, early dysregulation of FOXG1 and its target genes, FOXG1-dependent cell-cycle arrest, and apoptosis in human neural progenitors. The convergent effects result in depletion of the neural progenitor pool, possibly causing developmental alterations observed in congenital ZIKV syndrome.

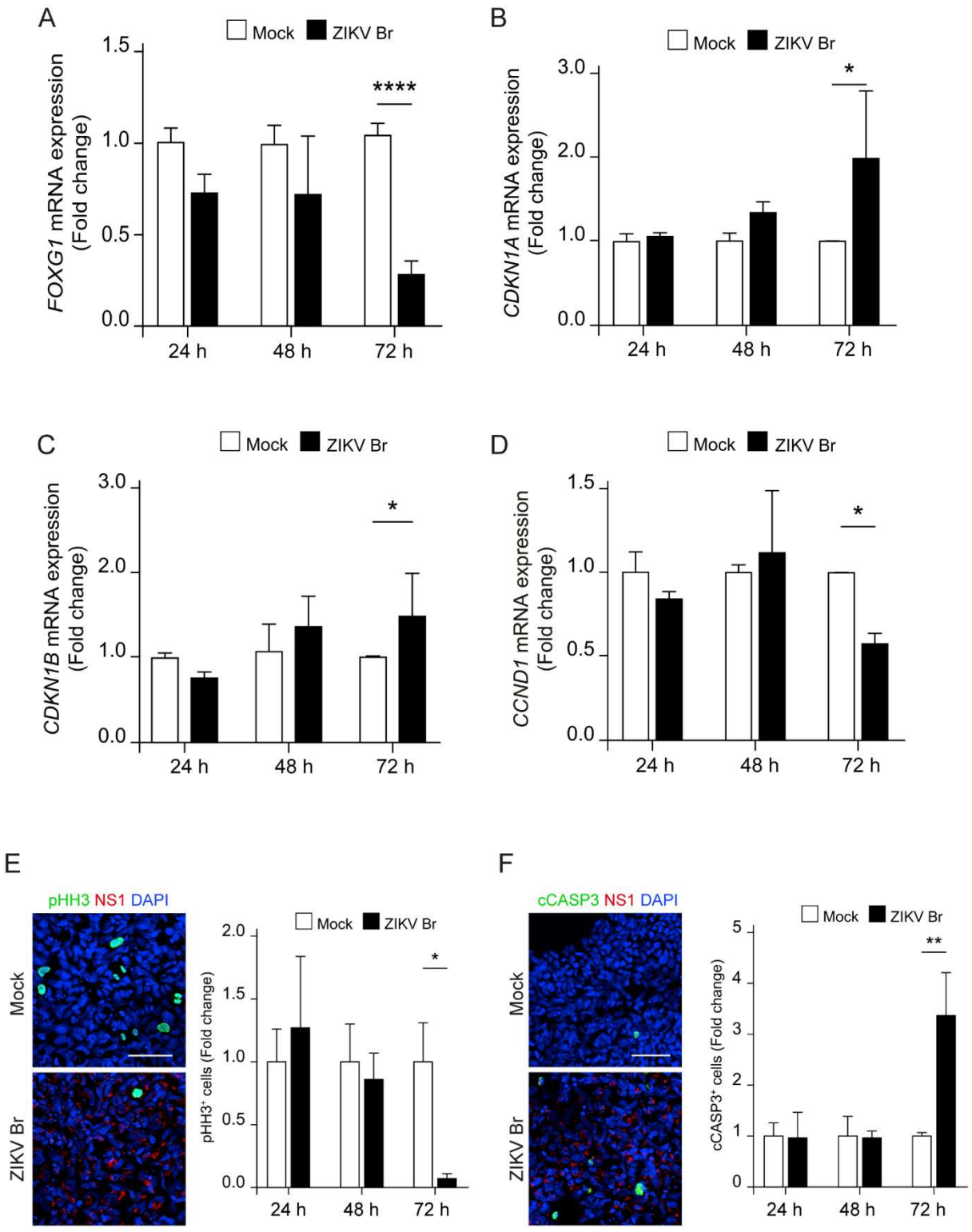

Figure 13. **ZIKV infection induces dysregulation in FOXG1 downstream genes affecting cell cycle progression and survival.**

Bar plot indicating fold change in (A) *FOXG1* (n = 3), $p < 0.0001$; (B) *CDKN1A* (n = 3), $p < 0.05$; (C) *CDKN1B* (n = 3), $p < 0.05$; and (D) *CCND1* (n = 3), $p < 0.05$, mRNA levels in mock- and ZIKV Br-infected conditions, 24 h, 48 h and 72 h pi. mRNA expression is assessed by real-

time PCR and analysed using the ΔΔCt method that compares the relative expression of each gene, normalized to *GAPDH* housekeeping, within each sample. Data are shown as mean ± SD; two-way ANOVA, post hoc Tukey's test.

(E) Representative confocal images of pHH3, ZIKV NS1, and DAPI in mock- and ZIKV Br-infected hiPS-NPCs 72 h pi. Scale bar, 50 μm. Bar plot indicating fold change in pHH3 positivity normalized to mock (total cells, n = 60.036), $p < 0.05$. Data are shown as mean ± SD; two-way ANOVA, post hoc Tukey's test.

(F) Confocal images of cleaved CASP3 (cCASP3), ZIKV NS1, and DAPI in mock- and ZIKV Br-infected hiPS-NPCs 72 h pi. Scale bar, 50 μm. Bar plot indicating fold change in cCASP3 positivity normalized to mock, in mock- and ZIKV Br-infected hiPS-NPCs (total cells, n = 58.209), $p < 0.01$. Data are shown as mean ± SD; two-way ANOVA, post hoc Tukey's test.

6.6 Only ZIKV, but not other viruses, causes Foxg1 displacement.

Next, to test whether FOXG1 relocation was a specific consequence of ZIKV infection, and not a non-specific effect following any viral infection, A549 transiently expressing Foxg1-GFP were infected with 1 MOI of two different ssRNA+ Arboviruses: USUV belonging to the same genus as ZIKV, and the Asian strain of CHIKV, belonging to the *Togaviridae* family. 24 h pi we fixed cells and stained both USUV NS1 and CHIKV envelope protein E1. Interestingly, we did not detect any significant changes in Foxg1 localization after either USUV or CHIKV infection in either cell line (Figures 14A and 14B).

These data reinforce the finding that ZIKV infection, but not other viruses, specifically perturbs FOXG1 nuclear pattern.

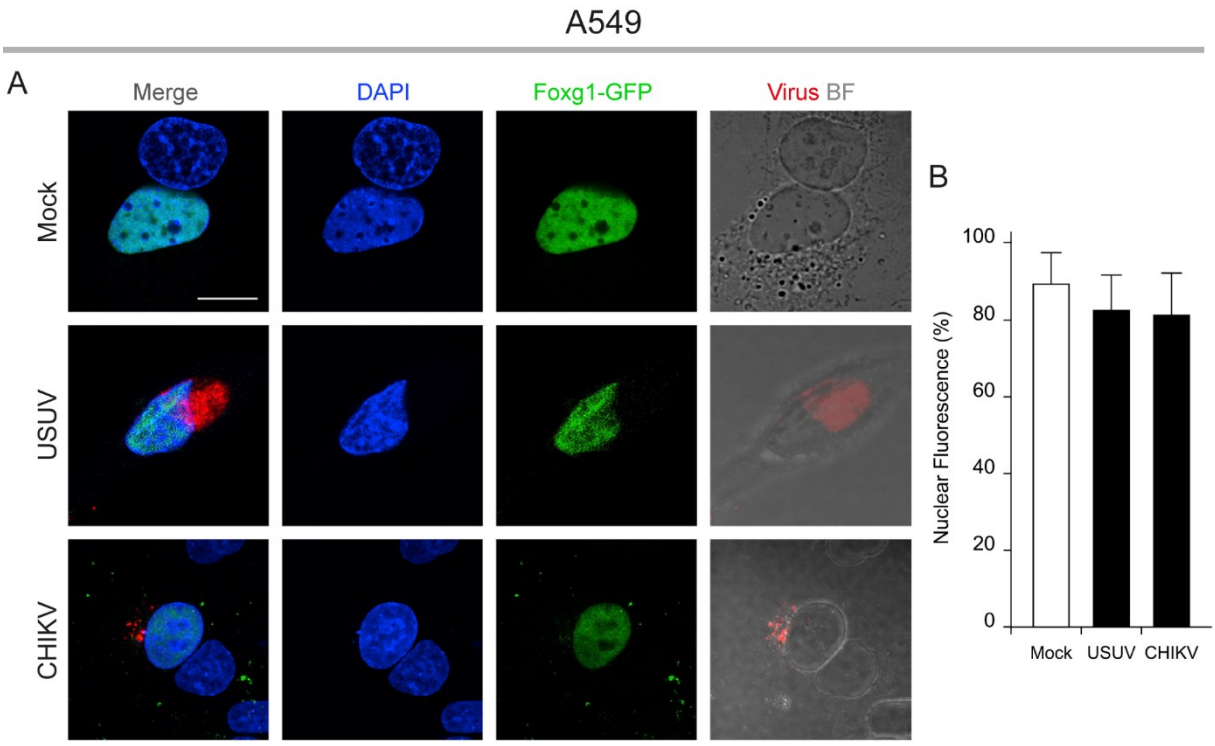

Figure 14. **Infection by other arboviruses does not affect FOXG1 localization.**
(A) Representative confocal images of Foxg1, Virus and DAPI of Foxg1-GFP transfected A549 mock- and infected with USUV or CHIKV. BF, Bright field. Analyses were performed at 24 h pi. Scale bar, 10 µm.
(B) Bar plot indicating the ratio of Foxg1 nuclear fluorescence on total fluorescence in mock-, USUV- and CHIKV-infected conditions (total cells, n = 36), $p > 0.05$. Data are shown as mean ± SD; one-way ANOVA, post hoc Tukey's test.

6.7 ZIKV infection affects FOXG1 only, but not other transcription factors.

Moreover, to evaluate whether the effect of ZIKV infection was specific to FOXG1 or could impinge also on other transcription factors, we examined the expression of SOX1 and SOX2, which are active in neural development and essential for maintaining NSC self-renewal (Graham et al., 1977; Kan et al., 2007). For this reason, we infected-hiPS-NPCs with 1 MOI of ZIKV Ug and 48 h pi infection we fixed cells and labelled SOX1, SOX2 and ZIKV NS1 proteins. Our results indicated that ZIKV Ug infection did not affect either transcription factor

localization because SOX1 (Figures 15A and 15B) and SOX2 (Figures 15C and 15D) stayed in the nucleus following infection.

In conclusion these data confirmed that ZIKV affects only FOXG1 localization and not localization of other transcription factors involved in neural development.

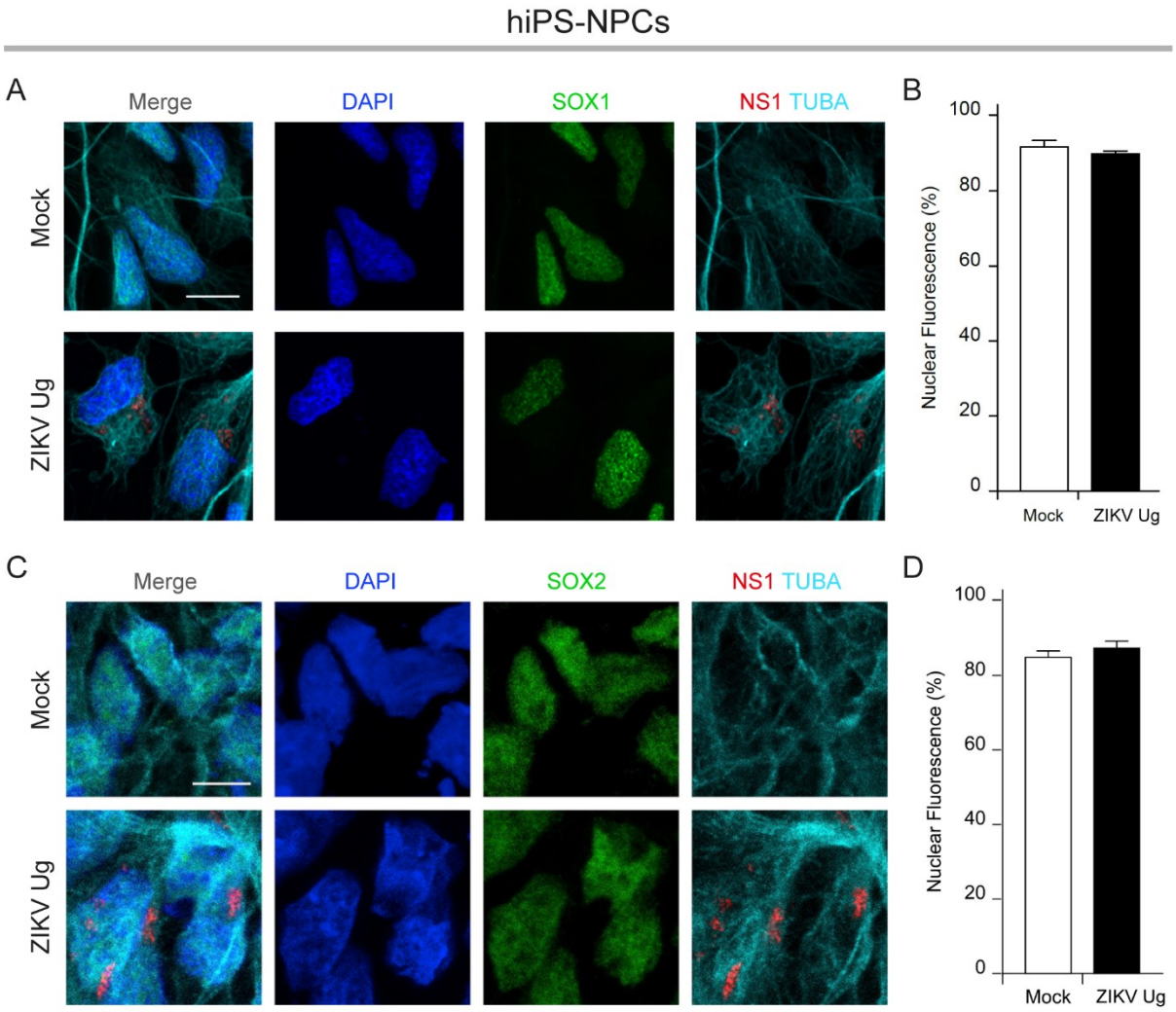

Figure 15. **ZIKV infection does not impinge on other transcription factor expression.**

(A) Representative confocal images of SOX1, ZIKV NS1, TUBA (α-tubulin), and DAPI in mock- and ZIKV Ug-infected hiPS-NPCs, 48 h pi. Scale bar = 10 µm.

(B) Bar plot indicating the ratio of SOX1 nuclear fluorescence on total fluorescence in mock- and ZIKV Ug-infected conditions (total cells, n = 40), p-value > 0.05 Data are shown as mean ± SD; unpaired Student's t-test.

(C) Representative confocal images of mock- and ZIKV Ug-infected hiPS-NPCs showing SOX2 pattern after ZIKV infection at 48 h pi. Scale bar, 10 µm.

(D) Bar plot indicating the ratio of SOX2 nuclear fluorescence on total fluorescence in mock- and ZIKV Ug-infected conditions (total cells, n = 40), $p > 0.05$. Data are shown as mean ± SD; unpaired Student's t test.

6.8 T271 in FOXG1 Akt domain is involved in ZIKV-induced FOXG1 nuclear displacement.

Subcellular localization of FoxG1 is mainly regulated post-translationally, i.e. by phosphorylation. Previous works shows that ectopic expression of FoxG1 increases the rate of cellular proliferation and protects cells from death, establishing Akt pathway as a major player in these cellular aspects (Dastidar et al., 2011; Li et al., 2016; Regad et al., 2007). In order to evaluate whether the effect of ZIKV infection on FOXG1 was mediated by Akt-dependent post-translational mechanisms, we studied whether the putative Foxg1 Akt domain (aa 266–271 RXRXXS*/T*X) and, specifically, T271 was involved in ZIKV-induced nuclear displacement and in the previously suggested role in apoptosis (Dastidar et al., 2011; Hettige & Ernst, 2019; Regad et al., 2007).

For this reason, we generated phospho-mimetic and phospho-defective mutants of Foxg1, fused to GFP at their C-terminal domain, where T271 was substituted with an aspartic acid (T271D) or an alanine (T271A), respectively (Figure 18F), and examined their effects on Foxg1 localization. 24 h after transfection of Foxg1 mutant in A549, we infected with 1 MOI of ZIKV Ug and 24 h later we stained cells to show infection (ZIKV NS1) and nuclei (DAPI). Consistently with the observation of Dastidar et al. but in contrast to what was observed by Regad et al. phospho-mimetic T271D mutants maintained their nuclear localization both in non-infected, as well as in ZIKV Ug-infected A549 cells. Similarly, phospho-defective Foxg1 T271A-GFP, that should be insensitive to Akt phosphorylation, turned out to be totally insensitive to ZIKV Ug infection, maintaining its nuclear localization (Figures 16A and 16B) (Dastidar et al., 2011; Regad et al., 2007).

All together, these data show that both mutants displayed a similar nuclear/cytoplasmatic ratio, typical of WT Foxg1, in A549 mock- and ZIKV Ug-infected cells.

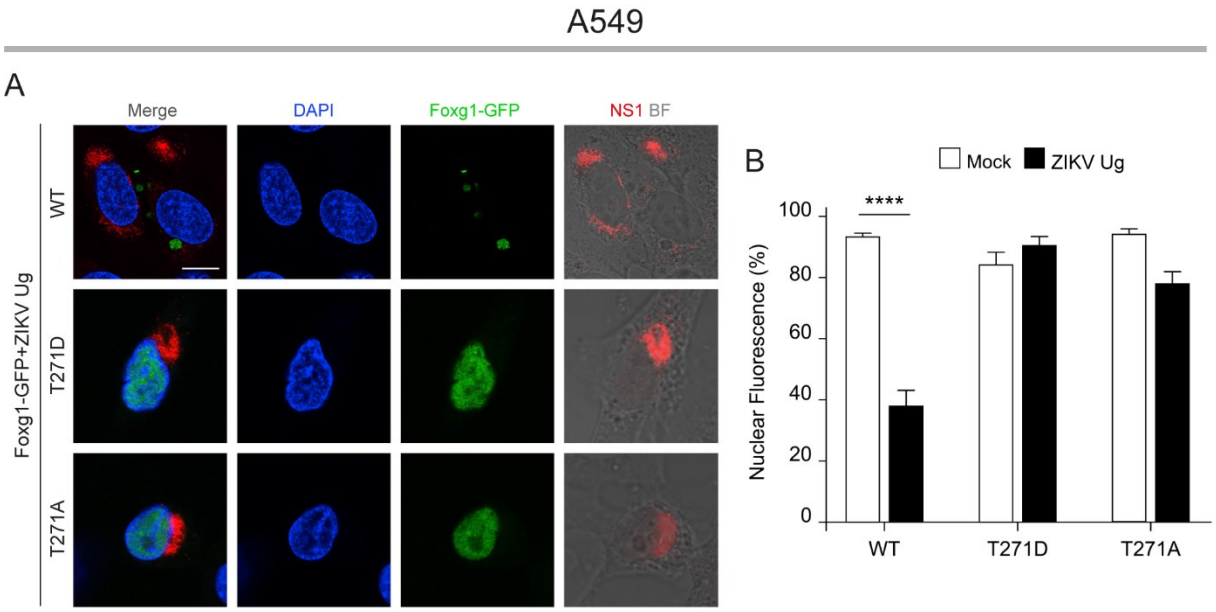

Figure 16. **T271 in FOXG1 Akt domain is essential for ZIKV-induced FOXG1 nuclear displacement.**

(A) Representative confocal images of WT Foxg1-GFP, Foxg1-GFP-T271D, and Foxg1-GFP-T271A transfected A549 cells and infected with 1 MOI of ZIKV Ug. BF, Bright field. Analyses were performed 24 h pi. Scale bar, 10 µm.

(B) Bar plot indicating the ratio of Foxg1 nuclear fluorescence on total fluorescence in mock- and ZIKV Ug-infected conditions, 24 h pi (total cells, n = 49), $p < 0.0001$. Data are shown as mean ± SD; two-way ANOVA, post hoc Tukey's test.

6.9 Akt phosphorylation increases following ZIKV infection.

As mentioned above, FOXG1 subcellular localization is controlled post-translationally and shuttles between nucleus and cytoplasm, following different stimuli, including the activation of the ERK and Akt pathways. Because we found that the putative Foxg1 Akt domain and, specifically, T271 is important for Foxg1 nuclear displacement following ZIKV infection, we investigated the state of Akt during ZIKV infection. Indeed, we hypothesized that ZIKV could have an effect on Akt pathway, which in turn could induce Foxg1 delocalization *via* T271

phosphorylation. For this reason, we infected A549 with 1 MOI of ZIKV Ug and performed WB analysis on cell lysates after 24h of infection to measure Akt phosphorylation levels. As positive control of Akt activation and phosphorylation, we also treated uninfected A549 with 100 ng/ml of insulin, and in parallel, with 200 nM of Wortmannin, that is PI3K inhibitor and negatively regulates Akt pathway. Both treatments were performed 30 min before cell detachment and lysis. According with observations by Airo's group, but in contrast with the results obtained by Liang, our result showed that following ZIKV infection there is a significant increase in the pAkt/Akt ratio, highlighting Akt activation, compared to uninfected cells (Figures 17A and 17B) (Airo et al., 2018; Liang et al., 2016).

Meanwhile, we also investigated the effect of ZIKV infection on PTEN expression. PTEN acts as a negative regulator of Akt pathway, usually exerting its tumor suppression function through the dephosphorylation of PIP_3, antagonizing PI3K-Akt signaling pathway. We infected A549 with 1 MOI of ZIKV Ug and, 24 h pi we expected that, if ZIKV infection enhanced Akt phosphorylation, it should in parallel decrease PTEN expression. However, we did not observe any significant change in either PTEN protein expression or mRNA levels following ZIKV infection (Figures 17C, 17D and 17E).

Next, to confirm the results and investigate the expression of FOXG1, PTEN and the phosphorylation of Akt in a time-dependent manner, we performed WB analysis of A549 infected with 1 MOI of ZIKV Br, lysed at different time points. We had already observed that A549 transfection led to non-specific Akt activation and that expression of FOXG1 was not optimized to be quantified by WB (data not shown). Thus, we transduced A549 with PLVs carrying *FOXG1* gene and, the following day, we infected with 1 MOI of ZIKV Br. Then, we extracted samples 8 h, 12 h, 16 h, 20 h and 24 h pi to perform WB. We observed that we had significant Akt phosphorylation at the same time as FOXG1 reduced expression, occurring at

24 h (Figures 17F, 17G and 17H). However, PTEN expression was not affected by ZIKV Br infection at any time point (Figures 17F and 17I).

Altogether, these findings showed that ZIKV affected Akt activation. This, in turn, could trigger FOXG1 phosphorylation and its following transition from nucleus to cytoplasm, and subsequent downregulation. However, Akt phosphorylation induced by ZIKV did not seem occur *via* dysregulation of PTEN expression.

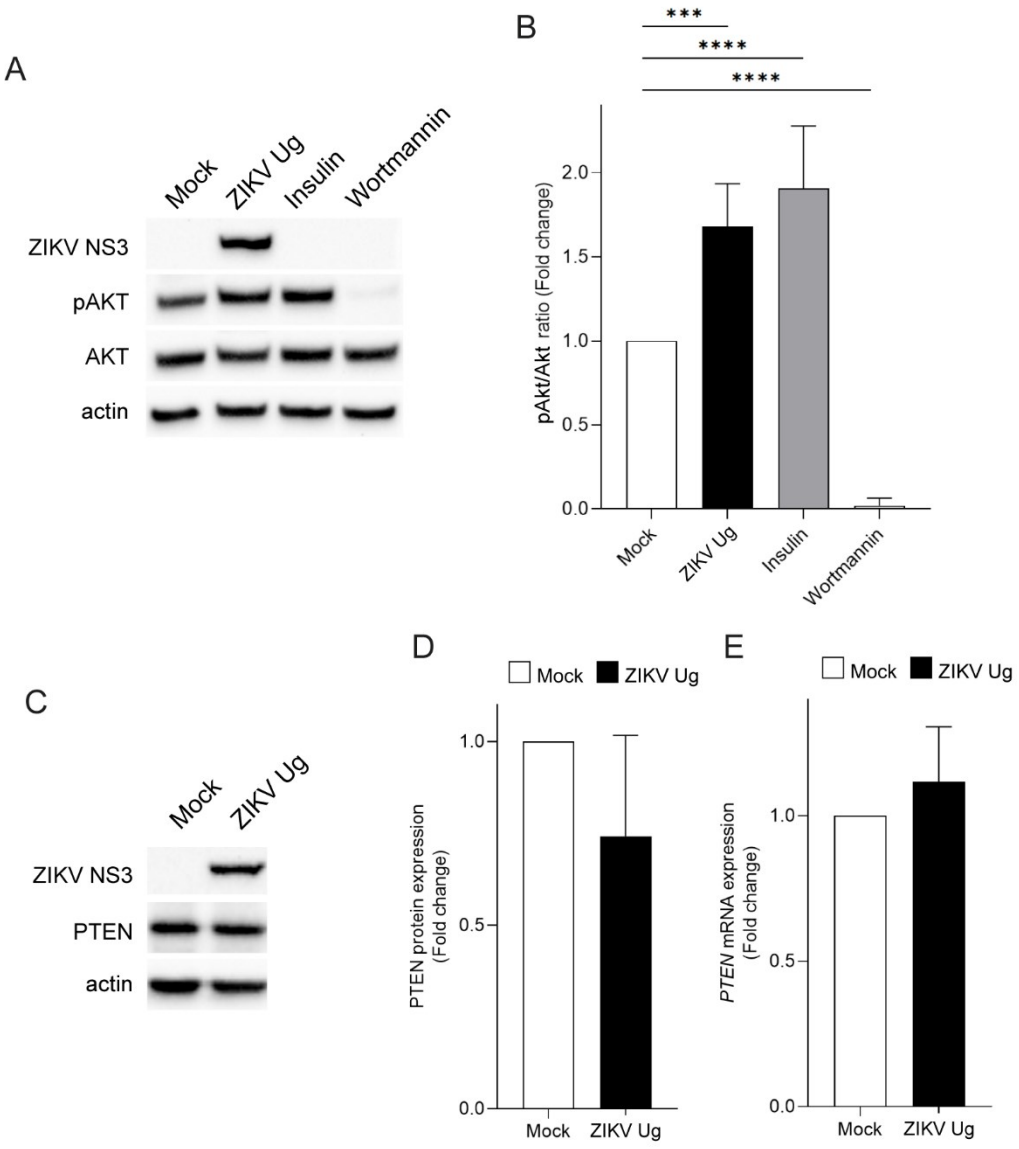

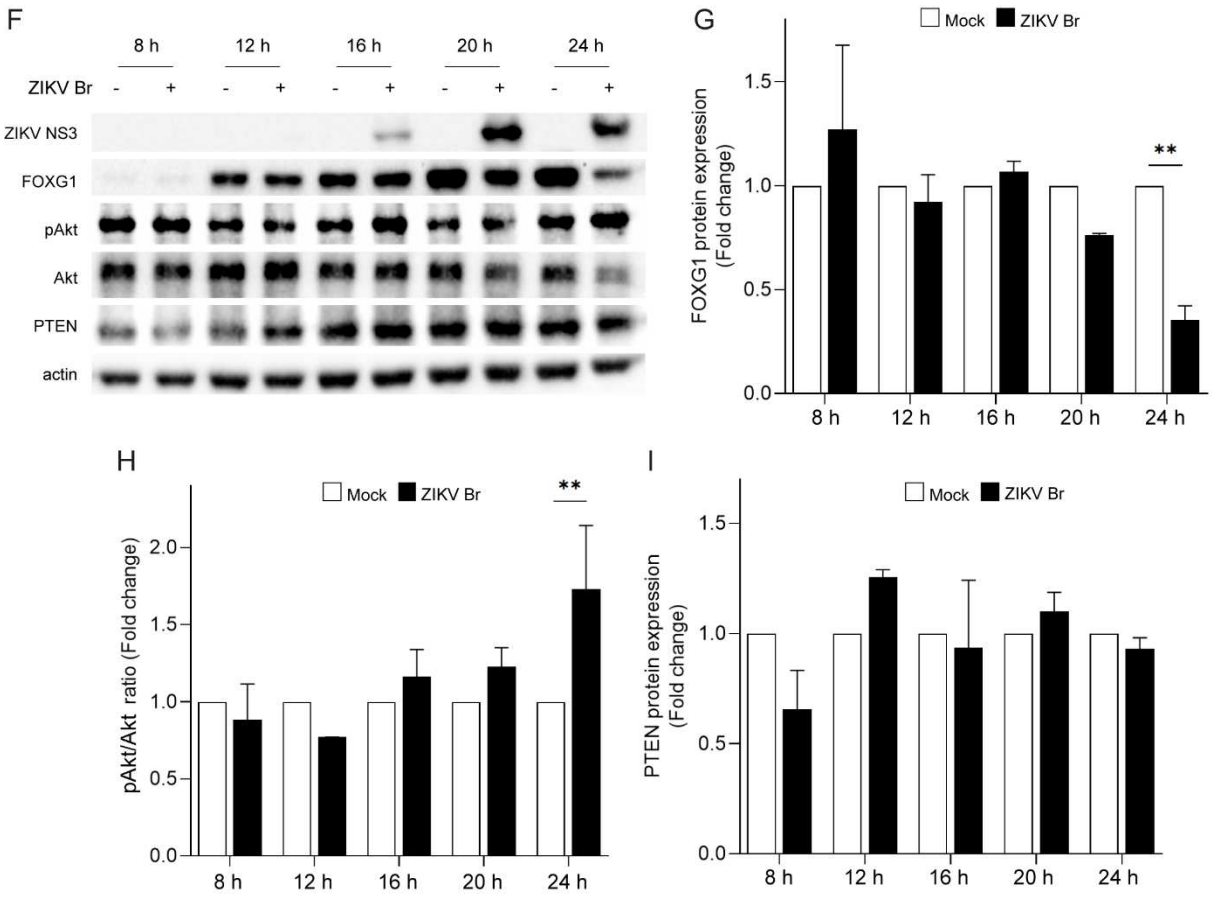

Figure 17. **ZIKV induces Akt activation and FOXG1 downregulation at 24h pi.**

(A) WB analysis comparing pAkt/Akt ratio in A549 mock-infected or infected with 1 MOI of ZIKV Ug, treated with 100 ng/ml of insulin, as a positive control of Akt phosphorylation, or 200 nM wortmannin, that is a negative regulator of Akt activation pathway. Actin is shown as loading control and ZIKV NS3 in infected cells. Analysis was performed 24 h pi and 30 min after insulin or wortmannin treatment.

(B) Densitometric analysis of (A). Bar plot indicating fold change in pAkt/Akt ratio, normalized to actin. Data are shown as mean ± SD. (n = 5), $p < 0.01$; one-way ANOVA, post hoc Tukey's test.

(C) WB analysis showing the comparison between the level of PTEN protein in mock- and ZIKV Ug-infected A549. Cells were lysed 24h pi. Actin is shown as loading control and ZIKV NS3 in infected cells.

(D) Densitometric analysis of (C). Bar plot indicating fold change in PTEN protein expression protein in mock- and ZIKV Ug-infected A549, normalized to actin. Data are shown as mean ± SD. (n = 4), $p > 0,05$; unpaired Student's t test.

(E) Bar plot indicating fold change in *PTEN* mRNA expression, assessed by real-time PCR and analyzed using the ΔΔCt method that compares the relative expression of *PTEN,* normalized to

GAPDH housekeeping, within each sample. Data are shown as mean ± SD (n = 3), p > 0,05; unpaired Student's t test.

(F) WB analysis showing the expression of FOXG1, pAkt/Akt ratio and PTEN in mock- and ZIKV Br-infected A549, transiently transduced with FOXG1-PLVs. Samples are collected every 4 h starting at 8 h pi to 24 h pi. Actin is shown as loading control and ZIKV NS3 in infected cells.

(G) Densitometric analysis of (F). Bar plot indicating fold change in FOXG1 protein expression in mock- and ZIKV Br-infected A549, normalized to actin, relatively to each time-point mock control. Data are shown as mean ± SD. (n = 2), p < 0.01; two-way ANOVA, post hoc Tukey's test.

(H) Densitometric analysis of (F). Bar plot indicating fold change in pAkt/Akt in mock- and ZIKV Br-infected A549, normalized to actin, relatively to each time-point for the mock control. Data are shown as mean ± SD. (n = 2), p < 0.01; two-way ANOVA, post hoc Tukey's test.

(I) Densitometric analysis of (F). Bar plot indicating fold change in PTEN protein expression, in mock- and ZIKV Br-infected A549, normalized to actin, relatively to each time-point mock control. Data are shown as mean ± SD. (n = 2), p > 0.05; two-way ANOVA, post hoc Tukey's test.

6.10 The C-terminus of FOXG1 is essential for ZIKV-induced downregulation.

To investigate if any other FOXG1 regions, in addition to T271, might contribute to its nuclear displacement in response to ZIKV, we used mouse Foxg1-GFP fusion peptides and generated further progressive deletions of Foxg1 at its N- and C-termini (Pancrazi et al., 2015).

In brief, N-terminal construct Foxg1-GFP$_{aa1-171}$ contained the nuclear targeting domain, which consist in poly-histidine (H) repeat (11H, aa 47-57), but did not have the Forkhead (FHD) component of the protein (Figure 18B) (Guen et al., 2011). Foxg1-GFP$_{aa234-391}$ contained FHD, GTB, JBD and MIT domain (Figure 18C). The GBD interacts with the Groucho protein, which is a transcription repressor involved in tightly controlled temporo-spatial development (Gasperowicz & Otto, 2005). The JBD recruits JARID1C demethylase, which is involved

transcriptional regulation and chromatin remodeling and silencing (Jensen et al., 2005). The MIT is mitochondrial localization domain, important to coordinate bioenergetics and the early phases of neuronal differentiation (Pancrazi et al., 2015). Foxg1-GFP$_{aa234-391}$ also contained the putative ZIKV protease cutting motif (Morazzani et al., 2019). C-terminal Foxg1-GFP$_{aa315-481}$ only contained JBD domain (Figure 18D) and, the shortest C-terminal Foxg1-GFP$_{aa428-481}$, not even that (Figure 18E).

In A549 cells, the intracellular distribution of N-termini Foxg1-GFP $_{aa1–171}$ fusion peptide was identical in both mock- and ZIKV Ug-infected cells, resulting diffused in both the nucleus and cytoplasm (Figures 18J and 18L). Then, we evaluated the role of the central region of Foxg1 (aa 234–391) containing FHD domain, T271 and the putative ZIKV serine protease cutting motif, but lacking the N- and C-termini. We transfected A549 cells with FoxG1-GFP$_{aa\ 234–391}$ (Figures 18K and 18L) and then infected with 1 MOI of ZIKV Ug. Also in this context, A549 cells displayed a fluorescence pattern that did not change following ZIKV infection. Finally, we transfected A549 with C-terminal Foxg1 fragments: Foxg1$_{aa315–481}$ and Foxg1$_{aa428–481}$. Both fragments were diffused in both the nucleus and cytoplasm, but following infection with 1 MOI of ZIKV Ug, they showed significant discrete cytoplasmic clusters (Figures 18M, 18N and 18O). These results suggest that Foxg1 domains located at the C-terminal domains contributed to nuclear displacement or, at least, to downregulation.

To exclude possible differences that may result from the N-terminal dissimilarity between mouse and human FOXG1, we fragmented human FOXG1 (Figure 18G) in two constructs generating human N-FOXG1-GFP$_{aa1–280}$, presenting the FHD (Figure 18H), and C-FOXG1-GFP$_{aa280–489}$ peptide, that instead contained GTB and JBD domains only (Figure 18I). We transfected N-FOXG1-GFP$_{aa1–280}$ in A549, which showed an intracellular localization predominantly nuclear, also when we infected cells with 1 MOI of ZIKV Ug for 24 h (Figures 18L and 18P). Then, consistently with the results with mouse Foxg1 fusion peptides, we

analyzed intracellular distribution of C-FOXG1-GFP$_{aa280–489}$, lacking the FHD, and we found that it diffused in both nuclear and cytoplasmic areas; however, following ZIKV Ug infection, discrete clusters became evident in the cytoplasm (Figure 18O and 18Q).

In conclusion, we identified the FOXG1 C-terminus as a critical region mediating the effect of ZIKV infection and we narrowed C-terminus, as important in modulating FOXG1 relocation after ZIKV infection.

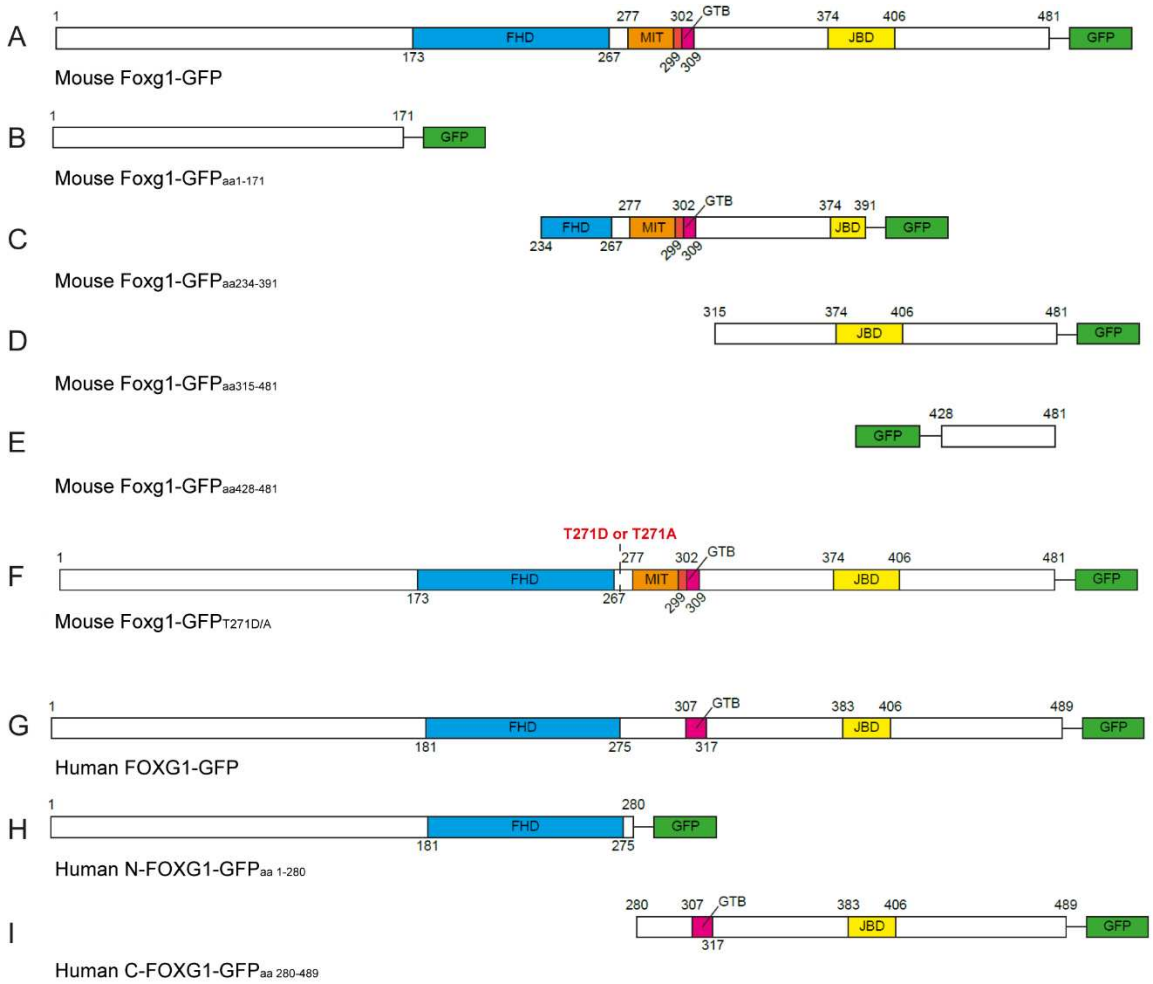

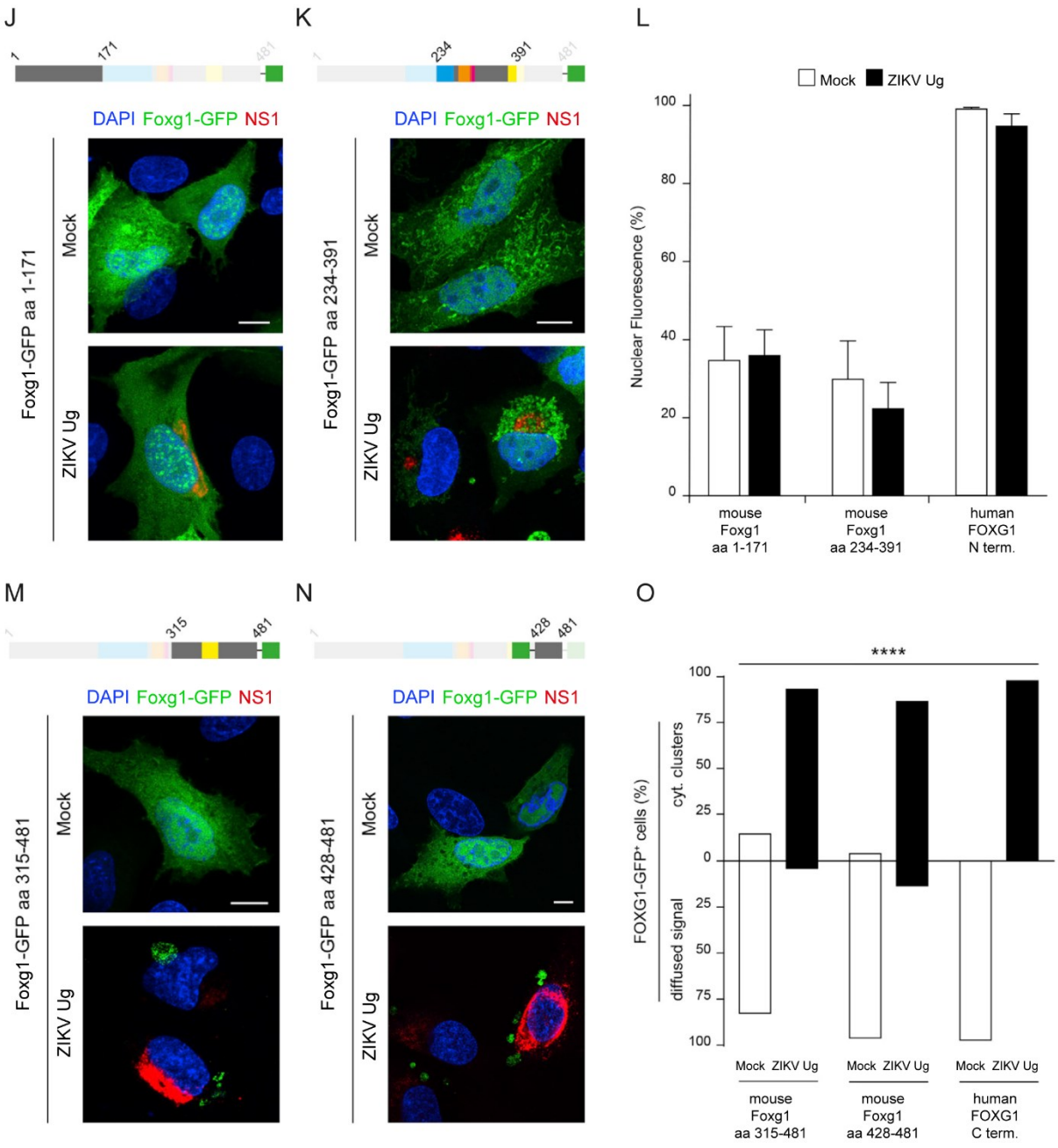
J
K
L
1
171
481
234
391
DAPI Foxg1-GFP NS1
Foxg1-GFP aa 1-171
Foxg1-GFP aa 234-391
Mock
ZIKV Ug
Mock
ZIKV Ug
Nuclear Fluorescence (%)
100
80
60
40
20
0
mouse Foxg1 aa 1-171
mouse Foxg1 aa 234-391
human FOXG1 N term.
M
N
O
315
428
Foxg1-GFP aa 315-481
Foxg1-GFP aa 428-481
****
FOXG1-GFP+ cells (%)
cyt. clusters
diffused signal
75
50
25
Mock ZIKV Ug
mouse Foxg1 aa 315-481
mouse Foxg1 aa 428-481
human FOXG1 C term.

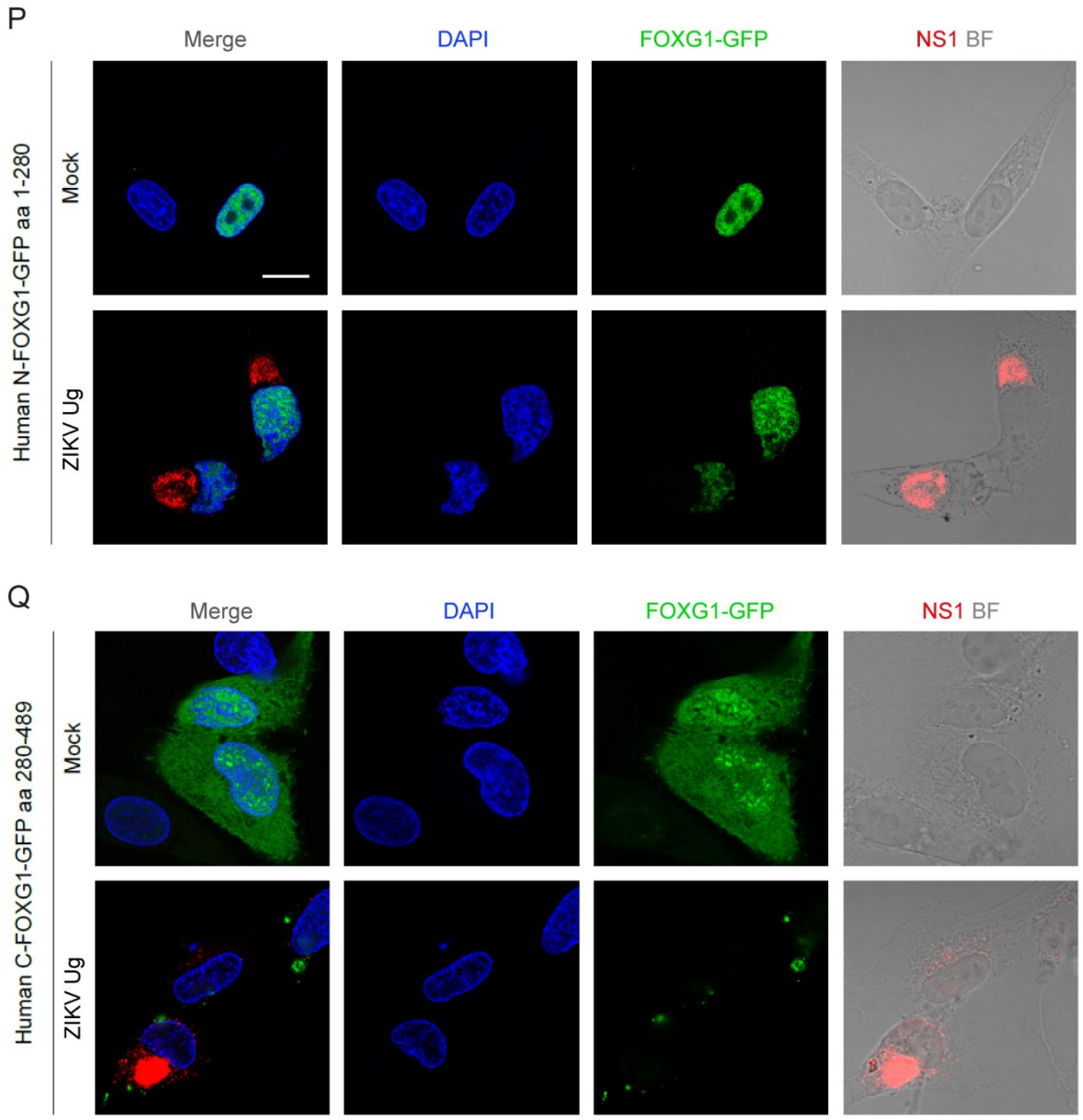

Figure 18. **FOXG1 C-terminus is involved in reacting to ZIKV infection.**

Schematic illustration of (A) mouse Foxg1-GFP WT, (B) N-terminal Foxg1-GFP$_{aa1-171}$, (C) central domain of Foxg1-GFP$_{aa234-391}$, (D) C-terminal Foxg1-GFP$_{aa315-481}$ and (E) final part of C-terminal Foxg1-GFP$_{aa428-481}$.

(F) Schematic illustration of mouse Foxg1-GFP $_{T271D/A}$ where T271 was substituted with aspartic acid (T271D) or alanine (T271A), respectively.

Schematic illustration of (G) human FOXG1-GFP WT, (H) N-terminal FOXG1-GFP$_{aa1-280}$ and (I) C-terminal FOXG1-GFP$_{aa280-489}$.

FHD, Forkhead Domain (blue); MIT, Mitochondrial domain (orange); ZIKV NS2B-NS3 cutting motif (red); GTB, GROUCHO/TLE-Binding domain (pink); JBD, JARID1B Binding Domain (yellow); GFP, Green Fluorescence Protein (green).

Representative confocal images of (J) N-terminal Foxg1-GFP$_{aa\ 1\text{-}171}$ transfected in A549 and infected with 1 MOI of ZIKV Ug; (K) central fragment Foxg1-GFP$_{aa234–391}$ transfected A549 cells in mock- and ZIKV Ug-infected conditions. Analyses were performed at 24 h pi, staining ZIKV (NS1) and nuclei (DAPI). Scale bar, 10 μm.

(L) Bar plot indicating the ratio of FOXG1 nuclear fluorescence on total fluorescence in mock- and ZIKV Ug-infected conditions in mouse Foxg1$_{aa1\text{-}171}$, mouse Foxg1$_{aa234\text{-}391}$ and human N-terminal FOXG1$_{aa1\text{-}280}$ transfected A549 cells. Data are shown as mean ± SD (total cells, n = 29), $p > 0.05$; two-way ANOVA, post hoc Tukey's test.

Representative confocal images of (M) C-terminal Foxg1-GFP$_{aa315\text{-}481}$ transfected in A549 and infected with 1 MOI of ZIKV Ug; (N) C-terminal Foxg1-GFP$_{aa428\text{-}481}$ transfected A549 cells in mock- and ZIKV Ug-infected conditions. Analyses were performed at 24 h pi, staining ZIKV (NS1) and nuclei (DAPI). Scale bar, 10 μm.

(O) Bar plot indicating the percentage of cells with FOXG1-GFP diffused signal or FOXG1-GFP cytoplasmic (cyt.) clusters in mock- and ZIKV Ug-infected conditions in mouse Foxg1$_{aa315\text{-}481}$, mouse Foxg1$_{aa428\text{-}481}$, and human C-terminal FOXG1$_{aa280\text{-}489}$ transfected A549 cells. Data are shown as mean (total cells, n = 30), $p < 0.0001$ (chi-square test).

Representative confocal images of (P) human N-terminal FOXG1-GFP$_{aa1\text{-}280}$ transfected in A549 and infected with 1 MOI of ZIKV Ug. Analyses were performed at 24 h pi, staining ZIKV (NS1) and nuclei (DAPI). Scale bar = 20 μm. (Q) human C-terminal FOXG1-GFP$_{aa280\text{-}489}$ transfected A549 cells in mock- and ZIKV Ug-infected conditions. Staining for ZIKV NS1 and nuclei (DAPI) was performed at 24 h pi. Scale bar = 20 μm.

6.11 ZIKV protease is not responsible of FOXG1 displacement and downregulation.

Recently, Morazzani et al. have shown that recombinant ZIKV protease is responsible for cleaving several cellular molecules in an *in vitro* system (Morazzani et al., 2019). Amongst these proteins, FOXG1 was cut, since it possesses the ZIKV serine protease cutting motif. Importantly, Li et al. have demonstrated that ZIKV protease (NS3) is responsible for Septin 2 cleavage, hindering neural progenitor cell division during ZIKV infection (H. Li et al., 2019). Because ZIKV NS3 and FOXG1 would be localized in different cellular compartments (NS3

in the cytoplasm and FOXG1 in the nucleus) it seemed unlikely that FOXG1 nuclear export could be caused by direct cutting by ZIKV NS3, but it could well be an indirect effect of protease activity. Therefore, we transiently transfected A549 with Foxg1-GFP and the following day we transfected again with ZIKV NS2B-NS3, to mimic ZIKV Br infection. This construct codes for residues 49 - 95 of ZIKV NS2B, the C terminus of which is covalently linked *via* GGGGSGGGG peptide to the N terminus of the NS3 (residues 1 to 170) (Lei et al., 2016). Indeed, the mature form of ZIKV serine protease consists of the N-terminal domain of NS3, which carries the catalytic triad S135-H51-D75, and the membrane-bound NS2B, essential to carry out its peptidolytic activity. As expected, following NS2B-NS3 transfection we did not observe any significant displacement of FOXG1 into the cytoplasm or any consequent protein degradation (Figures 19A and 19B). Next, to allow contact between ZIKV NS2B-NS3 and FOXG1, and subsequent FOXG1 cleavage, we performed NS2B-NS3 transfection of A549 already transduced with FOXG1-PLVs and the following day we lysed cells. Then, we incubated the samples at 37°C for 4 h, in order to allow ZIKV NS2B-NS3 to cut FOXG1 and other proteins in the mix, that have NS3-cutting motif. We hypothesized that the two exogenous proteins, that are localized in two different cellular compartments (FOXG1 into the nucleus and NS2B-NS3 into the cytoplasm), could physically interact with each other after cell disruption and supporting ZIKV NS2B-NS3 proteolytic activity in forced, but optimal condition. However, after WB analysis of FOXG1 expression in A549 mock- or infected with 1 MOI of ZIKV Br, or transiently transfected with NS2B-NS3 or a control plasmid (pCDNA), we did not observe any FOXG1 degradation or cleavage, when expressed together with NS2B-NS3 (Figures 19C and 19D).

We can conclude that ZIKV NS2B-NS3 alone do not seem responsible for FOXG1 protein degradation.

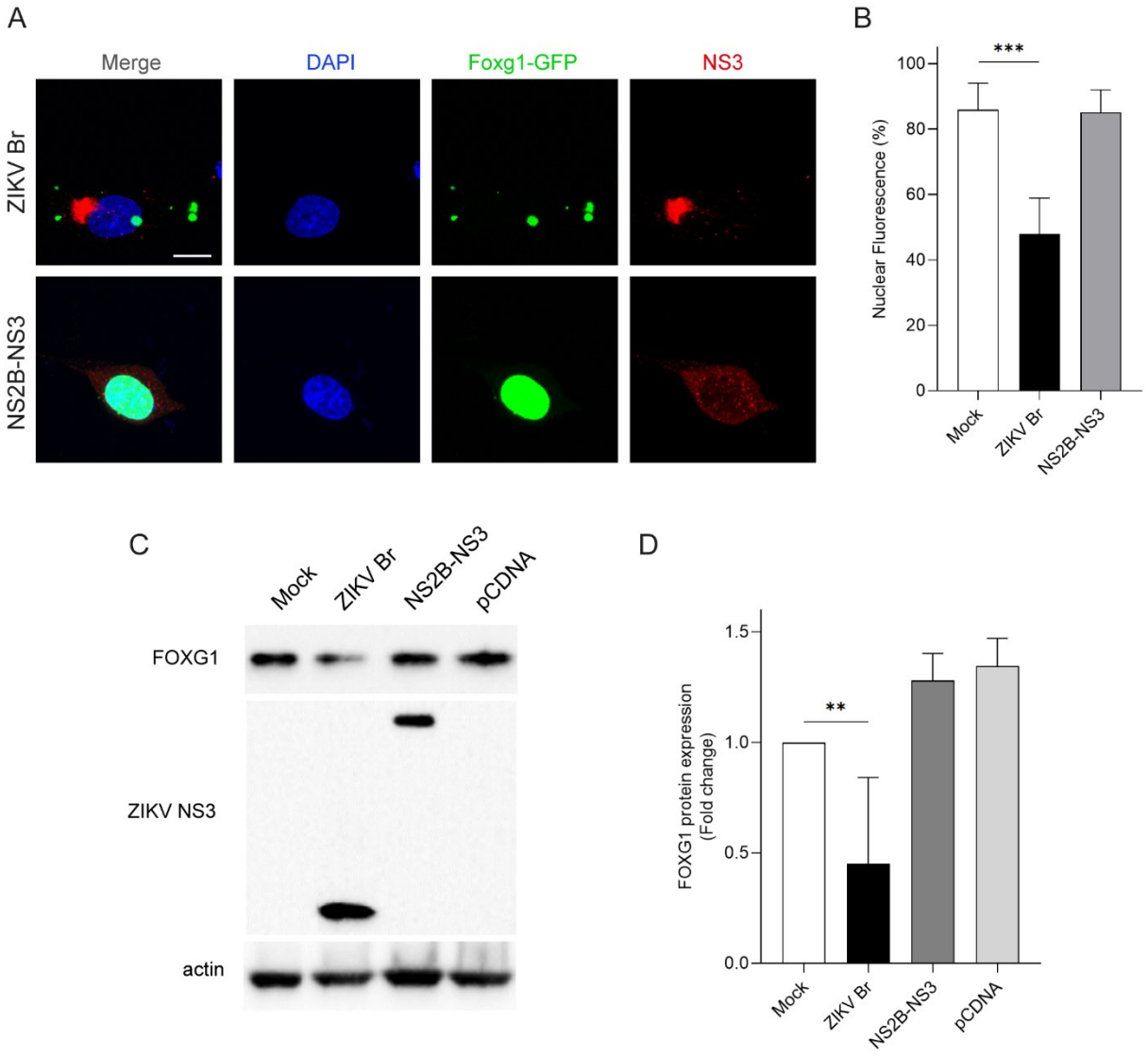

Figure 19. **FOXG1 nuclear export and degradation are not caused by to cutting by ZIKV protease.**

(A) Representative confocal images of Foxg1-GFP transfected A549 cells at 24 h from either infection with ZIKV Br or transfection with ZIKV NS3-NS2B. ZIKV NS3 and DAPI are shown. Analyses were performed at 24 h pi. Scale bar, 10 µm.

(B) Bar plot indicating the ratio of Foxg1 nuclear fluorescence on total fluorescence in ZIKV Br-infected or NS2B-NS3-transfected conditions (total cells, n = 20), $p < 0.001$. Data are shown as mean ± SD; one-way ANOVA, post hoc Tukey's test.

(C) WB analysis comparing the level of FOXG1 transiently expressed in A549. 24 h after transduction with FOXG1-PLVs, A549 are infected with 1 MOI of ZIKV Br or transfected with NS2B-NS3 and pCDNA, as control. Samples are collected 24 h pi or transfection. Actin is shown as loading control and ZIKV NS3 in infected cells.

(D) Densitometric analysis of (C). Bar plot indicating fold change in FOXG1 protein expression in mock-, ZIKV Br-infected or NS2B-NS3- and pCDNA-transfected A549, normalized to actin. Data are shown as mean ± SD. (n = 4), $p < 0.01$; one-way ANOVA, post hoc Tukey's test.

6.12 ZIKV enhances FGF2 expression and release.

There are several reports in the literature that show association of FGF2 levels with infection by ZIKV. Limonta et al. showed that ZIKV induces FGF2 expression and FGF2 facilitates virus replication and cell-to-cell spread (Limonta et al., 2019); moreover, in ZIKV-infected pregnant women, blood concentration of FGF2 correlates with the severity of the affected fetuses and, finally, FGF2 receptor inhibitors have been suggested as a promising approach for antiviral therapies (Carlin, 2022; Kam et al., 2017; Lottini et al., 2023; Maddaluno et al., 2020). GFs are also important to maintain neural stem cell self-renewal and orchestrate forebrain shaping during fetal development (Onorati et al., 2016).

To further explore the role of FGF2 in FOXG1 nuclear pattern disruption, we performed RT-qPCR to monitor *FGF2* expression in hiPS-NPCs. We infected hiPS-NPCs with 1 MOI of ZIKV Ug and we collected RNA extract every 24 h pi. Then we performed RT-qPCR using primers and protocol discussed in section 5.10 and we observed a time-dependent progressive increase of *FGF2* mRNA, following ZIKV infection (Figure 20A).

Moreover, we also performed ELISA (protocol shown in 5.14) to quantify FGF2 released in cell culture supernatant in a time-dependent manner. We infected A549 with 1 MOI of ZIKV, USUV, CHIKV, and, in parallel, we transfected with 200 ng/ml of Poly(I:C), transfected with expression plasmid (pCDNA) and transduced with FOXG1-PLVs. Next, we collected supernatant and cell lysates at different time points.

In agreement with Limonta et al., we observed a significant increase of FGF2 release following ZIKV Br infection, with a peak at 72 h pi, corresponding to 1.5 ng/ml of FGF2 released (Limonta et al., 2019). We can also observe lower but significant FGF2 release following

USUV infection, but not after CHIKV. However, we noticed significant production of FGF2 also following Poly(I:C) treatment (Figure 20B).

To shed further light into the subject, we infected A549 with 1 MOI of ZIKV Br, USUV, CHIKV or transfected with 200 ng/ml of Poly(I:C), with a control expression plasmid and transduced with FOXG1-PLVs. Interestingly, performing WB analysis on A549 either ZIKV Br-infected or treated as above, we did not observe an increase of FGF2 expression but rather a decrease, that we hypothesized to be the consequence of the loss of protein after release from cells (Figure 20C).

Altogether these results showed that ZIKV enhances FGF2 expression and release in both hiPS-NPCs and A549.

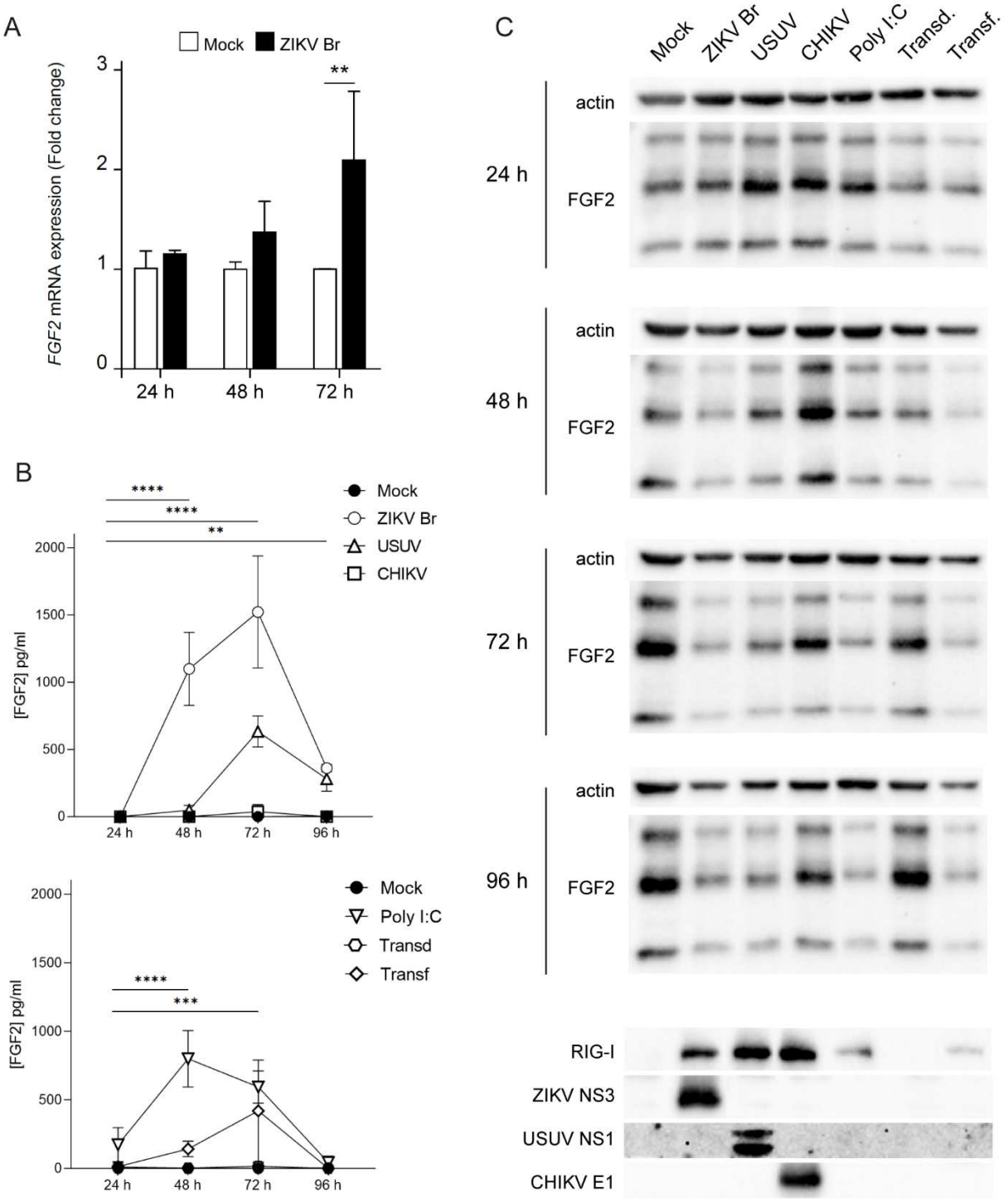

Figure 20. **ZIKV induces FGF2 expression and release in A549.**

(A) Bar plot indicating fold change in *FGF2* mRNA expression, assessed by real-time PCR and analyzed using the ΔΔCt method that compares the relative expression of *FGF2,* normalized to *GAPDH* housekeeping, within each sample. hiPS-NPCs were infected with 1 MOI of ZIKV Ug and collected 24 h, 48 h and 72 h pi. Data are shown as mean ± SD (n = 3), p-value < 0.01; Two-way ANOVA, post hoc Tukey's test.

(B) ELISA analysis and line graph showing FGF2 release in a time-dependent manner. Supernatants of A549 infected with ZIKV Br, USUV, CHIKV, transfected with Poly(I:C) or a control expression plasmid (Transf.) or transduced with control FOXG1-PLVs (Transd.), were collected 24 h, 48 h, 72 h and 96 h pi. Data are shown as mean ± SD. (n = 3), $p < 0.0001$; two-way ANOVA, post hoc Tukey's test.
(C) WB analysis showing A549 treated as in (B) and lysed after 24 h, 48 h, 72 h and 96 h. Images at every time point show FGF2 protein expression and actin as loading control. Representative images of RIG-I, ZIKV E, USUV NS1, CHIKV E1, in order to show infection or innate immunity stimulation, are taken 48 h pi.

6.13 FGF2 enhances ZIKV infection but not FOXG1 expression.

Kumar et al. showed that FGF2 was found to be dramatically upregulated in ZIKV-infected Sertoli cells. In turn, Limonta's group showed that FGF2 increased ZIKV replication through MAP kinase activation, in HFAs (Kumar et al., 2018; Limonta et al., 2019). For this reason, we asked whether ZIKV infection could be enhanced by FGF2 exposure and if it affected FOXG1 expression and cellular localization. We exposed A549 to different concentration of recombinant FGF2 (rFGF2) and 24h later we infected cells with 1 MOI of ZIKV Br for further 24 h, adding rFGF2 again. We also added rFGF2, at the same concentrations, only after viral adsorption; we fixed cells 24 h pi and performed IF analysis staining for ZIKV C protein (Figures 21A and 21B). According with Limonta et al., we observed that ZIKV protein expression and, presumably, ZIKV Br replication, significantly increased following both rFGF2 treatments, showing a peak after pre-treatment with 8 ng/ml rFGF2 (Figure 21D) and a peak at 4 ng/ml rFGF2, when added following ZIKV Br adsorption (Figure 21E) (Limonta et al., 2019). We also observed that following rFGF2 pre-treatment, we had higher percentages of ZIKV Br-infected cells, compared to simply adding rFGF2 pi. Because FGF2 can induce cellular proliferation, the effect of this cytokine on viral replication might be due to increased numbers of susceptible A549 and a longer exposure to FGF2 might boost replication. Next, because

FGF2 promoted ZIKV Br replication, we expected that blocking FGF2 from binding to receptors on the cell surface would have the opposite effect. However, addition of neutralizing anti-FGF2 antibody did not reduce ZIKV replication, but rather, it increased it (Figures 21C and 21F).

Then, because FOXG1 subcellular localization is controlled post-translationally by different stimuli, including GFs, and ZIKV Br replication increased following rFGF2 treatment, we wondered if increasing ZIKV Br by adding rFGF2 would affect FOXG1 expression and cytoplasmic localization. We treated A549 transduced with FOXG1-PLVs in different ways:

1) Adding 2.5 ng/ml of rFGF2 after virus adsorption, to bring the FGF2 concentration found after ZIKV infection (1.5 ng/ml) to the concentration of FGF2 that increased ZIKV replication in A549 (4 ng/ml);
2) Treating cells 24 h prior infection and again post-adsorption with 15 ng/ml of rFGF2, the concentration that Limonta et al. used to increase ZIKV infection in HFAs;
3) Adding 15 µg/ml of neutralizing FGF2 antibody to downregulate ZIKV infection, according to Limonta et al. (Limonta et al., 2019).

Then, we infected A549 with 1 MOI of ZIKV Br or USUV and we analyzed samples by WB 24 h pi (Figure 21G). Surprisingly, we did not observe any significant changes in FOXG1 expression following FGF2 or anti-FGF2 treatments (Figure 21H). Unfortunately, we did not observe the same significant increase in ZIKV Br or USUV protein expression, as shown in confocal images, but only a trend that showed an increase in ZIKV NS3 with 2.5 ng/ml of rFGF2 (Figures 21I and 21J).

Thus, ZIKV enhanced FGF2 expression and release, and also FGF2 treatment promoted ZIKV replication. However, FGF2 neutralization did not inhibit ZIKV replication. Moreover, we did not observe any significant change in FOXG1 expression following FGF2 treatment or

inhibition.

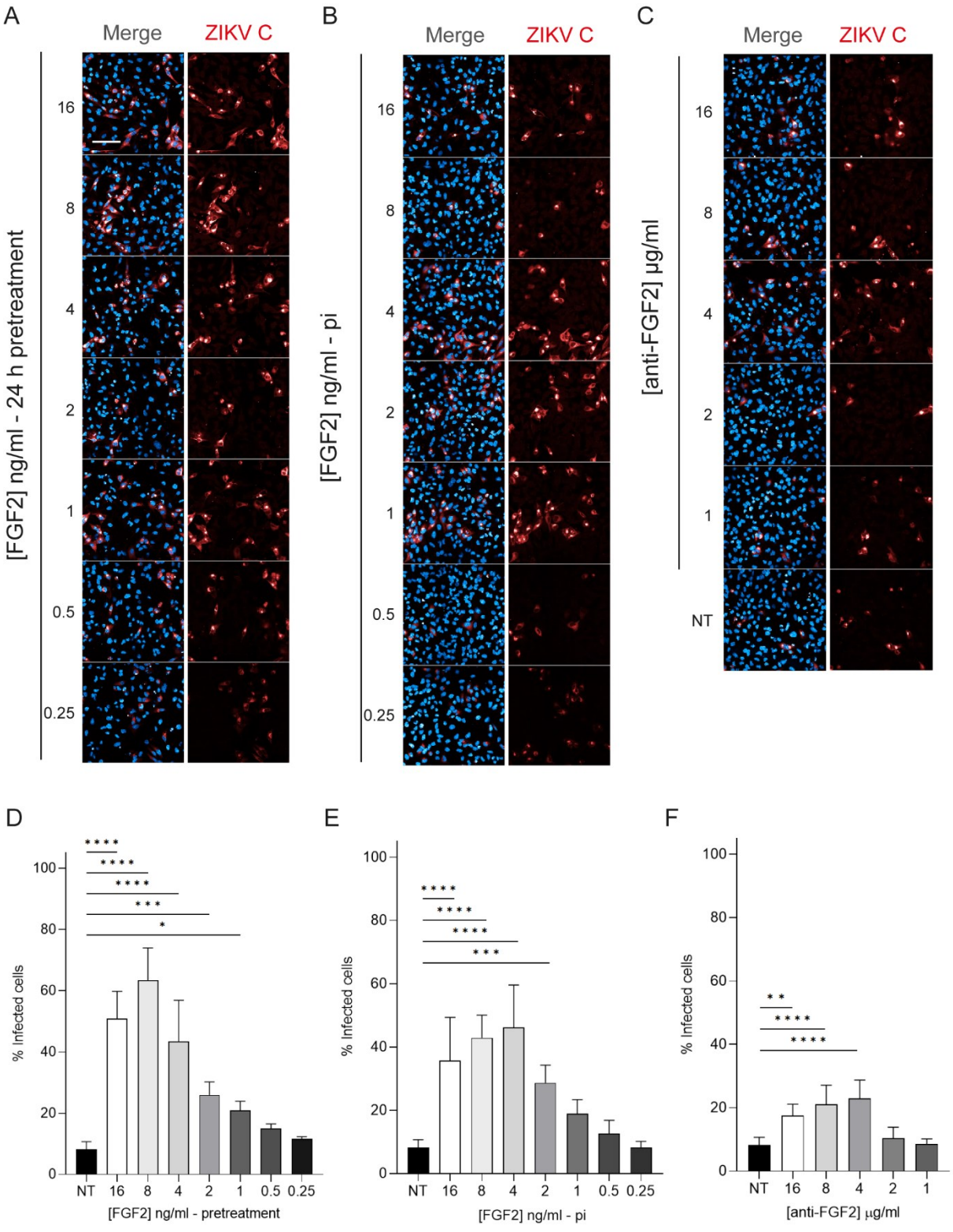
A
Merge
ZIKV C
[FGF2] ng/ml - 24 h pretreatment
16
8
4
2
1
0.5
0.25
B
Merge
ZIKV C
[FGF2] ng/ml - pi
16
8
4
2
1
0.5
0.25
C
Merge
ZIKV C
[anti-FGF2] µg/ml
16
8
4
2
1
NT
D
% Infected cells
100
80
60
40
20
0
NT 16 8 4 2 1 0.5 0.25
[FGF2] ng/ml - pretreatment
E
% Infected cells
100
80
60
40
20
0
NT 16 8 4 2 1 0.5 0.25
[FGF2] ng/ml - pi
F
% Infected cells
100
80
60
40
20
0
NT 16 8 4 2 1
[anti-FGF2] µg/ml

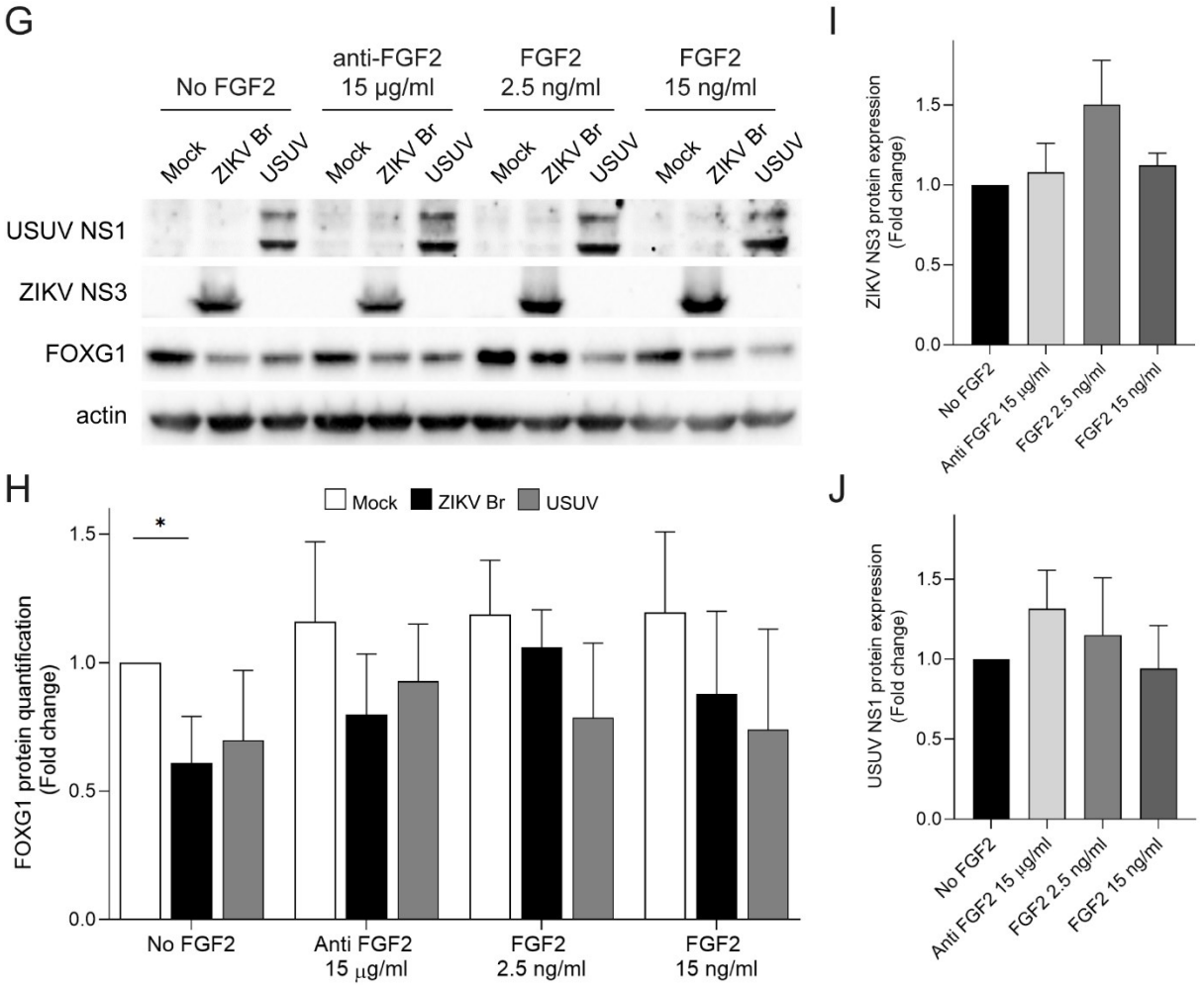

Figure 21. **FGF2 enhances ZIKV replication in A549 but not FOXG1 downregulation.**
Confocal images of (A) ZIKV Br-infected A549 pretreated for 24 h and treated after ZIKV Br adsorption or (B) treated pi with different concentrations of rFGF2 or (C) with neutralizing anti-FGF2 antibody. ZIKV Capsid (C) and DAPI are shown. NT, No treatment. Analyses were performed at 24 h pi. Scale bar, 100 µm.

Bar plot indicating (D) ZIKV infected cells (%) pretreated or (E) treated pi with different concentrations of rFGF2 or (F) neutralizing anti-FGF2 antibody. NT, No treatment. Data are shown as mean ± SD. (n = 6), $p < 0.0001$; one-way ANOVA, post hoc Tukey's test.

(G) WB analysis comparing the amount of FOXG1, ZIKV NS3 and USUV NS1 in mock-, ZIKV Br- and USUV-infected A549 transiently transduced with FOXG1-PLVs. A549 were treated pi with 15 µg/ml neutralizing anti-FGF2 antibody, with 2.5 ng/ml rFGF2 or both treated 24 h before infection and pi with 15 ng/ml of rFGF. Analysis is taken 24 h pi and actin is showed as loading control.

(H) Bar plot indicating fold change in FOXG1 protein expression normalized to actin. Data are shown as mean ± SD. (n = 5), $p < 0.05$; two-way ANOVA, post hoc Tukey's test.

(H) Bar plot indicating fold change in ZIKV NS3 protein expression normalized to actin. Data are shown as mean ± SD. (n = 3), $p > 0.05$; two-way ANOVA, post hoc Tukey's test.
(J) Bar plot indicating fold change in USUV NS1 protein expression normalized to actin. Data are shown as mean ± SD. (n = 3), $p > 0.05$; two-way ANOVA, post hoc Tukey's test.

6.14 Growth factors prevent FOXG1 displacement following ZIKV infection.

To further explore FOXG1 nuclear pattern disruption, we turned to NES cells, a model of human NSCs with neocortical identity, where the effect of ZIKV infection has been examined in detail (Onorati et al., 2016). NES cells are neurogenic, tripotent, and positive for neuroprogenitor markers, such as SOX1 and SOX2. Remarkably, they retain positional identity as confirmed by the expression of regional markers typical of the area they are derived from, including FOXG1. Unexpectedly, we could not detect any evident nuclear/total fluorescence ratio alteration of FOXG1 in ZIKV Ug-infected NES cells (Figures 22A and 22B).

To explain this result, we hypothesized that the different culture conditions between hiPS-NPCs and NES cells could affect FOXG1 shuttling, and again we focused on the role of GFs. Indeed, while NES cells are exposed to EGF and FGF2 to propel their self-renewal state, hiPS-NPCs are maintained into a neural medium devoid of GFs (Onorati et al., 2016). For this reason, we exposed hiPS-NPCs to 20 ng/ml EGF and 20 ng/ml FGF2, that are GFs concentrations supplied in NES cells maintenance medium, for 13 days, after which cells were infected with ZIKV Ug in the presence of both GFs. Similar to NES cells, no changes in FOXG1 nuclear localization were observed in this condition. Next, to evaluate the individual contribution of EGF and FGF2, we separately exposed hiPS-NPCs to each factor and found that EGF and/or FGF2 maintained FOXG1 nuclear localization following ZIKV infection (Figures 22C and 22D). In parallel, we evaluated whether treatment with the same cocktail of GFs exerted comparable effects in A549 cells expressing Foxg1-GFP. For this reason, we first adapted A549 to grown in low doses of

FBS (1%), reducing gradually FBS concentration in maintenance medium during cells splitting. Then we exposed A549 to 20 ng/ml EGF and 20 ng/ml FGF2 for 15 days and then performed experiment as always: we transfected A549 grown in GFs with Foxg1-GFP and the day after we infected with 1 MOI of ZIKV Ug. 24 h pi we found that GFs precluded FOXG1 relocation following ZIKV infection (Figures 22E and 22F).

Altogether, these data suggest that the impact of ZIKV infection on FOXG1 is modulated by the presence of EGF and/or FGF2.

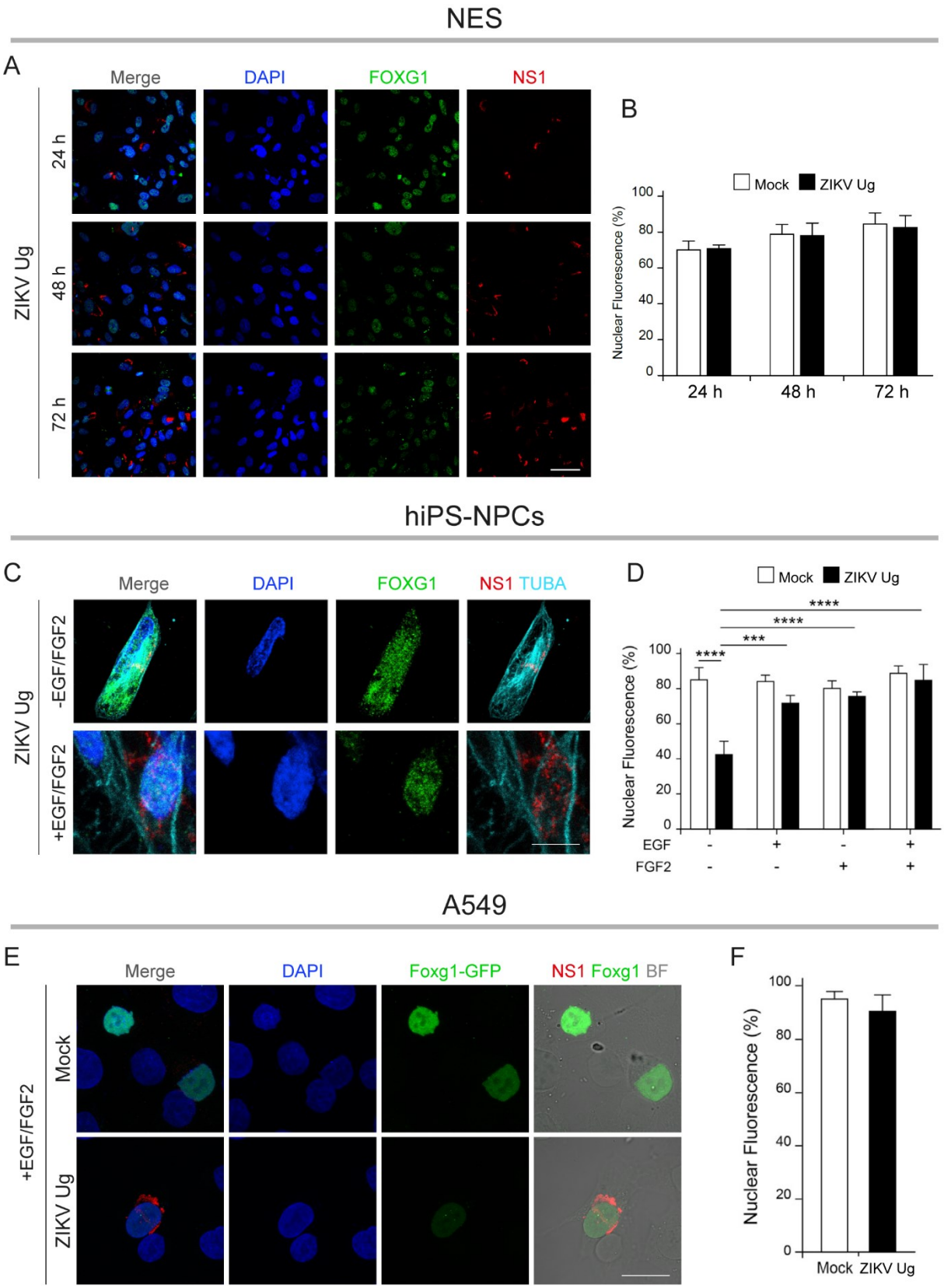

Figure 22. **ZIKV-induced FOXG1 displacement is inhibited by GF treatment in hiPS-NPCs and A549.**

(A) Representative confocal images of FOXG1, ZIKV NS1, and DAPI in mock- and ZIKV-infected NES cells 24 h, 48 h and 72 h pi. The time course analysis shows that FOXG1 does not mislocalize from the nucleus. Scale bar = 50 µm.

(B) Bar plot indicates the ratio of FOXG1 nuclear fluorescence on total fluorescence in mock- and ZIKV Br-infected NES cells at each time point. Data are shown as mean ± SD (total cells, n = 120), p-value > 0.05; Two-way ANOVA, post hoc Tukey's test.

(C) Representative confocal images of FOXG1, ZIKV NS1, TUBA (α-tubulin), and DAPI in ZIKV-infected hiPS-NPCs in the absence and in the presence of GFs (± 20 ng/ml of EGF and FGF2). Analyses were performed 48 h pi. Scale bar, 10 µm.

(D) Bar plot indicating the ratio of FOXG1 nuclear fluorescence on total fluorescence in mock- and ZIKV-infected hiPS-NPCs. Data are shown as mean ± SD (total cells, n = 160), $p < 0.001$; two-way ANOVA, post hoc Tukey's test.

(E) Representative confocal images of Foxg1-GFP transfected A549 cells in the presence of 20 ng/ml of EGF and FGF2, infected or not with 1 MOI of ZIKV Ug. BF, Bright field. Analyses were performed 24 h pi. Scale bar, 10 µm.

(F) Bar plot indicating the ratio of FOXG1 nuclear fluorescence on total fluorescence in mock- and ZIKV Br-infected A549. Data are shown as mean ± SD (total cells, n = 20), $p > 0.05$; unpaired Student's t test.

7 DISCUSSION AND CONCLUSION

ZIKV, belonging to the *Flavivirus* genus, is the only virus of its family known to be associated with complications in neuronal development, such as microcephaly. Epidemiological data indicate an increased association between ZIKV infection and microcephaly (Brasil et al., 2016a; Brasil et al., 2016b). Confirmation of this association occurred with the discovery of the ZIKV genome in the amniotic fluid of a microcephalic fetus in Brazil in 2016 (Calvet et al., 2016). Our laboratory, therefore, aimed at shedding light into the mechanisms that explain how ZIKV infection affects the activity of FOXG1, a transcription factor active in the early stages of neuronal development.

FOXG1 is expressed in various cell types of the nervous system, such as the cerebral cortex and telencephalon (Pauley et al., 2006). It plays a pleiotropic role in the development of the anterior brain, as evidenced by the fact that individuals with mutations in FOXG1 belong to a clinical entity known as "FOXG1-related encephalopathy", associated with Rett's syndrome (Wong et al., 2019). Therefore, correlation between clinical manifestations affecting the fetal brain following ZIKV infection and the activity of FOXG1seemed plausible.

In this study, confocal microscopy analyses were performed to observe the localization of the transcription factor Foxg1 in the presence and absence of ZIKV. A statistically significant difference was observed between uninfected and ZIKV-infected A549 cells transiently transfected with Foxg1-GFP. The same FOXG1 pattern was observed in mock- and ZIKV-infected hiPS-NPCs, that express FOXG1 endogenously. These results were confirmed using both ZIKV Uganda strain and the more interesting Brazilian strain, that is related to microcephaly (Figure 9). This allowed us to conclude that the export of Foxg1 from the nucleus to the cytoplasm is a mechanism induced specifically by ZIKV. Then, performing WB analysis were measured also the levels of FOXG1 protein expression in total or subcellular fractions and we found that in both endogenously and exogenously FOXG1 expressing cell lines there was a

reduction of FOXG1 protein expression following ZIKV infection (Figures 10 and 12). Moreover, to improve the transiently expression of Foxg1 and increase ZIKV infection levels in A549, transfection of Foxg1 plasmid was often replaced in several experiment by transduction with PLVs carrying *FOXG1* gene (Figure 11).

To determine whether the nuclear translocation of the Foxg1 factor, in the presence of ZIKV, was a specific response to ZIKV or was also caused by other viruses belonging to the *Flavivirus* genus or not, we proceeded with infections using USUV and CHIKV and confocal analyses following the same procedures as for ZIKV. The analysis yielded interesting results showing no variations in the nuclear fluorescence levels of Foxg1 in the presence of viruses other than ZIKV (Figure 14). Then, to ensure that the export from the nucleus to the cytoplasm was specific to FOXG1 and not to other transcription factors, we infected hiPS-NPCs with ZIKV and performed confocal imaging to also evaluate the localization of SOX1 and SOX2, two transcription factors involved in neural development. However, we found that following ZIKV infection SOX1 and SOX2 maintained nuclear localization, so we concluded that ZIKV affected only FOXG1 displacement (Figure 15).

These initial findings suggest that the export of the transcription factor into the cytoplasm, following ZIKV infection, is likely to result in its impaired function at the nuclear level, thus affecting its role in proper anterior brain development. We infected hiPS-NPCs with ZIKV, and we found that infection affects well-known downstream genes of FOXG1, such as *CCND1* involved in cell cycle progression, and *CDKN1A* and *CDKN1B*, involved in p53-dependent cell-cycle arrest. These effects lead to a reduction of proliferation and increased apoptosis in NPCs, as evidenced by decreased pHH3 and cCASP3 positivity, respectively (Figure 13). These findings are consistent with a previous study where ZIKV infection of hiPSC-NPCs resulted in transcriptional alterations, including *FOXG1* downregulation, upregulation of apoptotic signaling, and downregulation of cell-cycle pathways (Jiang et al., 2018).

Next, to investigate if a specific FOXG1 region might contribute to its nuclear displacement in response to ZIKV, we used both murine Foxg1 and human FOXG1 fusion peptides and generated further progressive deletions of at its N- and C-termini. The intracellular distribution of N-termini Foxg1-GFP (aa 1-171) was diffused in both the nucleus and cytoplasm, in mock- as in ZIKV-infected A549 cells. Instead, localization of human N-FOXG-GFP (aa 1-280) that contains FHD (the nuclear retention signal) was predominantly nuclear, and as murine N-terminal peptide, was not affected by ZIKV infection. We also analyzed the central region of FoxG1-GFP comprised between aa 234-391, containing FHD and the putative serine protease cutting motif, but also in this context, A549 cells displayed a fluorescence pattern that did not change following ZIKV infection. Then, we focused on C-terminal region of murine and human FOXG1. We transfected A549 with two Foxg1-GFP peptides (aa 315-481 and aa 428-481) and one human FOXG1-GFP peptide comprised between aa 280-489 and we found that they diffused in both nuclear and cytoplasmic areas; however, following ZIKV infection, we observed discrete clusters in the cytoplasm. These results suggest that FOXG1 domains located at the C-terminal domains contributed to nuclear displacement or, at least, to downregulation (Figure 18).

In light of this result, we also wondered if this fragment should be responsible of Foxg1 hypothetic degradation, because GFP signal drastically decreased in the cells, following ZIKV infection. Performing *in silico* analysis of the sequence of FoxG1 we can identify sequences involved in proteasome-mediated degradation at aa 438-442 (mouse) and aa 439-443 (human) and for this reason we can suppose that ZIKV infection stimulates the ubiquitination process leading to the degradation of Foxg1 once it is located in the cytoplasm. This would explain the drastic decrease in fluorescence levels observed in infected cells, but only future experiments will shed light on this mechanism.

Interestingly Li et al. have demonstrated that ZIKV protease impinge on neural cell division by degrading Septin-2 and FOXG1 has been shown also to possess the ZIKV serine protease (NS2B-NS3) cutting motif (H. Li et al., 2019; Morazzani et al., 2019). For this reason, to shed light on the mechanism by which ZIKV affect FOXG1 localization we transfected A549 with both Foxg1-GFP and ZIKV NS2B-NS3 plasmids. Because Foxg1 was into the nucleus and NS2B-NS3 instead showed a cytoplasmic localization we did not see any significant displacement of Foxg1 into the cytoplasm or any consequent protein degradation. However, when we attempt lo lyse A549 expressing both exogenous proteins, in order to allow contact between them, and subsequent FOXG1 cleavage, we didn't observe any effect associated with ZIKV infection (Figure 19).

Then, investigating on the mechanistic link between ZIKV and Foxg1 impairment, we learned from the literature, that the subcellular localization of FoxG1 is post-translationally regulated, for example, through phosphorylation and we found that ZIKV appears to activate a mechanism of nuclear-to-cytoplasmic export of Foxg1. Moreover, the Akt pathway has been identified as one of the main players in the functional activation and intracellular localization of the FOXG1 factor and we wondered if ZIKV could induce this putative phosphorylation, and then FOXG1 delocalization, by activation of Akt pathway. Indeed, it has been learned from the literature that the threonine residue of FOXG1, namely T226, is phosphorylated by Akt. In fact, Regad et al. demonstrated that the activation of the Akt pathway induced by FGF on T226 leads to the export and cytoplasmic localization of FoxG1, resulting in its impaired function as a differentiation repressor and, consequently, the induction of neuronal differentiation (Regad et al., 2007). Moreover, Akt acts on a specific threonine residue, T271, on the FoxG1 molecule (Baek et al., 2015). Confocal microscopy analysis allowed us to observe the function of the T271 residue in nuclear export: once T271A mutation was introduced into the FoxG1 gene, preventing phosphorylation at the hydroxyl of T, both in the presence and absence of ZIKV, the nuclear

localization of Foxg1 was maintained. Instead, analyzing T271D mutation, we expected to restore Foxg1 relocation following ZIKV infection, as aspartic acid could be phosphorylated as threonine, but our results showed that FOXG1 T271 mutants remain in the nucleus, similar to controls, suggesting that T271 is a key residue for FOXG1 mislocalization following ZIKV infection (Figure 16). Therefore, the data seem to suggest a correlation between the presence of T271 and export from the nucleus to the cytoplasm.

To confirm this hypothesis and to assess Akt activation pathway involvement, WB analysis was performed. In contrast to what was observed by Liang's research group, which demonstrated that ZIKV infection in human fetal NSCs inhibits the Akt-mTOR pathway, leading to defective neurogenesis and aberrant autophagy activation, we showed an increase in pAkt levels (active form) in the presence of ZIKV, in a time dependent-manner, consistent with FOXG1 downregulation (Liang et al., 2016). We also analyzed PTEN expression, that is the main negative regulator of the PI3K-Akt pathway in order to understand if ZIKV could inhibit its expression to induce Akt phosphorylation. However, by WB analysis we observed that in A549 infected with ZIKV, PTEN expression was not affected, and we can conclude that ZIKV mediated Akt activation could not occur *via* PTEN inhibition (Figure 17).

However, one of the significant pathways through which Akt influences cell growth, survival, and metabolism is its interaction with GFs. When GFs binds to its receptor on the cell surface, they trigger a series of events that ultimately lead to the activation of Akt. Once activated, Akt promotes cell survival by inhibiting programmed cell death and supports cell growth by stimulating protein synthesis and cell proliferation. FGF2 is a key signaling molecule involved in various cellular processes, including cell proliferation, differentiation, and tissue repair (Lottini et al., 2023; Ornitz & Itoh, 2015). Recent reports demonstrate that ZIKV induces the expression of FGF2, which in turn facilitates virus replication and cell-to-cell spread (Limonta

et al., 2019). Furthermore, in ZIKV-infected pregnant women, the blood concentration of FGF2 is positively correlated with the severity of fetal infection (Kam et al., 2017).

We found that *FGF2* mRNA expression in hiPS-NPCs increased in a time-dependent manner in ZIKV infected cells. Moreover, monitoring FGF2 released in supernatant of ZIKV-, USUV- and CHIKV-infected and poly(I:C)-transfected A549 we found that FGF2 secretion increased gradually, peaking at 72 h pi with 1.5 ng/ml of FGF2 released following ZIKV infection (Figure 20). In turn, we treated A549 cells with different concentration of rFGF2 and we found an increase in ZIKV infection. Because FGF2 can induce cellular proliferation, the effect of this cytokine on viral replication might be due to increased numbers of susceptible A549 and a longer exposure to FGF2 might boost replication. Then we wondered if repeating rFGF2 treatment in ZIKV-infected and transiently expressing FOXG1 A549, we would observe transcription factor further impairment, due to ZIKV infection increase. However, when we performed WB analysis, we cannot observe any significant changes in FOXG1 expression (Figure 21). Additionally, we analyzed FOXG1 expression in mock- and ZIKV-infected NES cells, a model of human neural stem cells that are typically maintained in a medium supplemented with FGF2 and EGF2. Interestingly, following ZIKV infection, we did not observe the typical FOXG1 displacement in these cells, concluding that the varying culture conditions between hiPS-NPCs and NES cells might influence the subcellular localization of FOXG1. NES cells receive EGF and FGF2 to support their self-renewal state, whereas hiPS-NPCs and A549 are kept in a neural medium without GFs. For this reason, we decided to maintain A549 and hiPS-NPCs in a medium supplemented with GFs and subjected them to ZIKV infection; we found that the treatment with GFs effectively prevented FOXG1 displacement, as in NES cells, concluding that the impact of ZIKV infection on FOXG1 is modulated by GFs (Figure 22).

All these findings suggest that the export of FOXG1 to the cytoplasm and its downregulation, following ZIKV infection, results in its impaired function at the nuclear level, thus compromising anterior brain development. FGFs might be important, but their exact role was not pinpointed in the present work. Further studies are needed to confirm this hypothesis and to conclude that in the presence of ZIKV, a proteasome-mediated degradation process could be activated.

8 BIBLIOGRAPHY

Abeyrathna, P., & Su, Y. (2015). The critical role of Akt in cardiovascular function. In *Vascular Pharmacology* (Vol. 74, pp. 38–48). Elsevier Inc. https://doi.org/10.1016/j.vph.2015.05.008

Airo, A. M., Urbanowski, M. D., Lopez-Orozco, J., You, J. H., Skene-Arnold, T. D., Holmes, C., Yamshchikov, V., Malik-Soni, N., Frappier, L., & Hobman, T. C. (2018). Expression of flavivirus capsids enhance the cellular environment for viral replication by activating Akt-signalling pathways. *Virology*, *516*, 147–157. https://doi.org/10.1016/j.virol.2018.01.009

Alfano, C., Gladwyn-Ng, I., Couderc, T., Lecuit, M., & Nguyen, L. (2019). The unfolded protein response: A key player in zika virus-associated congenital microcephaly. *Frontiers in Cellular Neuroscience*, *13*. https://doi.org/10.3389/fncel.2019.00094

Baek, S. T., Copeland, B., Yun, E. J., Kwon, S. K., Guemez-Gamboa, A., Schaffer, A. E., Kim, S., Kang, H. C., Song, S., Mathern, G. W., & Gleeson, J. G. (2015). An AKT3-FOXG1-reelin network underlies defective migration in human focal malformations of cortical development. *Nature Medicine*, *21*(12), 1445–1454. https://doi.org/10.1038/nm.3982

Bayer, A., Lennemann, N. J., Ouyang, Y., Bramley, J. C., Morosky, S., Marques, E. T. D. A., Cherry, S., Sadovsky, Y., & Coyne, C. B. (2016). Type III Interferons Produced by Human Placental Trophoblasts Confer Protection against Zika Virus Infection. *Cell Host and Microbe*, *19*(5), 705–712. https://doi.org/10.1016/j.chom.2016.03.008

Brasil, P., Calvet, G. A., Siqueira, A. M., Wakimoto, M., de Sequeira, P. C., Nobre, A., Quintana, M. de S. B., Mendonça, M. C. L. de, Lupi, O., de Souza, R. V., Romero, C., Zogbi, H., Bressan, C. da S., Alves, S. S., Lourenço-de-Oliveira, R., Nogueira, R. M. R., Carvalho, M. S., de Filippis, A. M. B., & Jaenisch, T. (2016). Zika Virus Outbreak in Rio de Janeiro, Brazil: Clinical Characterization, Epidemiological and Virological Aspects. *PLoS Neglected Tropical Diseases*, *10*(4). https://doi.org/10.1371/journal.pntd.0004636

Brasil, P., Pereira, J. P., Moreira, M. E., Ribeiro Nogueira, R. M., Damasceno, L., Wakimoto, M., Rabello, R. S., Valderramos, S. G., Halai, U.-A., Salles, T. S., Zin, A. A., Horovitz, D., Daltro, P., Boechat, M., Raja Gabaglia, C., Carvalho de Sequeira, P., Pilotto, J. H., Medialdea-Carrera, R., Cotrim da Cunha, D., … Nielsen-Saines, K. (2016). Zika Virus Infection in Pregnant Women in Rio de Janeiro. *New England Journal of Medicine*, *375*(24), 2321–2334. https://doi.org/10.1056/nejmoa1602412

Bredenkamp, N., Seoighe, C., & Illing, N. (2007). Comparative evolutionary analysis of the FoxG1 transcription factor from diverse vertebrates identifies conserved recognition sites for microRNA regulation. *Development Genes and Evolution*, *217*(3), 227–233. https://doi.org/10.1007/s00427-006-0128-x

Calvet, G., Aguiar, R. S., Melo, A. S. O., Sampaio, S. A., de Filippis, I., Fabri, A., Araujo, E. S. M., de Sequeira, P. C., de Mendonça, M. C. L., de Oliveira, L., Tschoeke, D. A., Schrago, C. G., Thompson, F. L., Brasil, P., dos Santos, F. B., Nogueira, R. M. R., Tanuri, A., & de Filippis, A. M. B. (2016). Detection and sequencing of Zika virus from amniotic fluid of fetuses with microcephaly in Brazil: a case study. *The Lancet Infectious Diseases*, *16*(6), 653–660. https://doi.org/10.1016/S1473-3099(16)00095-5

Carbaugh, D. L., Baric, R. S., & Lazear, H. M. (2019). Envelope Protein Glycosylation Mediates Zika Virus Pathogenesis. *Journal of Virology*, *93*(12). https://doi.org/10.1128/jvi.00113-19

Cargnin, F., Kwon, J. S., Katzman, S., Chen, B., Lee, J. W., & Lee, S. K. (2018). FOXG1 Orchestrates Neocortical Organization and Cortico-Cortical Connections. *Neuron*, *100*(5), 1083-1096.e5. https://doi.org/10.1016/j.neuron.2018.10.016

Carlin, C. R. (2022). Role of EGF Receptor Regulatory Networks in the Host Response to Viral Infections. In *Frontiers in Cellular and Infection Microbiology* (Vol. 11). Frontiers Media S.A. https://doi.org/10.3389/fcimb.2021.820355

Carnell, G., Grehan, K., Ferrara, F., Molesti, E., & Temperton, N. (2017). An Optimized Method for the Production Using PEI, Titration and Neutralization of SARS-CoV Spike Luciferase Pseudotypes. *BIO-PROTOCOL*, *7*(16). https://doi.org/10.21769/bioprotoc.2514

Chiramel, A. I., & Best, S. M. (2018). Role of autophagy in Zika virus infection and pathogenesis. In *Virus Research* (Vol. 254, pp. 34–40). Elsevier B.V. https://doi.org/10.1016/j.virusres.2017.09.006

Clé, M., Beck, C., Salinas, S., Lecollinet, S., Gutierrez, S., Van de Perre, P., Baldet, T., Foulongne, V., & Simonin, Y. (2019). Usutu virus: A new threat? In *Epidemiology and Infection* (Vol. 147, pp. 1–11). Cambridge University Press. https://doi.org/10.1017/S0950268819001213

Cugola, F. R., Fernandes, I. R., Russo, F. B., Freitas, B. C., Dias, J. L. M., Guimarães, K. P., Benazzato, C., Almeida, N., Pignatari, G. C., Romero, S., Polonio, C. M., Cunha, I., Freitas, C. L., Brandaõ, W. N., Rossato, C., Andrade, D. G., Faria, D. D. P., Garcez, A. T., Buchpigel, C. A., … Beltrao-Braga, P. C. B. B. (2016). The Brazilian Zika virus strain

causes birth defects in experimental models. *Nature*, *534*(7606), 267–271. https://doi.org/10.1038/nature18296

Dang, J., Tiwari, S. K., Lichinchi, G., Qin, Y., Patil, V. S., Eroshkin, A. M., & Rana, T. M. (2016). Zika Virus Depletes Neural Progenitors in Human Cerebral Organoids through Activation of the Innate Immune Receptor TLR3. *Cell Stem Cell*, *19*(2), 258–265. https://doi.org/10.1016/j.stem.2016.04.014

Dastidar, S. G., Landrieu, P. M. Z., & D'Mello, S. R. (2011). FoxG1 promotes the survival of postmitotic neurons. *Journal of Neuroscience*, *31*(2), 402–413. https://doi.org/10.1523/JNEUROSCI.2897-10.2011

Dell'Anno, M. T., Wang, X., Onorati, M., Li, M., Talpo, F., Sekine, Y., Ma, S., Liu, F., Cafferty, W. B. J., Sestan, N., & Strittmatter, S. M. (2018). Human neuroepithelial stem cell regional specificity enables spinal cord repair through a relay circuit. *Nature Communications*, *9*(1). https://doi.org/10.1038/s41467-018-05844-8

Dubridge, R. B., Tang, P., Chao Hsia, H., Leong, P.-M., Miller, J. H., & Calos1, M. P. (1987). Analysis of Mutation in Human Cells by Using an Epstein-Barr Virus Shuttle System. In *MOLECULAR AND CELLULAR BIOLOGY* (Vol. 7, Issue 1).

El Costa, H., Gouilly, J., Mansuy, J. M., Chen, Q., Levy, C., Cartron, G., Veas, F., Al-Daccak, R., Izopet, J., & Jabrane-Ferrat, N. (2016). ZIKA virus reveals broad tissue and cell tropism during the first trimester of pregnancy. *Scientific Reports*, *6*. https://doi.org/10.1038/srep35296

El Ghouzzi, V., Bianchi, F. T., Molineris, I., Mounce, B. C., Berto, G. E., Rak, M., Lebon, S., Aubry, L., Tocco, C., Gai, M., Chiotto, A. M. A., Sgrò, F., Pallavicini, G., Simon-Loriere, E., Passemard, S., Vignuzzi, M., Gressens, P., & Di Cunto, F. (2016). ZIKA virus elicits P53 activation and genotoxic stress in human neural progenitors similar to mutations involved in severe forms of genetic microcephaly and p53. *Cell Death and Disease*, *7*(10). https://doi.org/10.1038/cddis.2016.266

Faizan, M. I., Abdullah, M., Ali, S., Naqvi, I. H., Ahmed, A., & Parveen, S. (2017). Zika Virus-Induced Microcephaly and Its Possible Molecular Mechanism. In *Intervirology* (Vol. 59, Issue 3, pp. 152–158). S. Karger AG. https://doi.org/10.1159/000452950

Florian, C., Bahi-Buisson, N., & Bienvenu, T. (2012). FOXG1-related disorders: From clinical description to molecular genetics. *Molecular Syndromology*, *2*(3–5), 153–163. https://doi.org/10.1159/000327329

Garcez, P. P., Nascimento, J. M., De Vasconcelos, J. M., Madeiro Da Costa, R., Delvecchio, R., Trindade, P., Loiola, E. C., Higa, L. M., Cassoli, J. S., Vitória, G., Sequeira, P. C.,

Sochacki, J., Aguiar, R. S., Fuzii, H. T., De Filippis, A. M. B., Da Silva Gonçalves Vianez Júnior, J. L., Tanuri, A., Martins-De-Souza, D., & Rehen, S. K. (2017). Zika virus disrupts molecular fingerprinting of human neurospheres. *Scientific Reports*, *7*. https://doi.org/10.1038/srep40780

Gasperowicz, M., & Otto, F. (2005). Mammalian Groucho homologs: Redundancy or specificity? In *Journal of Cellular Biochemistry* (Vol. 95, Issue 4, pp. 670–687). https://doi.org/10.1002/jcb.20476

Genin, E. C., Caron, N., Vandenbosch, R., Nguyen, L., & Malgrange, B. (2014). Concise review: Forkhead pathway in the control of adult neurogenesis. In *Stem Cells* (Vol. 32, Issue 6, pp. 1398–1407). AlphaMed Press. https://doi.org/10.1002/stem.1673

Giard, D. J., Aaronson, S. A., Todaro, G. J., Arnstein, P., Kersey, J. H., Doslk, H., & Parks, W. P. (1973). *In Vitro Cultivation of Human Tumors: Establishment of Cell Lines Derived From a Series of Solid Tumors*. http://jnci.oxfordjournals.org/

Gill, C. M., Kapadia, R. K., Beckham, J. D., Piquet, A. L., Tyler, K. L., & Pastula, D. M. (2020). Usutu virus disease: a potential problem for North America? In *Journal of NeuroVirology* (Vol. 26, Issue 2, pp. 149–154). Springer. https://doi.org/10.1007/s13365-019-00818-y

Gladwyn-Ng, I., Cordón-Barris, L., Alfano, C., Creppe, C., Couderc, T., Morelli, G., Thelen, N., America, M., Bessières, B., Encha-Razavi, F., Bonnière, M., Suzuki, I. K., Flamand, M., Vanderhaeghen, P., Thiry, M., Lecuit, M., & Nguyen, L. (2018). Stress-induced unfolded protein response contributes to Zika virus-associated microcephaly. In *Nature Neuroscience* (Vol. 21, Issue 1, pp. 63–73). Nature Publishing Group. https://doi.org/10.1038/s41593-017-0038-4

Golson, M. L., & Kaestner, K. H. (2016). Fox transcription factors: From development to disease. *Development (Cambridge)*, *143*(24), 4558–4570. https://doi.org/10.1242/dev.112672

Graham, F. L., Smileyt, J., Russell, W. C., & Nairn, R. (1977). Characteristics of a Human Cell Line Transformed by DNA from Human Adenovirus Type 5. In *J. gen. Virol* (Vol. 36).

Gray, C. W., & Coster, A. C. F. (2016). The Akt switch model: Is location sufficient? *Journal of Theoretical Biology*, *398*, 103–111. https://doi.org/10.1016/j.jtbi.2016.03.005

Guen, T. Le, Fichou, Y., Nectoux, J., Bahi-Buisson, N., Rivier, F., Boddaert, N., Diebold, B., Héron, D., Chelly, J., & Bienvenu, T. (2011). A missense mutation within the fork-head domain of the forkhead box G1 Gene (FOXG1) affects its nuclear localization. *Human Mutation*, *32*(2). https://doi.org/10.1002/humu.21422

Gutierrez-Guerrero, A., Cosset, F. L., & Verhoeyen, E. (2020). Lentiviral Vector Pseudotypes: Precious Tools to Improve Gene Modification of Hematopoietic Cells for Research and Gene Therapy. In *Viruses* (Vol. 12, Issue 9). MDPI AG. https://doi.org/10.3390/v12091016

Hasan, S. S., Sevvana, M., Kuhn, R. J., & Rossmann, M. G. (2018). Structural biology of Zika virus and other flaviviruses. In *Nature Structural and Molecular Biology* (Vol. 25, Issue 1, pp. 13–20). Nature Publishing Group. https://doi.org/10.1038/s41594-017-0010-8

Hayes, E. B. (2009). Zika virus outside Africa. In *Emerging Infectious Diseases* (Vol. 15, Issue 9, pp. 1347–1350). https://doi.org/10.3201/eid1509.090442

Heinz, F. X., & Stiasny, K. (2017). The Antigenic Structure of Zika Virus and Its Relation to Other Flaviviruses: Implications for Infection and Immunoprophylaxis. *Microbiology and Molecular Biology Reviews*, *81*(1). https://doi.org/10.1128/mmbr.00055-16

Hettige, N. C., & Ernst, C. (2019). FOXG1 Dose in Brain Development. In *Frontiers in Pediatrics* (Vol. 7). Frontiers Media S.A. https://doi.org/10.3389/fped.2019.00482

Hettige, N. C., Fleming, P., Semenak, A., Zhang, X., Peng, H., Hagel, M. D., Theroux, J. F., Zhang, Y., Ni, A., Jefri, M., Antonyan, L., Alsuwaidi, S., Schuppert, A., Stumpf, P. S., & Ernst, C. (2023). FOXG1 targets BMP repressors and cell cycle inhibitors in human neural progenitor cells. *Human Molecular Genetics*, *32*(15), 2511–2522. https://doi.org/10.1093/hmg/ddad089

Himmelsbach, K., & Hildt, E. (2018). Identification of various cell culture models for the study of Zika virus. *World Journal of Virology*, *7*(1), 10–20. https://doi.org/10.5501/wjv.v7.i1.10

Hou, P. S., hAilín, D., Vogel, T., & Hanashima, C. (2020). Transcription and Beyond: Delineating FOXG1 Function in Cortical Development and Disorders. In *Frontiers in Cellular Neuroscience* (Vol. 14). Frontiers Media S.A. https://doi.org/10.3389/fncel.2020.00035

Hung, S. J., & Huang, S. W. (2021). Contributions of Genetic Evolution to Zika Virus Emergence. In *Frontiers in Microbiology* (Vol. 12). Frontiers Media S.A. https://doi.org/10.3389/fmicb.2021.655065

Jensen, L. R., Amende, M., Gurok, U., Moser, B., Gimmel, V., Tzschach, A., Janecke, A. R., Tariverdian, G., Chelly, J., Fryns, J.-P., Esch, H. Van, Kleefstra, T., Hamel, B., Moraine, C., Gécz, J., Turner, G., Reinhardt, R., Kalscheuer, V. M., Ropers, H.-H., & Lenzner, S. (2005). Mutations in the JARID1C Gene, Which Is Involved in Transcriptional Regulation

and Chromatin Remodeling, Cause X-Linked Mental Retardation. In *Am. J. Hum. Genet* (Vol. 76).

Jiang, X., Dong, X., Li, S. H., Zhou, Y. P., Rayner, S., Xia, H. M., Gao, G. F., Yuan, H., Tang, Y. P., & Luo, M. H. (2018). Proteomic analysis of Zika virus infected primary human fetal neural progenitors suggests a role for doublecortin in the pathological consequences of infection in the cortex. *Frontiers in Microbiology*, *9*(JUN). https://doi.org/10.3389/fmicb.2018.01067

Kaestner, K. H., Knö, W., & Martínez, D. E. (2000). *Unified nomenclature for the winged helix/forkhead transcription factors*. http://www.biology.pomona.edu/fox.

Kam, Y. W., Leite, J. A., Lum, F. M., Tan, J. J. L., Lee, B., Judice, C. C., De Toledo Teixeira, D. A., Andreata-Santos, R., Vinolo, M. A., Angerami, R., Resende, M. R., Freitas, A. R. R., Amaral, E., Passini, R., Costa, M. L., Guida, J. P., Arns, C. W., Ferreira, L. C. S., Rénia, L., … Costa, F. T. M. (2017). Specific biomarkers associated with neurological complications and congenital central nervous system abnormalities from Zika virus-infected patients in Brazil. *Journal of Infectious Diseases*, *216*(2), 172–181. https://doi.org/10.1093/infdis/jix261

Kan, L., Jalali, A., Zhao, L. R., Zhou, X., McGuire, T., Kazanis, I., Episkopou, V., Bassuk, A. G., & Kessler, J. A. (2007). Dual function of Sox1 in telencephalic progenitor cells. *Developmental Biology*, *310*(1), 85–98. https://doi.org/10.1016/j.ydbio.2007.07.026

King, B., Temperton, N. J., Grehan, K., Scott, S. D., Wright, E., Tarr, A. W., & Daly, J. M. (2016). Technical considerations for the generation of novel pseudotyped viruses. In *Future Virology* (Vol. 11, Issue 1, pp. 47–59). Future Medicine Ltd. https://doi.org/10.2217/fvl.15.106

Koyama, S., Ishii, K. J., Coban, C., & Akira, S. (2008). Innate immune response to viral infection. In *Cytokine* (Vol. 43, Issue 3, pp. 336–341). https://doi.org/10.1016/j.cyto.2008.07.009

Krauer, F., Riesen, M., Reveiz, L., Oladapo, O. T., Martínez-Vega, R., Porgo, T. V., Haefliger, A., Broutet, N. J., & Low, N. (2017). Zika Virus Infection as a Cause of Congenital Brain Abnormalities and Guillain–Barré Syndrome: Systematic Review. *PLoS Medicine*, *14*(1). https://doi.org/10.1371/journal.pmed.1002203

Kumamoto, T., & Hanashima, C. (2017). Evolutionary conservation and conversion of Foxg1 function in brain development. In *Development Growth and Differentiation* (Vol. 59, Issue 4, pp. 258–269). Blackwell Publishing. https://doi.org/10.1111/dgd.12367

Kumar, A., Jovel, J., Lopez-Orozco, J., Limonta, D., Airo, A. M., Hou, S., Stryapunina, I., Fibke, C., Moore, R. B., & Hobman, T. C. (2018). Human sertoli cells support high levels of zika virus replication and persistence. *Scientific Reports*, *8*(1). https://doi.org/10.1038/s41598-018-23899-x

Lai, M., Iacono, E., Spezia, P. G., Lottini, G., La Rocca, V., Quaranta, P., Pistello, M., & Freer, G. (2022). A low-cost simple test for weekly detection of Mycoplasma hyorhinis and arginini contaminations in cell cultures and viral preparations. *Journal of Virological Methods*, *299*. https://doi.org/10.1016/j.jviromet.2021.114327

Lai, M., La Rocca, V., Amato, R., Freer, G., Costa, M., Spezia, P. G., Quaranta, P., Lombardo, G., Piomelli, D., & Pistello, M. (2021). Ablation of acid ceramidase impairs autophagy and mitochondria activity in melanoma cells. *International Journal of Molecular Sciences*, *22*(6). https://doi.org/10.3390/ijms22063247

Lei, J., Hansen, G., Nitsche, C., Klein, C. D., Zhang, L., & Hilgenfeld, R. (2016). Crystal structure of Zika virus NS2B-NS3 protease in complex with a boronate inhibitor. *J. Exp. Bot*, *26*, 2023. https://doi.org/10.6084/m9.figshare.3470135

Li, C., Xu, D., Ye, Q., Hong, S., Jiang, Y., Zhang, N., Liu, X., Shi, L., Qin, C.-F., & Xu, Z. (2016). Zika Virus Disrupts Neural Progenitor Development and Leads to Microcephaly in Mice. *Cell Stem Cell*, *19*(1), 120–126. https://doi.org/10.1016/j.stem.2016.04.017

Li, H., Saucedo-Cuevas, L., Regla-Nava, J. A., Chai, G., Sheets, N., Tang, W., Terskikh, A. V., Shresta, S., & Gleeson, J. G. (2016). Zika Virus Infects Neural Progenitors in the Adult Mouse Brain and Alters Proliferation. *Cell Stem Cell*, *19*(5), 593–598. https://doi.org/10.1016/j.stem.2016.08.005

Li, H., Saucedo-Cuevas, L., Yuan, L., Ross, D., Johansen, A., Sands, D., Stanley, V., Guemez-Gamboa, A., Gregor, A., Evans, T., Chen, S., Tan, L., Molina, H., Sheets, N., Shiryaev, S. A., Terskikh, A. V., Gladfelter, A. S., Shresta, S., Xu, Z., & Gleeson, J. G. (2019). Zika Virus Protease Cleavage of Host Protein Septin-2 Mediates Mitotic Defects in Neural Progenitors. *Neuron*, *101*(6), 1089-1098.e4. https://doi.org/10.1016/j.neuron.2019.01.010

Li, X.-L., Boyanapalli, M., Weihua, X., Kalvakolanu, D. V, & Hassel1, B. A. (1998). Induction of Interferon Synthesis and Activation of Interferon-Stimulated Genes by Liposomal Transfection Reagents. In *JOURNAL OF INTERFERON AND CYTOKINE RESEARCH* (Vol. 18). Mary Ann Liebert, Inc.

Liang, Q., Luo, Z., Zeng, J., Chen, W., Foo, S. S., Lee, S. A., Ge, J., Wang, S., Goldman, S. A., Zlokovic, B. V., Zhao, Z., & Jung, J. U. (2016). Zika Virus NS4A and NS4B Proteins Deregulate Akt-mTOR Signaling in Human Fetal Neural Stem Cells to Inhibit

Neurogenesis and Induce Autophagy. *Cell Stem Cell*, *19*(5), 663–671. https://doi.org/10.1016/j.stem.2016.07.019

Limonta, D., Jovel, J., Kumar, A., Lu, J., Hou, S., Airo, A. M., Lopez-Orozco, J., Wong, C. P., Saito, L., Branton, W., Wong, G. K. S., Mason, A., Power, C., & Hobman, T. C. (2019). Fibroblast Growth Factor 2 Enhances Zika Virus Infection in Human Fetal Brain. *Journal of Infectious Diseases*, *220*(8), 1377–1387. https://doi.org/10.1093/infdis/jiz073

Lin, H. H., Yip, B. S., Huang, L. M., & Wu, S. C. (2018). Zika virus structural biology and progress in vaccine development. In *Biotechnology Advances* (Vol. 36, Issue 1, pp. 47–53). Elsevier Inc. https://doi.org/10.1016/j.biotechadv.2017.09.004

Lottini, G., Plicanti, E., Lai, M., Quaranta, P., Pistello, M., & Freer, G. (2023). Canonical fibroblast growth factors in viral infection. In *Reviews in Medical Virology* (Vol. 33, Issue 4). John Wiley and Sons Ltd. https://doi.org/10.1002/rmv.2452

Ma, J., Benitez, J. A., Li, J., Miki, S., Ponte de Albuquerque, C., Galatro, T., Orellana, L., Zanca, C., Reed, R., Boyer, A., Koga, T., Varki, N. M., Fenton, T. R., Nagahashi Marie, S. K., Lindahl, E., Gahman, T. C., Shiau, A. K., Zhou, H., DeGroot, J., … Furnari, F. B. (2019). Inhibition of Nuclear PTEN Tyrosine Phosphorylation Enhances Glioma Radiation Sensitivity through Attenuated DNA Repair. *Cancer Cell*, *35*(3), 504-518.e7. https://doi.org/10.1016/j.ccell.2019.01.020

Maddaluno, L., Urwyler, C., Rauschendorfer, T., Meyer, M., Stefanova, D., Spörri, R., Wietecha, M., Ferrarese, L., Stoycheva, D., Bender, D., Li, N., Strittmatter, G., Nasirujjaman, K., Beer, H., Staeheli, P., Hildt, E., Oxenius, A., & Werner, S. (2020). Antagonism of interferon signaling by fibroblast growth factors promotes viral replication. *EMBO Molecular Medicine*, *12*(9). https://doi.org/10.15252/emmm.201911793

Means, J. C., & Passarelli, A. L. (2010). Viral fibroblast growth factor, matrix metalloproteases, and caspases are associated with enhancing systemic infection by baculoviruses. *Proceedings of the National Academy of Sciences of the United States of America*, *107*(21), 9825–9830. https://doi.org/10.1073/pnas.0913582107

Merten, O. W., Hebben, M., & Bovolenta, C. (2016). Production of lentiviral vectors. In *Molecular Therapy - Methods and Clinical Development* (Vol. 3, p. 16017). Elsevier Inc. https://doi.org/10.1038/mtm.2016.17

Miner, J. J., Cao, B., Govero, J., Smith, A. M., Fernandez, E., Cabrera, O. H., Garber, C., Noll, M., Klein, R. S., Noguchi, K. K., Mysorekar, I. U., & Diamond, M. S. (2016). Zika Virus Infection during Pregnancy in Mice Causes Placental Damage and Fetal Demise. *Cell*, *165*(5), 1081–1091. https://doi.org/10.1016/j.cell.2016.05.008

Mlakar, J., Korva, M., Tul, N., Popović, M., Poljšak-Prijatelj, M., Mraz, J., Kolenc, M., Resman Rus, K., Vesnaver Vipotnik, T., Fabjan Vodušek, V., Vizjak, A., Pižem, J., Petrovec, M., & Avšič Županc, T. (2016). Zika Virus Associated with Microcephaly. *New England Journal of Medicine*, *374*(10), 951–958. https://doi.org/10.1056/nejmoa1600651

Morazzani, E. M., Compton, J. R., Leary, D. H., Berry, A. V., Hu, X., Marugan, J., Glass, P. J., & Legler, P. M. (2019). Proteolytic cleavage of host proteins by the Group IV viral proteases of Venezuelan equine encephalitis virus and Zika virus. *Antiviral Research*, *164*, 106–122. https://doi.org/10.1016/j.antiviral.2019.02.001

Mukhopadhyay, S., Kuhn, R. J., & Rossmann, M. G. (2005). A structural perspective of the Flavivirus life cycle. In *Nature Reviews Microbiology* (Vol. 3, Issue 1, pp. 13–22). https://doi.org/10.1038/nrmicro1067

Onorati, M., Castiglioni, V., Biasci, D., Cesana, E., Menon, R., Vuono, R., Talpo, F., Laguna Goya, R., Lyons, P. A., Bulfamante, G. P., Muzio, L., Martino, G., Toselli, M., Farina, C., A Barker, R., Biella, G., & Cattaneo, E. (2014). Molecular and functional definition of the developing human striatum. *Nature Neuroscience*, *17*(12), 1804–1815. https://doi.org/10.1038/nn.3860

Onorati, M., Li, Z., Liu, F., Sousa, A. M. M., Nakagawa, N., Li, M., Dell'Anno, M. T., Gulden, F. O., Pochareddy, S., Tebbenkamp, A. T. N., Han, W., Pletikos, M., Gao, T., Zhu, Y., Bichsel, C., Varela, L., Szigeti-Buck, K., Lisgo, S., Zhang, Y., … Sestan, N. (2016). Zika Virus Disrupts Phospho-TBK1 Localization and Mitosis in Human Neuroepithelial Stem Cells and Radial Glia. *Cell Reports*, *16*(10), 2576–2592. https://doi.org/10.1016/j.celrep.2016.08.038

Ornelas, A. M. M., Pezzuto, P., Silveira, P. P., Melo, F. O., Ferreira, T. A., Oliveira-Szejnfeld, P. S., Leal, J. I., Amorim, M. M. R., Hamilton, S., Rawlinson, W. D., Cardoso, C. C., Nixon, D. F., Tanuri, A., Melo, A. S., & Aguiar, R. S. (2017). Immune activation in amniotic fluid from Zika virus–associated microcephaly. *Annals of Neurology*, *81*(1), 152–156. https://doi.org/10.1002/ana.24839

Ornitz, D. M., & Itoh, N. (2015). The fibroblast growth factor signaling pathway. *Wiley Interdisciplinary Reviews: Developmental Biology*, *4*(3), 215–266. https://doi.org/10.1002/wdev.176

Pancrazi, L., Benedetto, G. Di, Colombaioni, L., Sala, G. Della, Testa, G., Olimpico, F., Reyes, A., Zeviani, M., Pozzan, T., & Costa, M. (2015). Foxg1 localizes to mitochondria and coordinates cell differentiation and bioenergetics. *Proceedings of the National Academy*

of Sciences of the United States of America, *112*(45), 13910–13915. https://doi.org/10.1073/pnas.1515190112

Passemard, S., Kaindl, A. M., & Verloes, A. (2013). Microcephaly. In *Handbook of Clinical Neurology* (Vol. 111, pp. 129–141). Elsevier B.V. https://doi.org/10.1016/B978-0-444-52891-9.00013-0

Pauley, S., Lai, E., & Fritzsch, B. (2006). Foxg1 is required for morphogenesis and histogenesis of the mammalian inner ear. *Developmental Dynamics*, *235*(9), 2470–2482. https://doi.org/10.1002/dvdy.20839

Petersen, L. R., Jamieson, D. J., Powers, A. M., & Honein, M. A. (2016). Zika Virus. *New England Journal of Medicine*, *374*(16), 1552–1563. https://doi.org/10.1056/NEJMra1602113

Phin, S., Moore, M. W., & Cotter, P. D. (2013). Genomic rearrangements of PTEN in prostate cancer. *Frontiers in Oncology*, *3 SEP*. https://doi.org/10.3389/fonc.2013.00240

Pierson, T. C., & Diamond, M. S. (2020). The continued threat of emerging flaviviruses. In *Nature Microbiology* (Vol. 5, Issue 6, pp. 796–812). Nature Research. https://doi.org/10.1038/s41564-020-0714-0

Prudovsky, I. (2021). Cellular mechanisms of fgf-stimulated tissue repair. In *Cells* (Vol. 10, Issue 7). MDPI. https://doi.org/10.3390/cells10071830

Quicke, K. M., Bowen, J. R., Johnson, E. L., McDonald, C. E., Ma, H., O'Neal, J. T., Rajakumar, A., Wrammert, J., Rimawi, B. H., Pulendran, B., Schinazi, R. F., Chakraborty, R., & Suthar, M. S. (2016). Zika Virus Infects Human Placental Macrophages. *Cell Host and Microbe*, *20*(1), 83–90. https://doi.org/10.1016/j.chom.2016.05.015

Regad, T., Roth, M., Bredenkamp, N., Illing, N., & Papalopulu, N. (2007). The neural progenitor-specifying activity of FoxG1 is antagonistically regulated by CKI and FGF. *Nature Cell Biology*, *9*(5), 531–540. https://doi.org/10.1038/ncb1573

Revathidevi, S., & Munirajan, A. K. (2019). Akt in cancer: Mediator and more. In *Seminars in Cancer Biology* (Vol. 59, pp. 80–91). Academic Press. https://doi.org/10.1016/j.semcancer.2019.06.002

Rey, F. A., Stiasny, K., & Heinz, F. X. (2017). Flavivirus structural heterogeneity: implications for cell entry. In *Current Opinion in Virology* (Vol. 24, pp. 132–139). Elsevier B.V. https://doi.org/10.1016/j.coviro.2017.06.009

Rossi, S. L., Ebel, G. D., Shan, C., Shi, P. Y., & Vasilakis, N. (2018). Did Zika Virus Mutate to Cause Severe Outbreaks? In *Trends in Microbiology* (Vol. 26, Issue 10, pp. 877–885). Elsevier Ltd. https://doi.org/10.1016/j.tim.2018.05.007

Sager, G., Gabaglio, S., Sztul, E., & Belov, G. A. (2018). Role of host cell secretory machinery in zika virus life cycle. In *Viruses* (Vol. 10, Issue 10). MDPI AG. https://doi.org/10.3390/v10100559

Sakuma, T., Barry, M. A., & Ikeda, Y. (2012). Lentiviral vectors: Basic to translational. In *Biochemical Journal* (Vol. 443, Issue 3, pp. 603–618). https://doi.org/10.1042/BJ20120146

Schäfer, T., Zentgraf, H., Zehe, C., Brügger, B., Bernhagen, J., & Nickel, W. (2004). Unconventional Secretion of Fibroblast Growth Factor 2 Is Mediated by Direct Translocation across the Plasma Membrane of Mammalian Cells. *Journal of Biological Chemistry*, *279*(8), 6244–6251. https://doi.org/10.1074/jbc.M310500200

Schnierle, B. S. (2019). Cellular attachment and entry factors for chikungunya virus. In *Viruses* (Vol. 11, Issue 11). MDPI AG. https://doi.org/10.3390/v11111078

Seoane, J., Le, H.-V., Shen, L., Anderson, S. A., & Massague, J. M. (2004). Integration of Smad and Forkhead Pathways in the Control of Neuroepithelial and Glioblastoma Cell Proliferation. *Cell*, *117*, 211–223.

Silva, L. A., & Dermody, T. S. (2017). Chikungunya virus: Epidemiology, replication, disease mechanisms, and prospective intervention strategies. In *Journal of Clinical Investigation* (Vol. 127, Issue 3, pp. 737–749). American Society for Clinical Investigation. https://doi.org/10.1172/JCI84417

Smith, D. W., & Mackenzie, J. (2016). Zika virus and Guillain-Barré syndrome: Another viral cause to add to the list. In *The Lancet* (Vol. 387, Issue 10027, pp. 1486–1488). Lancet Publishing Group. https://doi.org/10.1016/S0140-6736(16)00564-X

Sousa, A. M. M., Zhu, Y., Raghanti, M. A., Kitchen, R. R., Onorati, M., Tebbenkamp, A. T. N., Stutz, B., Meyer, K. A., Li, M., Kawasawa, Y. I., Liu, F., Perez, R. G., Mele, M., Carvalho, T., Skarica, M., Gulden, F. O., Pletikos, M., Shibata, A., Stephenson, A. R., … Sestan, N. (2017). Molecular and cellular reorganization of neural circuits in the human lineage. *Science*, *358*(6366), 1027–1032. https://doi.org/10.1126/science.aan3456

Subissi, L., Dub, T., Besnard, M., Mariteragi-Helle, T., Nhan, T., Lutringer-Magnin, D., Barboza, P., Gurry, C., Brindel, P., Nilles, E. J., Baud, D., Merianos, A., Musso, D., Glynn, J. R., Dupuis, G., Cao-Lormeau, V. M., Giard, M., & Mallet, H. P. (2018). Zika virus infection during pregnancy and effects on early childhood development, French Polynesia, 2013–2016. *Emerging Infectious Diseases*, *24*(10), 1850–1858. https://doi.org/10.3201/eid2410.172079

Tang, H., Hammack, C., Ogden, S. C., Wen, Z., Qian, X., Li, Y., Yao, B., Shin, J., Zhang, F., Lee, E. M., Christian, K. M., Didier, R. A., Jin, P., Song, H., & Ming, G. L. (2016). Zika virus infects human cortical neural progenitors and attenuates their growth. *Cell Stem Cell*, *18*(5), 587–590. https://doi.org/10.1016/j.stem.2016.02.016

Van Den Elsen, K., Quek, J. P., & Luo, D. (2021). Molecular insights into the flavivirus replication complex. *Viruses*, *13*(6). https://doi.org/10.3390/v13060956

Van der Linden, H., Carvalho, M. D., van der Linden, V., Lacerda, K. M., Pessoa, A., Carneiro, M. L., Cordeiro, M. T., & Valente, K. D. (2018). Epilepsy Profile in Infants with Congenital Zika Virus Infection. *New England Journal of Medicine*, *379*(9), 891–892. https://doi.org/10.1056/nejmc1716070

Vegas, N., Cavallin, M., Maillard, C., Boddaert, N., Toulouse, J., Schaefer, E., Lerman-Sagie, T., Lev, D., Magalie, B., Moutton, S., Haan, E., Isidor, B., Heron, D., Milh, M., Rondeau, S., Michot, C., Valence, S., Wagner, S., Hully, M., … Bahi-Buisson, N. (2018). Delineating FOXG1 syndrome: From congenital microcephaly to hyperkinetic encephalopathy. *Neurology: Genetics*, *4*(6). https://doi.org/10.1212/NXG.0000000000000281

Weigel, D., Gerd, ', Irgens, J., Kiittner, F., Seifert, E., & Jlckle, H. (1989). The Homeotic Gene fork head Encodes a Nuclear Protein and Is Expressed in the Terminal Regions of the Drosophila Embryo. In *Cell* (Vol. 57).

Wen, Z., Song, H., & Ming, G.-L. (2017). *How does Zika virus cause microcephaly?* https://doi.org/10.1101/gad.298216

West, K. A., Castillo, S. S., & Dennis, P. A. (2002). Activation of the PI3K/Akt pathway and chemotherapeutic resistance. In *Drug Resistance Updates* (Vol. 5).

Wolff, J. H., & Mikkelsen, J. G. (2022). Delivering genes with human immunodeficiency virus-derived vehicles: still state-of-the-art after 25 years. In *Journal of Biomedical Science* (Vol. 29, Issue 1). BioMed Central Ltd. https://doi.org/10.1186/s12929-022-00865-4

Wong, L. C., Singh, S., Wang, H. P., Hsu, C. J., Hu, S. C., & Lee, W. T. (2019). FOXG1-related syndrome: From clinical to molecular genetics and pathogenic mechanisms. In *International Journal of Molecular Sciences* (Vol. 20, Issue 17). MDPI AG. https://doi.org/10.3390/ijms20174176

Xiong, Y., Zhang, Y., Xiong, S., & Williams-Villalobo, A. E. (2020). A glance of p53 functions in brain development, neural stem cells, and brain cancer. In *Biology* (Vol. 9, Issue 9, pp. 1–13). MDPI AG. https://doi.org/10.3390/biology9090285

Yu, I.-M., Zhang, W., Holdaway, H. A., Li, L., Kostyuchenko, V. A., Chipman, P. R., Kuhn, R. J., Rossmann, M. G., & Chen, J. (2008). The flavivirus precursor membrane-envelope protein complex: Structure and maturation. *Science*, *319*(5871), 1830–1834. https://doi.org/10.1126/science.1153263

Zanluca, C., De Melo, V. C. A., Mosimann, A. L. P., Dos Santos, G. I. V., dos Santos, C. N. D., & Luz, K. (2015). First report of autochthonous transmission of Zika virus in Brazil. *Memorias Do Instituto Oswaldo Cruz*, *110*(4), 569–572. https://doi.org/10.1590/0074-02760150192

Zhang, F., Hammack, C., Ogden, S. C., Cheng, Y., Lee, E. M., Wen, Z., Qian, X., Nguyen, H. N., Li, Y., Yao, B., Xu, M., Xu, T., Chen, L., Wang, Z., Feng, H., Huang, W. K., Yoon, K. J., Shan, C., Huang, L., … Jin, P. (2016). Molecular signatures associated with ZIKV exposure in human cortical neural progenitors. *Nucleic Acids Research*, *44*(18), 8610–8620. https://doi.org/10.1093/nar/gkw765

Zhao, X., Bian, R., Wang, F., Wang, Y., Li, X., Guo, Y., Zhang, X., Luo, G., & Zhan, R. (2021). GDF-5 promotes epidermal stem cells proliferation via Foxg1-cyclin D1 signaling. *Stem Cell Research and Therapy*, *12*(1). https://doi.org/10.1186/s13287-020-02106-7